Spring 1-1-2013

Spatio-Temporal Variability and Predictability of Relative

Daniel Paul Broman
University of Colorado at Boulder, daniel.p.broman@gmail.com

SPATIO-TEMPORAL VARIABILITY AND PREDICTABILITY OF RELATIVE HUMIDITY AND MENINGOCOCCAL MENINGITIS INCIDENCE IN THE WEST AFRICAN MONSOON REGION

by

DANIEL PAUL BROMAN

B.S., University of New Hampshire, 2011

A thesis submitted to the

Faculty of the Graduate School of the

University of Colorado in partial fulfillment

of the requirement for the degree of

Master of Science

Department of Civil, Environmental, and Architectural Engineering

2013

This thesis entitled:
Spatio-Temporal Variability and Predictability of Relative Humidity and Meningococcal Meningitis Incidence in the West African Monsoon Region
written Daniel Paul Broman
has been approved for the Department of Civil, Environmental, and Architectural Engineering

_____
(Dr. Balaji Rajagopalan, Committee Chair)

_____
(Dr. Thomas Hopson, Committee Member)

_____
(Dr. Edith Zagona, Committee Member)

Date_____

The final copy of this thesis has been examined by the signatories, and we find that both the content and the form meet acceptable presentation standards of scholarly work in the above mentioned discipline.

Broman, Daniel Paul (M.S., Civil Engineering, Department of Civil, Environmental, and Architectural Engineering)

Spatio-Temporal Variability and Predictability of Relative Humidity and Meningococcal Meningitis Incidence in the West African Monsoon Region

Thesis directed by Professor Balaji Rajagopalan

Meningococcal meningitis (meningitis) is endemic to West Africa, with the disease being fatal in 50% of the cases if left untreated. This region relies upon the international community for assistance in prevention and treatment. The International Coordinating Group for Vaccine Provision (ICG) oversees the monitoring of meningitis cases and the allocation of vaccine to limit case spread. Given the limited supply of vaccine, determining its deployment is contingent upon a number of factors including predictions of future cases. An inverse relationship exists between relative humidity and the incidence of meningitis cases providing a method of prediction based on understanding of climate variability. This research focused on first examining the interseasonal variability of relative humidity to develop predictive models based on climate features and then extend those models to forecast meningitis case counts.

The annual latitudinal migration of the Intertropical Convergence Zone (ITCZ) drives the monsoon onset and retreat, however ancillary factors such as sea-surface temperatures can have a large influence on monsoon timing and strength. This onset and retreat of the monsoon plays an important role in the occurrence of meningococcal meningitis in the region. The first part of the thesis involves a systematic analysis of relative humidity during the onset, peak and retreat periods of the monsoon over Western Africa. A K-means cluster analysis was performed to identify spatially coherent regions of relative humidity variability during the three periods. The cluster average of the relative humidity provides a robust representative index of the strength and timing of the WAM. Correlating the cluster anomalies with large-scale dynamical and thermodynamical features indicate that the anomalies are most strongly connected to the land-ocean temperature gradient and the corresponding circulation, tropical Atlantic sea surface temperatures (SSTs), and to a somewhat lesser extent SSTs over the tropical

Pacific. These connections to large-scale climate features were also found to be persistent over intraseasonal time scales, and thus best linear predictive models were developed to enable skillful forecasts of relative humidity during the two periods at 15-75 day lead times.

The second part of the research involved analyzing the meningitis incidence within four countries of West Africa (Benin, Chad, Nigeria, and Togo) and their links to meteorological variables. The predictive models of relative humidity during the onset and withdrawal season of the monsoon, which also coincides with the withdrawal and onset of meningitis season, respectively, were used to model the occurrences of meningitis cases. Skill scores were found to determine the effectiveness of these models in forecasting meningitis case counts. These two components of the research make important contributions towards understanding the processes that govern meningitis occurrences and provide the tools for improving the efficiency of mitigation strategies.

TABLE OF CONTENTS

TABLES

FIGURES

ACKNOWLEDGEMENT

I would first like to express my gratitude to the University of Colorado, Boulder, the Department of Civil, Environmental, and Architectural Engineering, and the Hydrology, Water Resources, and Environmental Fluid Mechanics Graduate Program for accepting me and assisting me as I discovered my passion as I had little direction at the begining. I would like to especially thank my adviser Balaji Rajagopalan for finding and offering me the opportunity that led to this research, and for all his assistance along the way. Tom Hopson, my research associate at the National Center for Atmospheric Research, who's work this paper is built off has been an exceptional resource through the entire project. I am grateful for his assistance and advocacy on my behalf trying to locate additional opportunities to continue and expand upon this work. I would like to thank Edith Zagona for serving on my graduate committee in short order. Conversations with Rajul Pandya from UCAR and Tom Yoksas from Unidata gave me a much better understanding of intricacies in working on an international interdisciplinary project and the resources they provided gave me a much better understanding of the "big picture".

1 INTRODUCTION AND BACKGROUND

1.1 INTRODUCTION

> *"Whoever wishes to investigate medicine properly, should proceed thus: in the first place to consider the seasons of the year, and what effects each of them produces for they are not at all alike, but differ much from themselves in regard to their changes. Then the winds, the hot and the cold, especially such as are common to all countries, and then such as are peculiar to each locality. We must also consider the qualities of the waters, for as they differ from one another in taste and weight, so also do they differ much in their qualities."*
> -Hippocrates, *On Airs, Waters, and Places* (trans. by Francis Adams)

Environmental conditions, have, since the emergence of western medicine, been linked to human health. Infectious disease can be directly or indirectly linked to these conditions through physiological effects, societal changes, and vector influences, i.e. breeding of mosquitoes. This paper explores the connection between meningococcal meningitis and relative humidity in West Africa. The first section below gives an overview of meningococcal meningitis in the region, describing its history, current management methods, and links to environmental conditions. The second section describes large-scale climate features, and their influence on relative humidity.

1.2 MENINGITIS IN AFRICA

Meningococcal meningitis (hereafter referred to as meningitis) is endemic to Africa to an extent Lapeyssonnie and others have identified a 'meningitis belt' stretching across sub-Saharan Africa (Lapeyssonnie, 1963; Molesworth, 2002). Greenwood (1998) posits that the disease first reached this region in the late 19th or early 20th century brought by

Muslim pilgrims returning from the Hajj, given evidence that this period saw the first large epidemics. These epidemics are now commonplace, occurring every 7 – 14 years (WHO Fact Sheet Nº141). Meningitis is a bacterial disease caused by *Neisseria meningitides* (Nm). The disease affects the protective membrane surrounding the brain and spinal column, resulting in a stiff neck, nausea, and high fever. The World Health Organization estimates that 50% of untreated cases lead to death. Even in cases treated, 10 – 20% develop neurological sequelae, which can have long-term implications including additional medical expenses and loss of productivity (WHO 2005). The total direct cost to treat a case of meningitis is estimated to be approximately US $90 in Burkina Faso, 34% of GDP per capita. Indirect costs are estimated to be much higher. Meningitis is spread person-to-person through the exchange of respiratory droplets, though there are varying local beliefs in the cause of the disease, from the wind and sun to supernatural causes (Colombini et. al. 2009). Regardless of local belief, modern prevention methods, vaccination, and treatment methods are effective in managing meningitis. The most prevalent serogroup, A (Nm A), is responsible for 80 - 85% of the historical cases of meningitis in the meningitis belt (*WHO Fact Sheet Nº141*).

1.3 MENINGITIS MANAGEMENT

The International Coordinating Group for Vaccine Provision (ICG) was created in 1997 to manage responses to meningitis outbreaks. The WHO, Medicines Sans Frontiers (MSF), the International Federation of the Red Cross and Red Crescent (IFRC), and UNICEF are founding partners; the ICG also collaborates with technical partners including the U.S. Centers for Disease Control and Prevention. The ICG coordinates targeted reactive vaccination campaigns using either a bivalent Nm A/C polysaccharide

vaccine or a trivalent Nm A/C/W135 polysaccharide vaccine. These vaccine provide immunity in individuals against meningitis for roughly three years, but do not confer herd immunity, meaning disease transmission is still possible. Vaccination is conducted at the sub-national district level and is based on a districts incidence rate, cases per 100,000. This rate is calculated from the weekly reporting of district case counts. Threshold levels for vaccination, based on work by Varaine et. al. (1997); Lewis et. al. (2001) were established to ensure good sensitivity and specificity in detecting epidemics and allow for timely response. Table 1.1 lists these threshold levels.

Table 1.1: ICG meningitis monitoring and treatment strategy (from *Weekly epidemiological record,* 22 September, 2000, WHO)

	Population	
Intervention	> 30 000	< 30 000
Alert threshold / Seuil d'alerte • Inform authorities / Informer les autorités • Investigate / Enquêter • Confirm / Confirmer • Treat cases / Traiter les cas • Strengthen surveillance / Renforcer la surveillance • Prepare / Préparer	• 5 cases per 100 000 inhabitants per week / 5 cas pour 100 000 habitants par semaine	• 2 cases in 1 week / 2 cas en 1 semaine *Or / Ou* • An increase in the number of cases compared to previous non-epidemic years / Une augmentation du nombre de cas par rapport aux années non épidémiques précédentes
Epidemic threshold / Seuil épidémique • Mass vaccination / Vaccination de masse • Distribute treatment to health centres / Distribuer traitements aux centres de santé • Treat according to epidemic protocol / Prise en charge selon le protocole épidémique • Inform the public / Informer la population	*If (1) no epidemic for 3 years and vaccination coverage <80% or (2) alert threshold crossed early in the dry season*[b] */ Si 1) pas d'épidémie depuis 3 ans et couverture vaccinale <80% ou 2) seuil d'alerte franchi tôt dans la saison sèche*[b] • 10 cases per 100 000 inhabitants per week / 10 cas pour 100 000 habitants par semaine *Other situations / Autres situations* • 15 cases per 100 000 inhabitants per week / 15 cas pour 100 000 habitants par semaine	• 5 cases in 1 week / 5 cas en 1 semaine *Or / Ou* • Doubling of the number of cases in a 3-week period[c] / Doublement des cas sur une période de 3 semaines[c] *Or / Ou* • Other situations should be studied on a case-by-case basis[b, d] Les autres situations doivent être étudiées au cas par cas[b, d]
	If there is an epidemic in a neighbouring area / En cas d'épidémie dans une zone proche • the alert threshold becomes the epidemic threshold / Le seuil d'alerte devient le seuil épidémique	

[a] Recommendation of the Consensus meeting on detection of meningitis epidemics in Africa, Paris, 20 June 2000. – Recommandation de la Réunion de consensus sur la détection des épidémies de méningite en Afrique, Paris, le 20 juin 2000.

[b] Early in the dry season: before March. Other epidemic risk factor that may be considered: high population density. – Tôt dans la saison sèche: avant mars. Autre facteur de risque épidémique qui peut être pris en considération: forte densité de population.

[c] For example: *week 1*: 1 case; *week 2*: 2 cases; *week 3*: 4 cases. – Par exemple, *semaine 1* : 1 cas; *semaine 2*: 2 cas; *semaine 3*: 4 cas.

[d] For mass gatherings, refugees and displaced persons, 2 confirmed cases in 1 week are enough to vaccinate the population. – Pour les regroupements de populations, réfugiés et personnes déplacées, 2 cas confirmés en 1 semaine suffisent pour vacciner la population.

In districts with populations greater than 30,000, instances of 5 cases per 100,000, the alert level, trigger increased surveillance and a determination of the meningitis strain responsible. 10 cases per 100,000, the epidemic level, trigger vaccination within the district. Alert level districts adjacent to epidemic level districts are also vaccinated. MenAfriVac, a new conjugate vaccine designed to provide long-term immunity against Nm A has greatly reduced the number of Nm A cases, and is hoped will severely limit or eliminate Nm A when the inoculation campaign is complete. As of 2013, this project has successfully inoculated the under-30 population in six countries: Burkina Faso, Mali, Niger, Chad, and Cameroon. This inoculation campaign is ongoing in five countries including three in West Africa: Ghana, Benin, and Nigeria. MenAfriVac has produced the desired response, conferring herd immunity against Nm A. Kristiansen et. al. (2013) sampled persons in Burkina Faso pre and post vaccination. Pre-vaccination, 0.39% of the sampled persons carried Nm A. Post-vaccination, none of the sampled persons carried Nm A in any of the five sampling campaigns. The reactive vaccination strategy managed by the ICG is still useful in regions that have not received MenAfriVac, and remains the primary response to outbreaks of Nm W135 or other serotypes. Forecasts of meningitis incidence using connections to environmental factors could provide greater response time to contain epidemics and reduce overall incidence.

1.4 LINKS TO ENVIRONMENTAL FACTORS

Local knowledge of the disease suggests an awareness of its link to environmental factors; both the Bambara word for meningitis, *finyabana*, and the Mossi word, *segba banga* mean wind disease (Besancenot et. al. 1997; Colombini et. al. 2009). Meningitis

incidence exhibits a strong seasonal cycle, with almost all cases occurring during the dry season, November through May. During the dry season, the Harmattan winds transport hot, dry, dusty air southwest from the Sahara Desert. Temperature, humidity, and dust have all been suggested as being linked to meningitis incidence. Sultan et. al. (2005) compared the start week of the meningitis season, found by examining the weekly anomaly case anomaly as compared to the weekly mean cases, with an index of the strength of the Harmattan winds. Their analysis was performed using nine years of case data from Mali, and found a strong linear relationship between the case anomalies and the Harmattan winds ($R^2 = 0.8498$). Molesworth et. al. (2003) aggregated historical cases of meningitis and compared case counts at the district level to environmental factors. The two strongest predictors were a classification based on the seasonal specific humidity profile and land cover. Thomson et. al. (2006) used rainfall and aerosol anomalies spatially classified by land cover types as predictors of meningitis incidence. The R^2 for all land cover types was 0.38 using a linear regression with the above environmental factors and monthly meningitis incidence anomaly.

A conceptual model of meningitis incidence was put forth by Mueller et. al. (2010) and is shown in Figure 1.1.

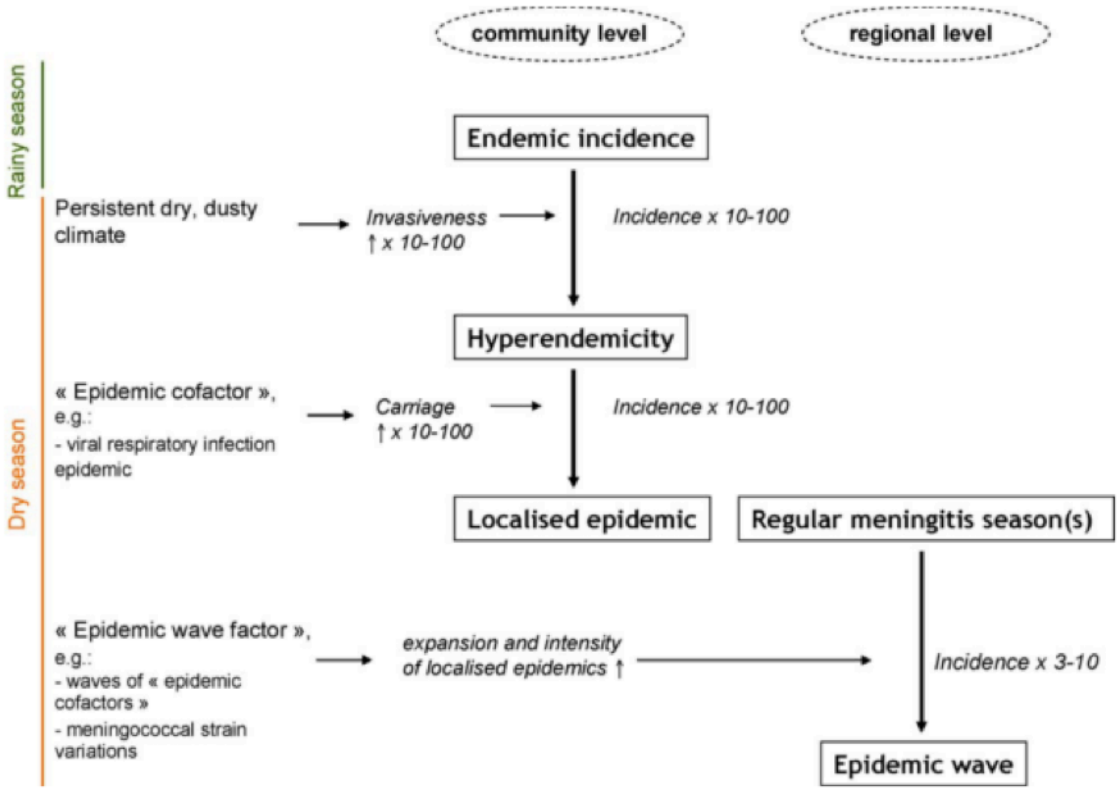

Figure 1.1: Conceptual meningitis model from Mueller et. al. (2010)

Environmental factors are responsible for the increase in incidence from the rainy to dry season; dry, dusty conditions lead to a transition from endemic to hyperenedmic incidence. Viral respiratory infections provide for weakened mucosal defenses leading to epidemics. Expansion to a regional-level epidemic is contingent on a new strain of meningitis or a high prevalence of epidemic cofactors. In Figure 1.2, I have expanded on this conceptual model in an attempt to identify causes of increased meningitis incidence. Three categories of causes have been identified: social, biologic, and physiological.

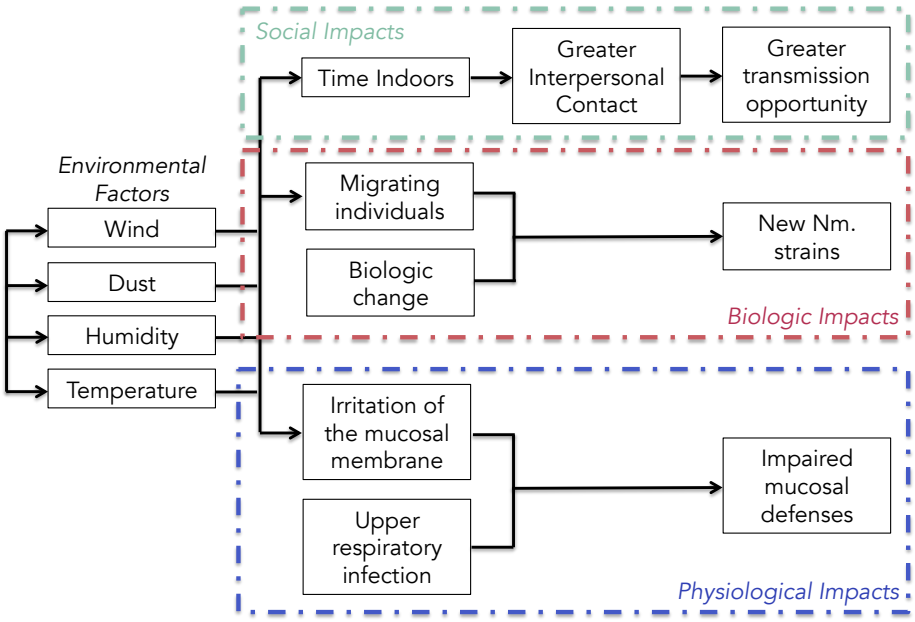

Figure 1.2: New conceptual model of meningitis incidence

Dry season conditions encourage individuals to spend more time indoors, which increases interpersonal contact. This increased contact offers greater opportunity for disease transmission as meningitis is spread person to person. Carriage rates of the same serogroup between individuals living together were higher than between contacts outside the home suggesting that this greater opportunity does result in higher transmission (Greenwood et. al. 1978; Hassan-King et. al. 1988; Gugnani et. al. 1989; Cheesbrough et. al. 1995; Boisier and Djibo 2006; Trotter and Greenwood 2007).

Local populations have little defense against new emergent strains of meningitis. Two methods of introduction are suggested here: in situ mutation, and migration. In situ mutation of Nm to produce a new strain of the disease would directly introduce it into the local population. Seasonal migration, which is prevalent in the region, could also transport new strains of Nm from other locations. The United Nations Environment

Programme (UNEP) investigated seasonal migration and identified two primary motivations: farmers seeking work in the city during the dry season, and seasonal migration of livestock herdsmen, both potential vectors new meningitis strains. Long-distance human transport of meningitis is thought to be responsible for its introduction into the region at the turn of the 20th century, and for the introduction of a new serotype, Nm W135 within the past 15 years (Greenwood, 1998). The meningitis modeling study presented in Chapter 3 does not attempt to account for all causes shown in Figure 1.2, rather, it focuses on the demonstrated link between meningitis incidence and relative humidity and uses prior meningitis incidence as a surrogate for the other causes. Two predominant seasons exist in West Africa: a winter dry season, and a summer wet season. An understanding of the connections between relative humidity and large-scale climate is needed to make use of the link between meningitis incidence and relative humidity. The section below presents an overview of climate in West Africa with a focus on moisture transport.

1.5 CLIMATE SEASONAL VARIABILITY

Seasonal weather patterns in our region of interest, including the countries Ghana, Togo, Benin, Nigeria, Chad, Niger, Mali, and Burkina Faso, are dominated by the West African Monsoon (WAM). The WAM is a low-level southwesterly flow existing during the boreal summer, advecting moisture inland from the Gulf of Guinea. Meningitis incidence almost exclusively occurs during the winter dry season, making an understanding of the transition periods key to understanding the seasonal cycle of meningitis. These transition periods are termed *monsoon onset*, and *monsoon retreat*. Seasonal migration of the Intertropical Convergence Zone (ITCZ) and the Intertropical

Front (ITF), the later the interface between monsoon and Harmattan winds, control monsoon onset and retreat. The WAM is largely driven by a pressure gradient existing between two centers of action, the South Atlantic High, and the West African Heat Low (WAHL). The relative strength of these centers determines the strength of monsoon winds, and indirectly controls moisture advection onshore. Preferential heating controlled by surface albedo and solar insolation determine the strength and location of the WAHL (Ramel et al. 2006). Drobinski et. al. (2005) points to the orography of North Africa, the Hoggar Massive and Atlas Mountains in particular, as influencers in the deepening of the WAHL in late spring and determining its location centered over the Sahara Desert. North of the mountains, subsidence from the descending branches of the Hadley cell and the WAHL increase the pressure gradient rotating wind direction from the southeast to the northeast. This strengthens WAHL circulation, deepening the low-pressure region. Monsoon "preonset" identifies the data the ITF reaches 15ºN (with the ITF defined as the zero mean zonal wind component at 925mb). This marks the start of the rain season, and the mean date of occurrence is 14 May with a 9.8 day standard deviation. An abrupt transition or "jump" of the ITCZ from 5º to 10ºN indicates monsoon onset, whose mean occurrence is 25 June with a 9 day standard deviation. This corresponds to increasing rainfall and a deepening of the WAHL (Sultan and Janicot, 2003). The mean date of occurrence for WAHL deepening is 20 June, 5 days before the mean date of monsoon jump (Lavaysse et. al. 2009). Sea-surface temperature (SSTs) in the Gulf of Guinea also influence the strength of the cross-equator pressure gradient driving monsoon flow. A precipitation dipole identified by Lough (1986) between the Guinea Coast and the Sahel has been linked to these SSTs by Vizy and Cook (2002), Fontaine and Louvet (2006),

and Caniaux et al. (2011). Northward movement of the ITCZ strengthens the cross-equator southeast trade winds in April, producing Ekman pumping north of the equator lowering SSTs. The region of lower SSTs has been termed the "Atlantic cold tongue" and is well developed during the monsoon season. SST anomalies in the Gulf of Guinea, weaken the cold tongue, increase evaporation, and thus enhance precipitation over the Guinea Coast. Concomitant low-level winds from the Sahara extend further south producing subsidence and suppressed precipitation in the Sahel. Sources of precipitation in West Africa include the tropical Atlantic, 23%, Central Africa, 17%, and precipitation recycling within West Africa 27% (Eltahir and Gong, 1996). Nieto et. al. employed a Lagrangian approach to track sources of moisture in the Sahel and found that during the monsoon, precipitation recycling was the most important. The tropical Atlantic, Central Africa, and the Eastern Mediterranean were the other identified sources. This tropical Atlantic source is controlled by monsoon winds. Lavaysse et. al. (2009) identified several dynamical elements of the WAM that influence regional moisture transport including the African Easterly Jet (AEJ), the Tropical Easterly Jet (TEJ), and African Easterly Waves (AEW). Nicholson (2009) suggests the AEJ and TEJ have a large influence on regional rainfall moisture advection. She termed the region between the jets the "tropical rainbelt". Instability in the region produced by conservation of vorticity promotes convection. Mesoscale convective systems (MCS) responsible for large-scale regional precipitation are transported westward by the AEJ (Mohr and Thorncroft 2006). The location and propagation of AEWs, which help organize MCS are controlled by the strengths of the AEJ and TEJ. The timing and number of AEWs produce the interseasonal variability seen in WAM rainfall (Jackson et al. 2009). The strength of the AEJ centered at 650mb is

controlled by WAHL meridional circulation (Thorncroft and Blackburn 1999). Uplift in the WAHL generates an anticyclone aloft whose easterly circulation strengthens the AEJ. A low-level westerly jet produced by the cross-equator pressure gradient driving monsoon flow is seen in years with high rainfall. This westerly jet is weak or nonexistent in dry years (Nicholson, 2009). Long-term trends in precipitation saw a decrease from 1970 through 1985, and a slow increase from 1985 though the present. Hagos and Cook (2008) have linked this precipitation decrease to increased SSTs in the Indian Ocean. These higher SSTs produced subsidence over the Sahel blocking monsoon-advected moisture from the Atlantic. Further increase in Indian Ocean SSTs have shifted this subsidence westward to the Atlantic, producing the increases in rainfall seen over the past 25 years. Forecasts for future behavior are largely uncertain, with low GCM model agreement. The IPCC AR4 assessment suggests that the precipitation dipole between the Guinea Coast and Sahel will strengthen as SSTs increase in the Gulf of Guinea. This would increase rainfall over the Guinea Coast and decrease rainfall over the Sahel. Findings by Haarsma (2005) who investigated rainfall variability over the Sahel suggest increases in Sahel precipitation. He found a strong link between rainfall and mean sea level pressure (MSLP) over the Sahara. Increasing surface air temperatures suggest that MSLP over the Sahara would strengthen, increasing Sahelian rainfall. Cook and Vizy (2006) looked at CGCMs used by the IPCC and found they did not capture well the precipitation distribution or monsoon dynamics.

1.6 THESIS ORGANIZATION

This understanding of West African climate was used as a basis for modeling the seasonal relative humidity. Additional understanding of the interseasonal variability of relative humidity could provide more informed forecasting of meningitis incidence and improve health resource allocation. Chapter 2 describes the interseasonal variability of relative humidity during the transition periods and the large-scale dynamics driving the transitions. Climate predictors are identified from these large-scale dynamics and used to forecast the relative humidity at several lead-times. Chapter 3 extends these forecasts to meningitis, using direct relative humidity and the identified climate predictors to forecast cases in two periods: the peak and shoulder meningitis seasons. Chapter 4 discusses the results of these forecasts and suggests their application in improving health resource allocation in West Africa.

2 RELATIVE HUMIDITY SEASONAL FORECASTING

The results presented in this chapter will be published in modified form as Broman et. al. 2013: Spatio-Temporal Variability and Predictability of Relative Humidity Over West African Monsoon Region. J. Clim.

2.1 ABSTRACT

Spatial and temporal variability of relative humidity over the Western African Monsoon (WAM) region is investigated. In particular, the variability during the onset and retreat periods of the monsoon is considered. A K-means cluster analysis was performed to identify spatially coherent regions of relative humidity variability during the two periods. The cluster average of the relative humidity provides a robust representative index of the strength and timing of the transition periods between the dry and wet periods. Correlating the cluster indices with large-scale circulation and sea surface temperatures indicate that the land-ocean temperature gradient and the corresponding circulation, tropical Atlantic sea surface temperatures (SSTs), and to a somewhat lesser extent SSTs over the tropical Pacific, all play a role in modulating the timing of the monsoon season relative humidity onset and retreat. These connections to large-scale climate features were also found to be persistent over interseasonal time scales and thus best linear predictive models were developed to enable skillful forecasts of relative humidity during the two periods at 15-75 day lead times. The public health risk due to meningitis epidemics are of grave concern to the population in this region, and these risks are strongly tied to regional humidity levels. Because of this linkage, the understanding

and predictability of relative humidity variability is of use in meningitis epidemic risk mitigation, which motivated this research.

2.2 BACKGROUND AND MOTIVATION

This project focuses on the interaction between climate and disease incidence in eight countries in West Africa: Ghana, Togo, Benin, Nigeria, Chad, Niger, Mali, and Burkina Faso. All or parts of these countries lie within the African 'Meningitis Belt', and whose seasonal weather patterns are controlled by the West African Monsoon (WAM). Limited healthcare networks exist in this region, with international organizations providing logistic and material support for the prevention and treatment of meningococcal meningitis (hereafter referred to as meningitis). This includes the allocation of vaccines to sub-national districts given the incidence of meningitis[1]. Understanding of the interseasonal variability of the WAM system could provide more informed decision-support in allocating healthcare supplies given identified links between meningococcal meningitis epidemics and climate. One of the strongest links identified is with relative humidity, motiving this study. We have investigated the relative humidity during the transitions between the dry and monsoon seasons. The spring transition from dry to monsoon season marks the end of the meningitis season, and the fall transition from monsoon to dry season can influence the start of the proceeding meningitis season.

[1] International Coordinating Group on Vaccine Provision. http://www.who.int/csr/disease/meningococcal/icg/en/

The traditional measure of monsoon variability has been seasonal rainfall. The region experiences periods of low and high rainfall, including the Sahelian drought of the 1970s and 80s. Past investigation has looked at identifying causes of both the annual rainfall cycle and the larger decadal scale patterns. Connections have been made with global sea-surface temperatures, circulation patterns, along with other ocean and land-surface processes including soil moisture.

The WAM is a dominant low-level southwesterly flow affecting sub-Saharan Africa temperature and precipitation patterns. This seasonal flow advects moisture from the Gulf of Guinea and equatorial Atlantic onshore during the boreal summer in sharp contrast to the dry northeasterly Harmattan winds that exist throughout the rest of the year. Monsoon behavior is linked to the seasonal latitudinal migration of the intertropical convergence zone (ITCZ) and the intertropical front (ITF) the latter representing the interface between monsoon winds and Harmatton winds. Eltahir and Gong 1996 investigated the sources of precipitation in West Africa and found the Tropical Atlantic contributes 23%, Central Africa 17%, and precipitation recycling within West African contributes 27%. The Gulf of Guinea source is controlled by the southwest monsoon flow, the Central African source by westerly flows generated by monsoon circulation, and the precipitation recycling by land surface properties. Using a Lagrangian approach, Nieto et al. (2006) tracked the sources of moisture for the Sahel and found that in summer, precipitation recycling over the Sahel was the most important. Other identified sources included the Tropical Atlantic, Central Africa, and the Eastern Mediterranean. For this last source, increased SSTs increased local evaporation and the moisture was advected to the Sahel through low-level transport. Lavaysse et al. (2009) identify several

dynamical elements of the West African Monsoon that represent and influence its behavior including the West African Heat Low (WAHL), the African Easterly Jet (AEJ), the Tropical Easterly Jet (TEJ), and African Easterly Waves (AEW). The pressure gradient between the WAHL and the South Atlantic anticyclone drives the southwesterly monsoon winds. The strength and position of the West African Heat Low (WAHL) is dependent on preferential heating controlled by surface albedo and solar heating conditions (Ramel et al. 2006). These controls also influence the shape of the WAHL that can be more zonally elongated than round in some years (Lavaysse et al. 2009). Work by Drobinski et al. (2005) suggest that the orography of North Africa, the Hoggar Massive and Atlas Mountains in particular, aid in the deepening of the WAHL in late spring and describe its location centered over the Sahara Desert. Subsidence to the north of the mountains from the northern branches of the Hadley cell and the WAHL increase the pressure gradient rotating southeasterly winds to northeasterly winds. This behavior strengthens WAHL circulation, deepening the low pressure region. Monsoon onset as defined by Sultan and Janicot (2003) is split into two phases a "preonset" identified as the date the ITF reaches 15ºN (with the ITF being the zero mean zonal wind component at 925mb). This phase represents the start of the rainy season in the region and the mean date of occurrence is the 14 May with 9.8 day standard deviation. Monsoon onset is defined by an abrupt transition or "jump" of the ITCZ from 5º to 10ºN corresponding with increases in rainfall and a deepening of the heat low. The mean date of occurrence is 25 June with 9 day standard deviation. The deepening of the WAHL occurs on a mean date of 20 June, five days before the mean date of monsoon jump (Lavaysse et al. 2009).

Nicholson (2009) presented a "new look" on WAM dynamics and suggested the importance of the African Easterly Jet (AEJ) and Tropical Easterly Jet (TEJ) to rainfall and moisture advection. She identified the region between the waves as the "tropical rainbelt". Instability resulting from conservation of vorticity promotes convection in this region. The cross-equator pressure gradient driving monsoon flows produces in some years a low-level westerly jet whose strength is strongly correlated with rainfall. A weak pressure gradient and a weak or nonexistent westerly jet occur during dry years and a strong pressure gradient and strong well-defined westerly jet occur during wet years. The AEJ transports mesoscale convective systems (MCS) westward, which are responsible for large-scale precipitation in the region (Mohr and Thorncroft 2006). The speed of the AEJ centered at 650mb is controlled by WAHL meridional circulation (Thorncroft and Blackburn 1999). Uplift in the WAHL generates an anticyclone aloft whose easterly circulation strengthens the AEJ. The strengths of the AEJ and TEJ control the location and propagation of African Easterly Waves (AEW) which help organize MSC (Jackson et al. 2009). The number and timing of AEWs are responsible for the interseasonal variability of WAM rainfall. The strength of the cross-equator pressure gradient has been linked to sea-surface temperatures (SST) in the Gulf of Guinea. Lough (1986) identified a precipitation dipole between the Guinea Coast and the Sahel. Future work by Vizy and Cook (2002), Fontaine and Louvet (2006), and Caniaux et al. (2011) have investigated this dipole and linked it to SST anomalies in the Gulf of Guinea. In April, cross-equator southeast trade winds strengthen as the ITCZ shifts northward. These trades produce Ekman pumping north of the equator lowering SSTs and lead to the formation of the "Atlantic cold tongue". This feature is well developed during the peak of the monsoon.

Positive SST anomalies in the Gulf of Guinea increase evaporation enhancing precipitation over the Guinea Coast. Concomitant low-level winds from the Sahara extends further south leading to subsidence and suppressed precipitation in the Sahel. Modeling studies by Koster et al. (2004) suggest a strong land-atmosphere coupling between soil moisture and precipitation in boreal summer. This supports the precipitation recycling findings mentioned above. Hagos and Cook (2008) explain the decreasing Sahelian rainfall in the 1980s through increased sea-surface temperatures in the Indian Ocean. Warming produced a region of subsidence over the Sahel blocking monsoon-advected moisture from the Atlantic. Continued increases in Indian Ocean SSTs have shifted this zone westward over the Atlantic leading to an increase, though still depressed rainfall over the Sahel. IPCC AR4 Assessment suggests due to the increased SST in the tropics an amplification of the precipitation dipole between the Sahel and Guinea Coast with decreased rainfall over the Sahel and increased rainfall over the Guinea Coast. Haarsma (2005) investigate rainfall variability over the Sahel using climate reanalysis data and found a strong link between rainfall and mean sea-level pressure over the Sahara, the summer location of the WAHL. Increases in surface air temperatures suggest a deepened heat low and increased rainfall over the Sahel. Cook and Vizy (2006) address this uncertainty. There is low model agreement for much of West Africa, and the CGCMs used in the ensemble did not capture well the precipitation distribution or monsoon dynamics.

Coinciding with the West African Monsoon region is the African meningitis belt (Lapeyssonnie 1963) extending through the semi-arid region south of the Sahara. Several studies have indicated a strong link between atmospheric moisture, in the form of relative

humidity or specific humidity, and meningococcal meningitis susceptibility. (Molesworth et al. 2003) classified districts by their seasonal specific humidity profiles found that this classification along with land cover were the best predictors in a meningitis epidemic risk model. This relationship appears robust as studies by Besancenot et al. (1997) in Benin, Yaka et al. (2008) in Niger and Burkina Faso reached similar conclusions. This link between relative humidity and its predictive capability of meningitis risk is corroborated from preliminary analysis shown in Figure 2.1 (Hopson et. al., unpublished).

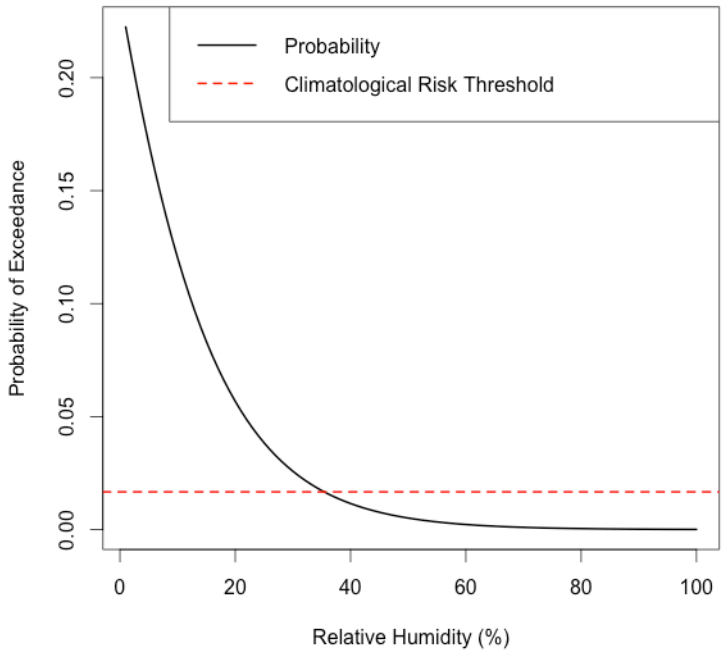

Figure 2.1: Empirical relationship between meningitis epidemic risk and relative humidity. Dashed red line indicates the inherent background risk of epidemic.

This figure indicates an inverse relationship between relative humidity and meningitis epidemic risk. The probability of exceedance is based on the mean relative humidity for the proceeding four weeks at a two-week lag. The red dashed line indicates the inherent background risk of a meningitis epidemic independent of relative humidity. Humidity in the region and more importantly the timing of humidity increase and

decrease are controlled by the WAM system. Thus, understanding monsoon dynamics to better predict monsoon onset and retreat in the context of increasing and decreasing relative humidity would allow better prediction of meningitis epidemic risk. Prior to the development of a conjugate vaccine for NmA meningococcal meningitis the primary method of treating all epidemics of meningococcal meningitis relied on the distribution of a polysaccharide vaccine to regions at risk for epidemics. The motivation was to contain the disease before it spread to surrounding districts. Districts at alert level, 5 cases in 100,000 received the vaccine if surrounding districts had already reached the epidemic level of 10 cases in 100,000. If a district reached the alert level without neighboring a district at the epidemic level, the decision to allocate vaccine was based on vaccine supply and time to the end of meningitis season. This allocation, managed by the *International Coordinating Group on Vaccine Provision* (ICG), is still used to manage epidemics of other meningococcal meningitis serogroups, particularly NmW135. While prior research efforts largely focused on monsoon seasonal rainfall and its variability, this study is motivated by the need to provide better tools to help mitigate and manage the meningitis risk. To this end, here we propose to investigate the interannual variability and predictability of relative humidity during the onset and retreat phase of the monsoon season, which coincides with the retreat and onset season of meningitis risk. This research offers a unique and complementary perspective to the existing body of literature. The paper is organized as follows. The study region and data sets used are first described followed by the methods. Next, results from climate diagnostics and predictability are presented followed by results from predictive models and concluding with summary and discussion of the results. An understanding of the interseasonal variability of relative

humidity could provide better prediction of the end of the meningitis season allowing for more informed decisions while allocating vaccine and healthcare resources. This study aims to investigate this interseasonal variability. Weather station data for the time period 1973 – 2012 were used along with climate reanalysis data to identify potential predictors of relative humidity behavior. Identified predictors were used to develop predictive models of relative humidity.

2.3 DATA AND STUDY REGION

The study region encompasses countries falling within both the meningitis belt and WAM region and includes Mali, Burkina Faso, Togo, Benin, Chad, and Cameroon as shown in Figure 2.2.

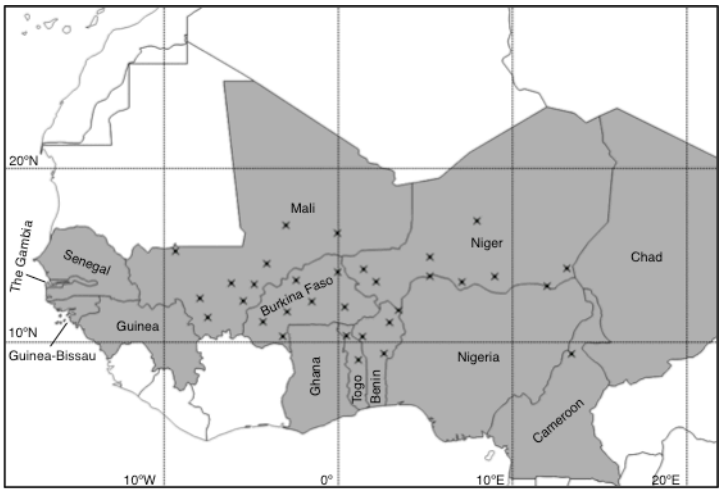

Figure 2.2: Study region showing weather station locations. The shading indicates the countries lying within the 'Meningitis Belt' as defined by the U.S. CDC[2]

[2] U.S. Centers for Disease Control and Prevention Meningococcal Disease / http://wwwnc.cdc.gov/travel/yellowbook/2012/chapter-3-infectious-diseases-related-to-travel/meningococcal-disease

Daily calculated relative humidity data from the Global Historical Climatology Network (GHCN) were obtained through NOAAs' Climate Data Online (CDO) portal[3]. The World Meteorological Organization (WMO) maintains the GHCN network, constructed from data collected by national meteorological services. These data were obtained for 32 stations (Figure 2.2) within the study region with at least 90% coverage over 1973 – 2012. Investigations of large-scale climate variability used the gridded NCEP/NCAR reanalysis data (Kalnay et al. 1996) and gridded Kaplan sea-surface temperature reconstructions (Kaplan et al. 1998).

2.4 METHODS

Monsoon dynamics were examined through variations in relative humidity in three periods defined as: monsoon onset, 15 May – 30 June; monsoon peak, 30 June – 15 September; and monsoon retreat, 15 September – 15 October. These periods are similar to those selected by the African Monsoon Multidisciplinary Analysis for their Special Observing Period (Redelsperger et al. 2006). For each period mean relative humidity was computed for each station and year providing a forty-year time series. The seasonal relative humidity climatologies for three stations within the study area are shown in Figure 2.3.

[3] NOAA CDO: http://www.ncdc.noaa.gov/cdo-web/

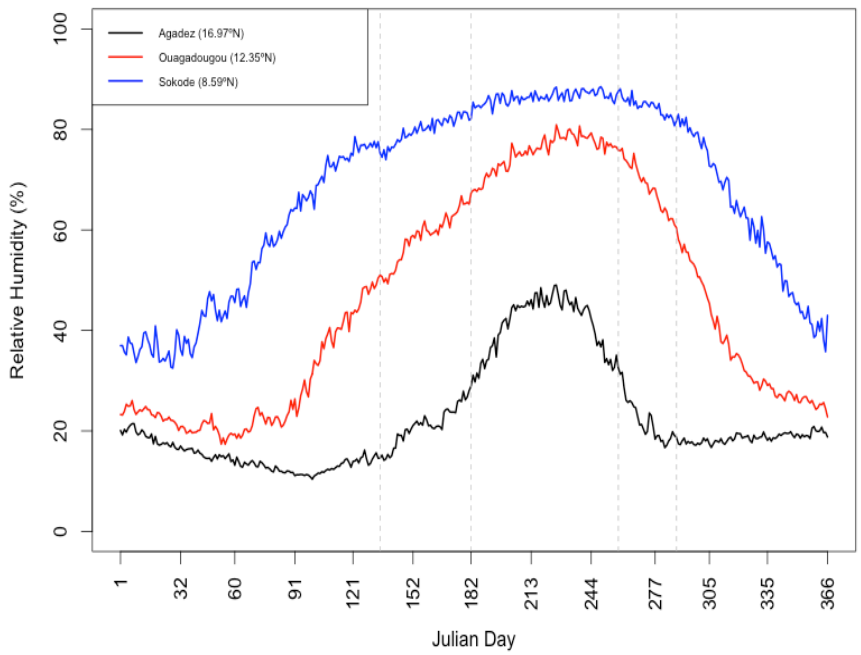

Figure 2.3: Mean seasonal relative humidity profiles for three locations. Vertical lines show the onset and retreat periods

A K-means cluster analysis (Scott and Knott 1974) was performed separately for each period to identify the spatial variability and coherence of relative humidity. In this, locations are grouped in homogeneous clusters such that within cluster variability is minimum and between-cluster variability is maximum. A cluster index was then computed by averaging the relative humidity across stations in each cluster, to produce representative time series for each spatial region (cluster).

The cluster indices of relative humidity for each period were then correlated with a suite of contemporaneous global circulation fields including sea level pressure, zonal and meridional winds at 925mb, 600mb and 200mb, sensible and latent heat fluxes using the reanalysis data set; and with global Kaplan SST. The resulting spatial correlation maps were used to identify the large-scale ocean and atmospheric mechanism that drive the variability of relative humidity in the study region. Composite maps of selected fields

corresponding to ‘high’ and ‘low’ relative humidity years were also produced to understand the physical links to extremes in relative humidity. To explore the predictability of relative humidity in the region lagged correlation maps were produced with circulation fields and SST – in that the relative humidity in a period is correlated with large-scale fields from preceding time periods. For example, the onset period relative humidity index is correlated with large-scale fields from preceding April, March, February and January. Regions of high correlation values are used to develop potential predictors by spatially averaging over this region. The predictors are then used in a generalized linear modeling framework to develop predictive models at different lead times. This method has been widely used in application to western US streamflow forecasting (Grantz et al. 2005; Regonda et al. 2006; Bracken et al. 2010).

2.5 RESULTS AND DISCUSSION

2.5.1 Spatial Variability

A K-means cluster analysis was performed on the average relative humidity at all the locations for the onset, peak and retreat periods. The data is grouped into several clusters and for each the within cluster variance is computed. The number of clusters where this variance drops off and stabilizes is the optimal number selected. Figure 2.4 shows the within cluster variance versus number of clusters for the three periods.

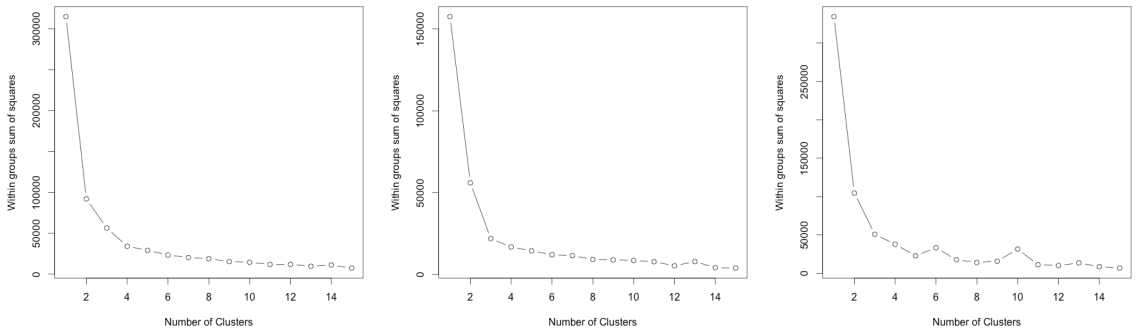

(a) (b) (c)

Figure 2.4: K-means cluster diagnostics for (a) Onset, (b) Peak, and (c) Retreat periods

It can be seen that the variance drops off around three clusters in all the periods, indicating that higher number of clusters is unlikely to result in distinct homogeneous clusters. The spatial locations of the clusters in the three periods are shown in Figure 2.5.

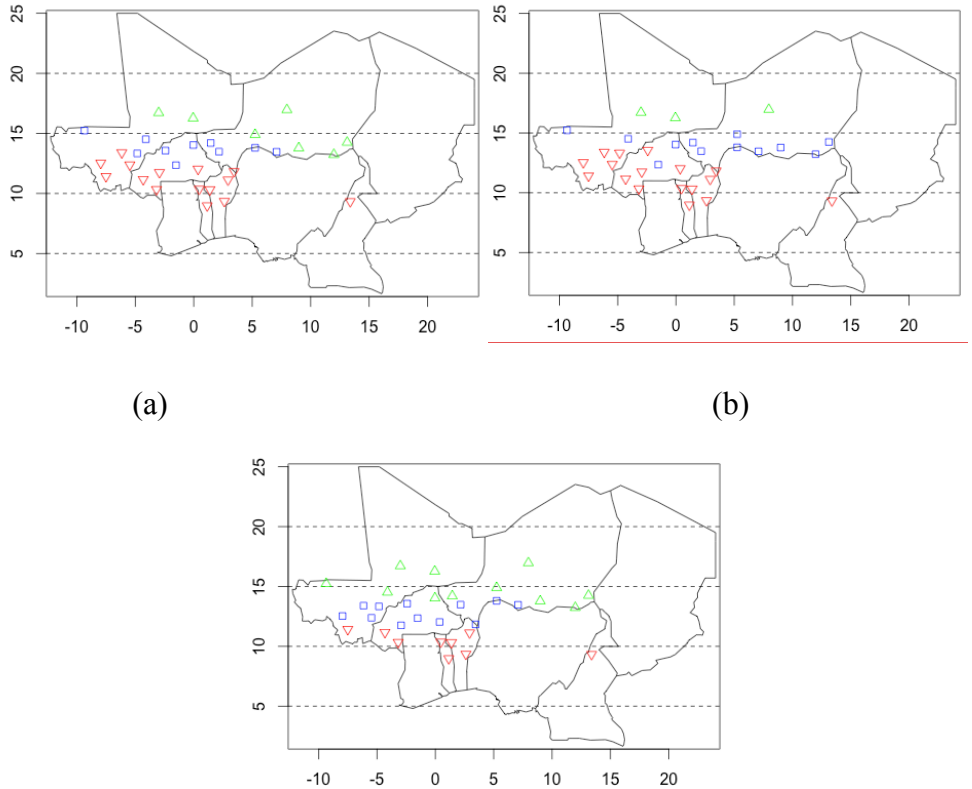

(a) (b)

(c)

Figure 2.5: K-means station clusters for onset (a), and retreat (b) periods

In all the periods the three clusters exhibit a clear north-south spatial pattern with stations grouped along east-west. The north-south stratification is consistent with movement of the ITCZ through the monsoon season and the background strong climatological humidity gradient in the region. The stations in the three clusters for the onset and retreat periods are almost identical with slight differences only at the cluster boundaries. This similarity can be attributed to the onset northward and retreat southward movement of the ITCZ being fairly uniform. Slight differences between the onset ITCZ transition, with its 'jump' from ~10º to 15º N in June, and the retreat ITCZ transition, with its smooth transition explain the slight variations. During the peak season the ITCZ is within 10º to 15º N latitudes, hence the diffusion of cluster boundaries. Several of the stations found in the northern cluster during onset and retreat are found in the middle cluster during peak monsoon period. Only the three most northern stations, Tombouctou, Mali, Gao, Mali and Agadez, Niger, all located close or within the Sahara remain in the northern cluster in all three periods. The relative humidity is then averaged over the stations in each cluster to obtain cluster indices for the three periods and a time series their standardized values are shown in Figure 2.6.

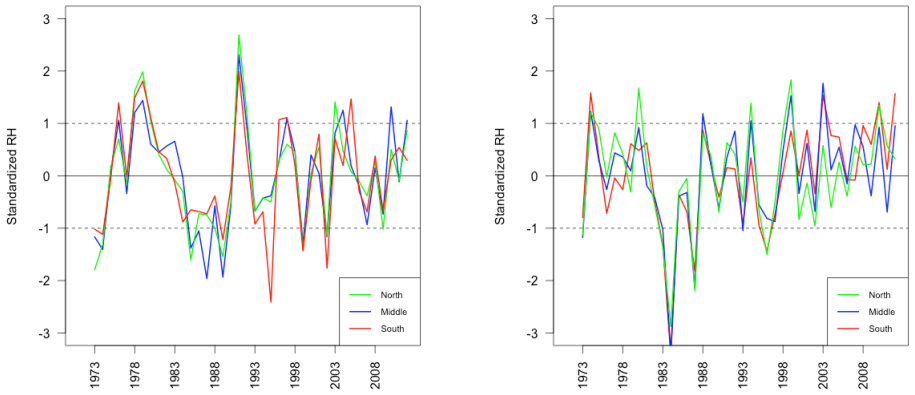

(a)

(b)

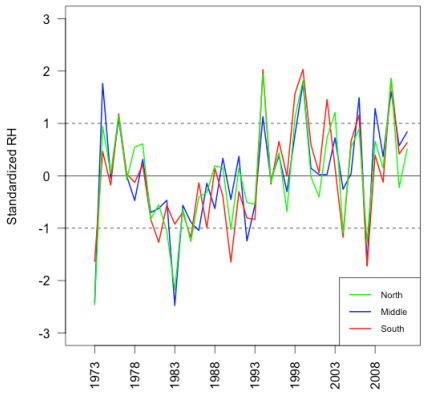

(c)

Figure 2.6: Standardized relative humidity timeseries for onset (a), peak (b), and retreat (c)

Although the actual relative humidity varies between each cluster, the figure shows that they all have similar temporal variability (not shown). All three periods exhibit an upward trend from ~1988 through 2012, which corresponds to the upward trend found in the Sahel rainfall index (Janowiak 1988). The Sahel drought is also clearly visible in Figure 4 during the peak period, with a strong dip in relative humidity in the mid 1980s.

2.5.2 Links to Large-Scale Climate

In order to understand the drivers of year-to-year variability of the relative humidity, the cluster indices were correlated with large-scale climate fields of the concurrent period. In particular, we selected five variables to correlate – surface temperature, mean sea level pressure, zonal winds, meridional winds, and global SST. The sea level pressure and average winds were selected to capture the links to atmospheric circulation such as the African Easterly Jet and Tropical Easterly Jet; while the surface temperatures and SSTs are for large-scale oceanic features such as ENSO, Atlantic equatorial patterns etc. Figure 2.7 shows the correlations with each of the variables' fields for the three clusters during the onset period.

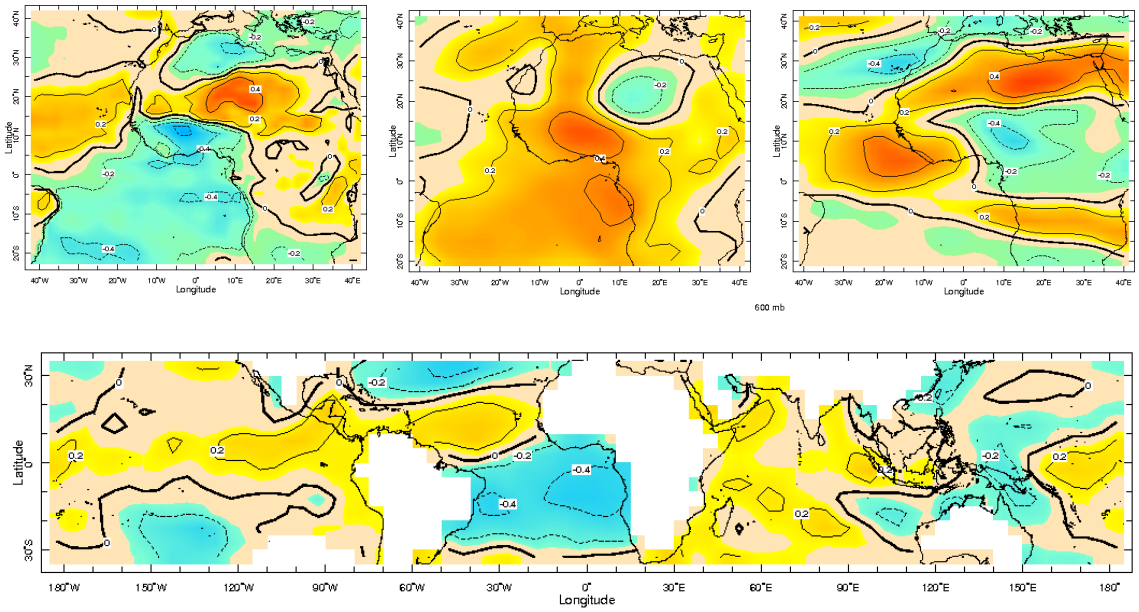

(a)

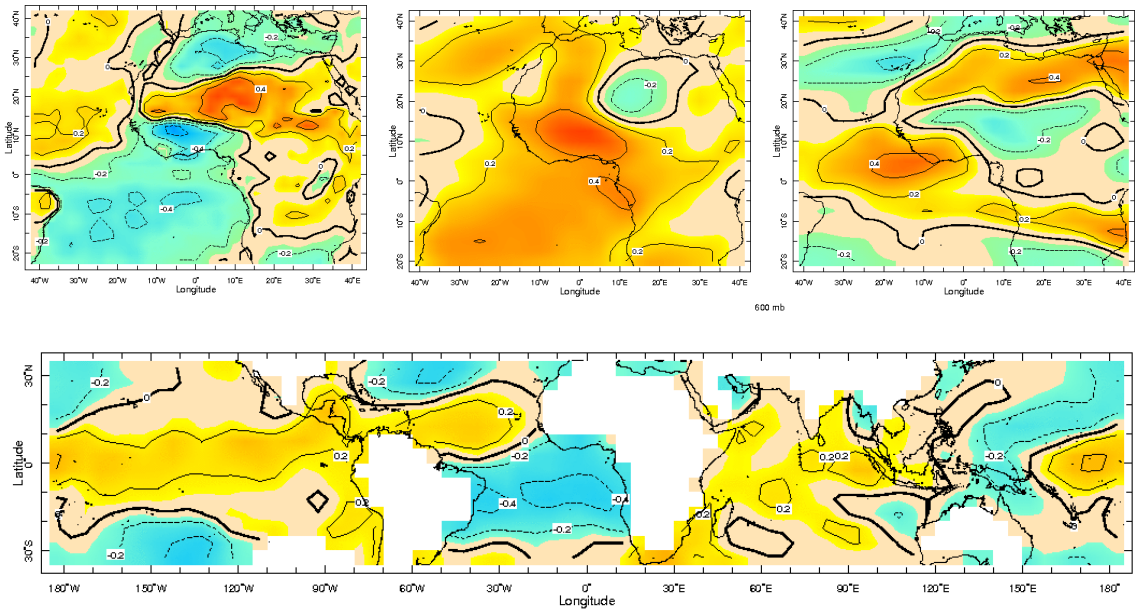

(b)

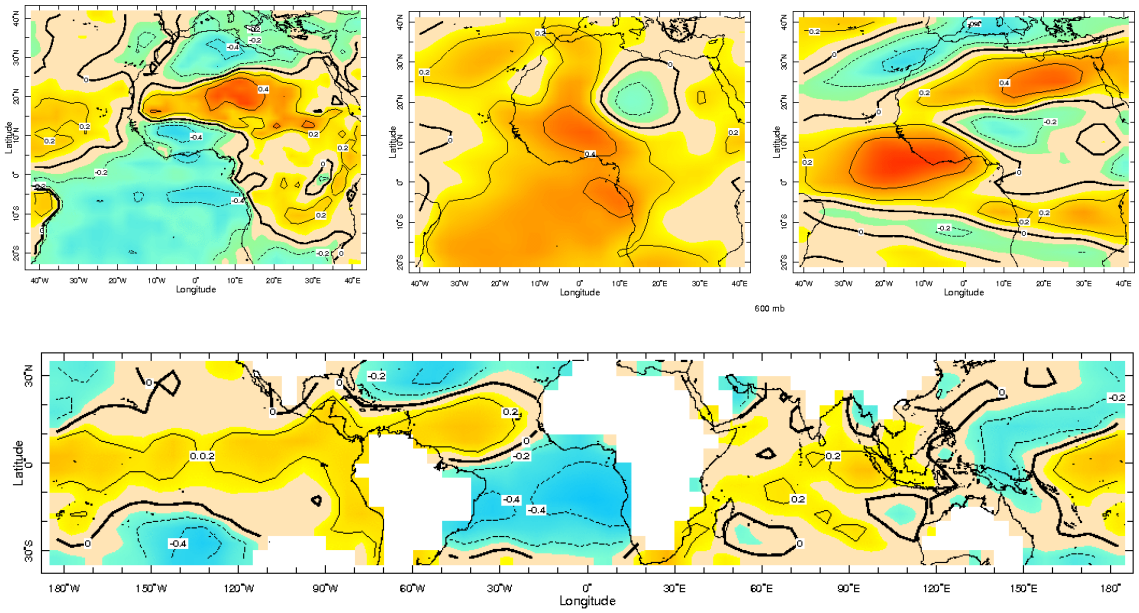

(c)

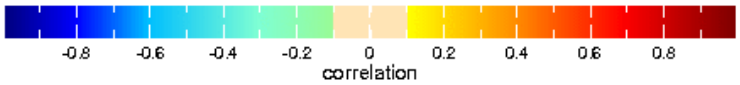

Figure 2.7: Onset north (a), middle (b), and south (c) cluster correlation maps with surface temperature (left), mean sea-level pressure (middle), 600mb zonal winds (right), and global sea-surface temperature (bottom).

In the onset period, all three clusters have positive correlation with the Sahara desert surface temperature, and negative correlation with the Guinea Coast surface temperature. This negative correlation extends to Gulf of Guinea and South Atlantic sea-surface temperatures. This dipole pattern of positive correlation over land coupled with negative correlation to the south and over the ocean is indicative of a strong land-ocean thermal gradient, a key component of the monsoon. The correlation pattern with sea level pressure is opposite and consistent – over the warmer land of the Sahara, the approximate location of West African Heat Low, the pressure is low leading to a negative correlation, with the opposite holding true to the south and along the Guinea Coast. With SSTs, a diploe pattern is apparent in the tropical Atlantic Ocean, with positive correlation in the northern tropical Atlantic and negative to the south. This dipole is well known as influencing the rainfall over North Eastern Brazil and Western Africa (Nobre and Srukla, 1996). In the Pacific there is a weak positive correlation in the central and eastern tropical Pacific and a weak negative correlation in the west – reminiscent of ENSO pattern. The correlation patterns are remarkably similar for the middle and southern clusters (Figures 2.7 b-c).

Retreat period correlations are shown in Figure 2.8.

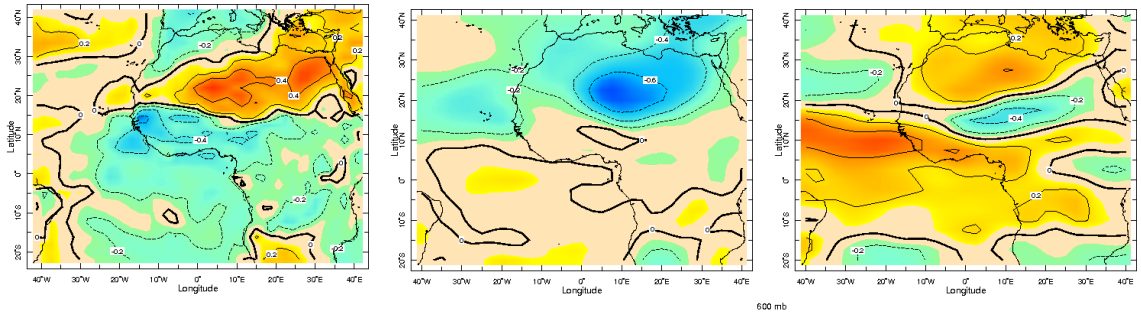

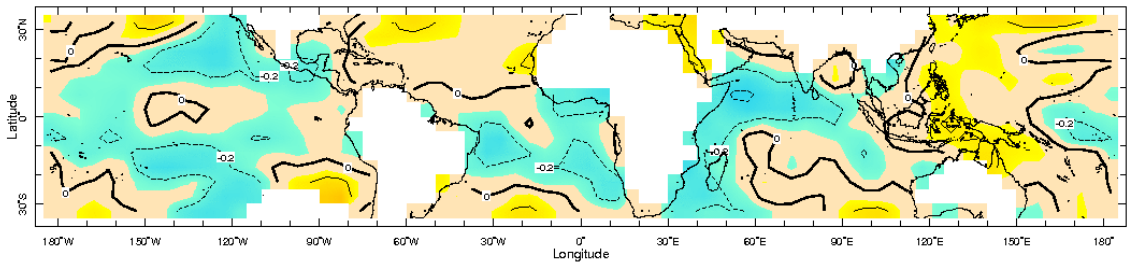
Latitude
Longitude

(a)

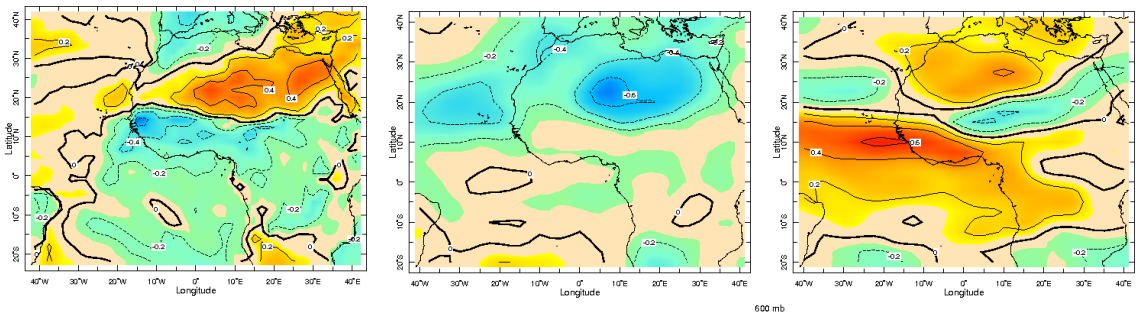
Latitude
Longitude
600 mb

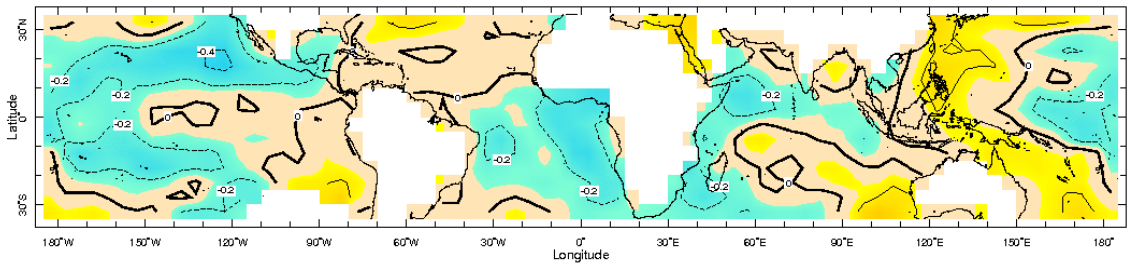
Latitude
Longitude

(b)

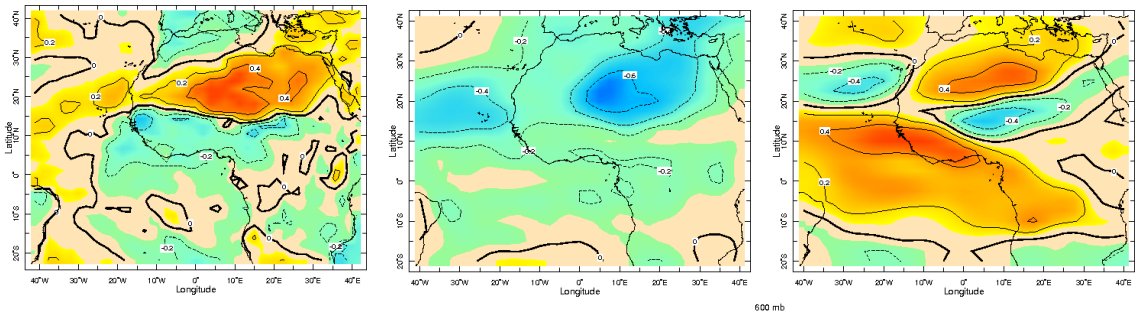
Latitude
Longitude
600 mb

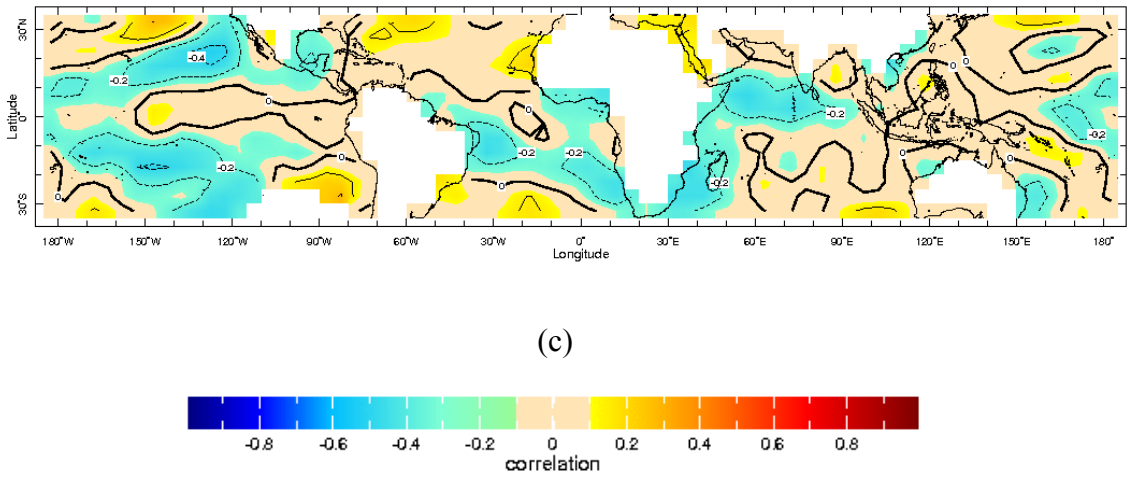

(c)

Figure 2.8: Retreat north (a), middle (b), and south (c) cluster correlation maps with surface temperature (left), mean sea-level pressure (middle), 600mb zonal winds (right), and global sea-surface temperature (bottom).

For all clusters, the land temperature correlations show positive correlation over western Africa similar to that in the onset period (Figure 2.7), but a negative correlation to the south that is much weaker. The correlations with SLP also mirror this (Figure 2.8). The correlation pattern with 600mb zonal winds shows a stronger negative correlation over the region of the African Easterly Jet, also the location of the ITCZ (Figure 2.8). This is stronger and coherent than its counterpart in the onset period (Figure 2.7). This is due to the fact the most of the activity is on the land as the monsoon period starts to wind down. The correlation with SST is much weaker than that observed during onset – this is consistent with the fact that during the end of the monsoon season the tropical Atlantic SST gradient is much diminished as the ITCZ is in the northern hemisphere and on its way south – and the gradient gets established in fall.

Composite analysis was performed to investigate the large-scale climate features responsible for relative humidity extremes. For this, we selected years with ‘high’ and

'low' relative humidity, outside of one standard deviation away from the mean, for a given period and maps of climate variables averaged over these years are produced. We show representative composite maps for the south cluster for onset (Figure 2.9) and retreat periods (Figure 2.10).

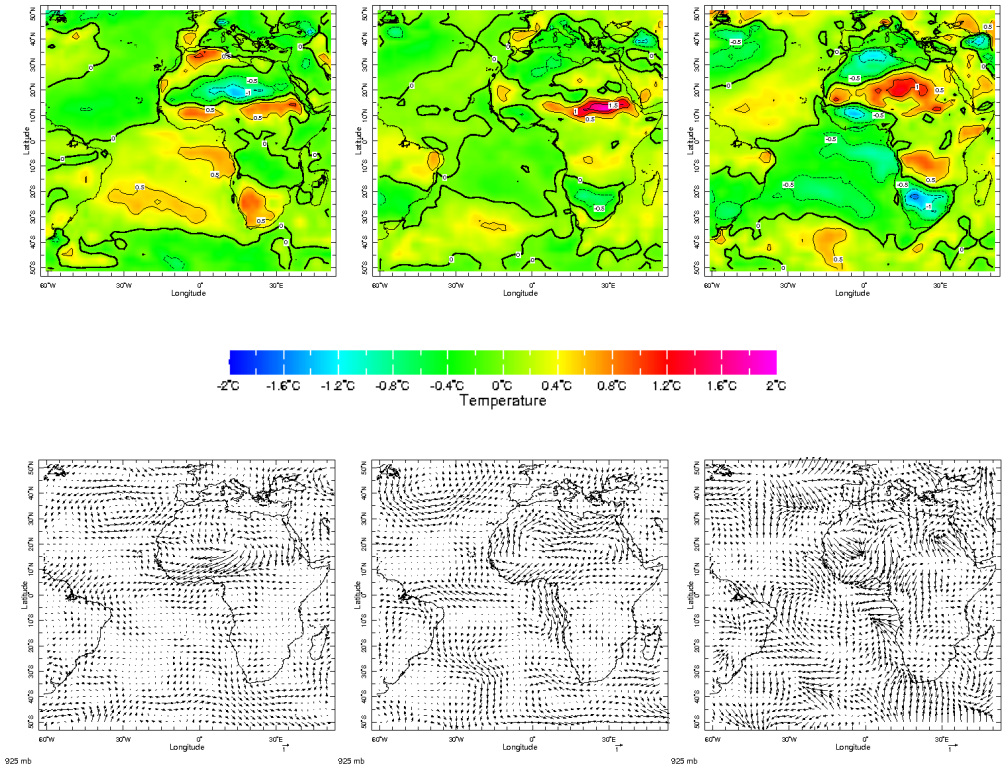

Figure 2.9: Onset south cluster composite plots showing surface temperature (top) and 925mb winds (bottom) for low years (left), high years (middle) and the low – high years (right)

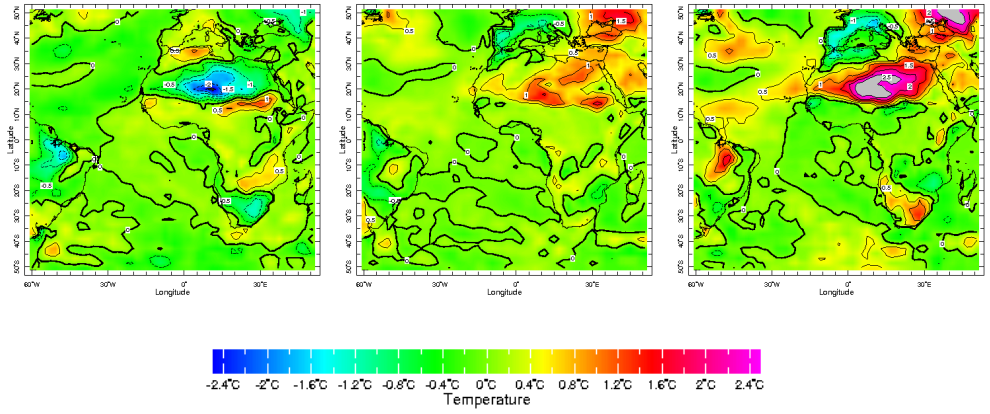

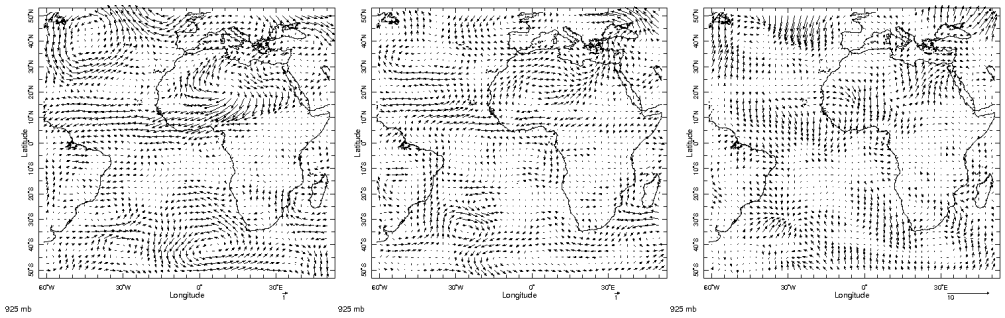

Figure 2.10: Retreat south cluster composite plots showing surface temperature (top) and 925mb winds (bottom) for low years (left), high years (middle) and the low – high years (right)

Composite maps of surface temperature for low years for onset period (Figure 2.9) shows a cooler land and warmer ocean, indicative of a weaker land-ocean temperature gradient - the winds show an anomalously southerly flow consistent with the temperature pattern. During high years the patterns are reversed, although the warming over land is a bit stronger than during low years, also the wind pattern is weaker than that of the low years. The asymmetry in the relationship during low and high years indicates nonlinearity in the relationship and the difference maps in the same figure show this. These patterns are similar during retreat (Figure 2.10) and also for other clusters (see Appendix A).

2.5.3 Predictability

As mentioned in the motivation, relative humidity during onset and withdrawal periods are important for the retreat and onset of meningitis season, respectively - thus, the ability to predict the relative humidity during these periods is of specific interest. To

this end, predictors and forecasting models are developed understand the predictability and the potential long-lead skill. To identify predictors, the cluster time indices are correlated with large-scale climate variables from preceding periods. We selected three lead times to issue forecasts for the onset – i.e., the first of Mar, Apr and May, giving a lead time of 75, 45 and 15 day lead times, respectively. Figure 2.11 shows the correlation between the onset index of the southern cluster with January climate variables.

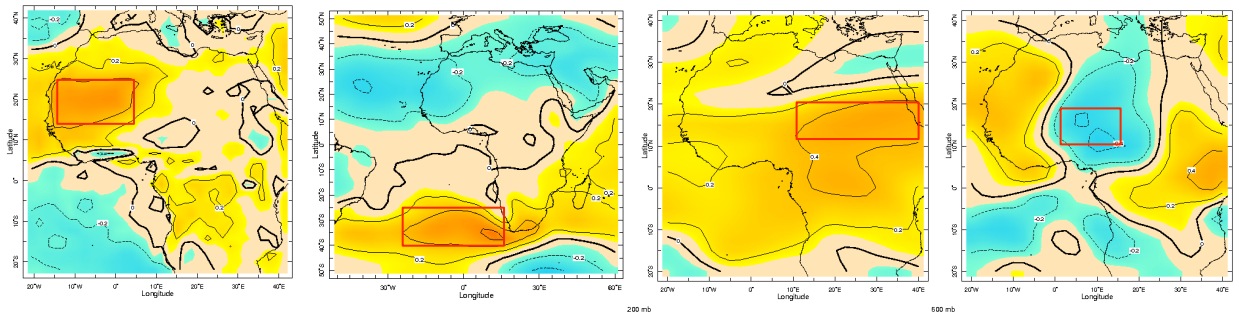

(a) (b) (c) (d)

Figure 2.11: Onset South Cluster correlation plots with January (a) Surface Temperature, (b) MSLP, (c) 200mb Zonal Winds, (d) 600mb Meridional Winds

It can be noticed that the correlation patters with surface temperature, sea level pressure and winds are similar to the correlation patterns seen during the concurrent period (Figure 2.7) – indicating that the large scale patterns are persistent and thus, lending potential predictability. The boxes indicate regions of high absolute correlation. Correlations with climate variables on May 1 (Figure 2.12) also show similar patterns.

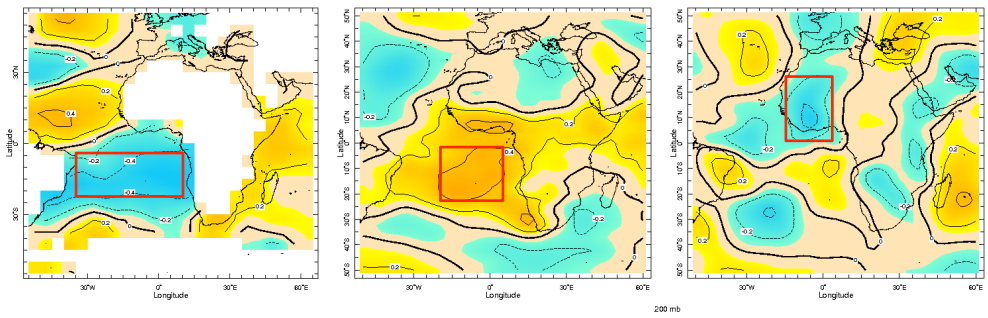

(a) (b) (c)

Figure 2.12: Onset South Cluster correlation plots with April (a) SST, (b) MSLP, (c) 200mb Zonal Winds

Regions with high absolute correlation, approximately 0.4 or above in these maps are identified and the corresponding climate variables averaged over these regions provide potential predictors. Figures 2.13 and 2.14 show the correlation plots for June and August used to select retreat predictors.

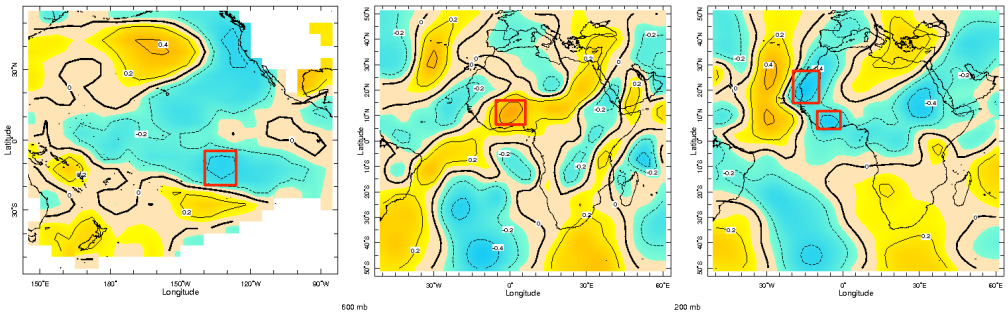

(a) (b) (c)

Figure 2.13: Retreat South Cluster correlation plots with June (a) SST, (b) 600mb Zonal Winds, (c) 200mb Zonal Winds

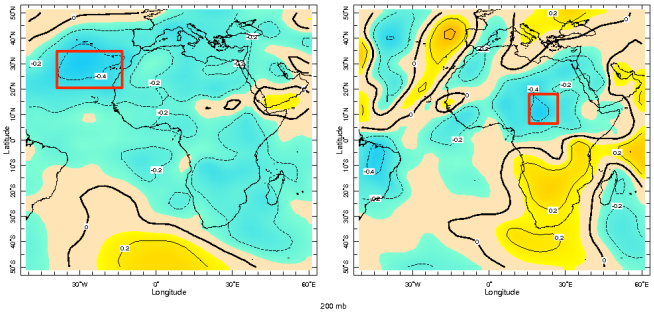

(a) (b)

Figure 2.14: Retreat South Cluster correlation plots with August (a) MSLP, (b) 200mb Zonal Winds

The red boxes in Figures 2.11 – 2.14 show the regions used to generate these predictors. The list of predictors identified for the different lead times and for onset and withdrawal are shown in Tables 2.1 and 2.2.

Table 2.1: Onset Period model predictors

Predictor	Cluster	Parameter	Time Period	X1 (º)	X2 (º)	Y1 (º)	Y2 (º)
oaj01	South	Surf. Temp.	January	-16	4	14	25
oaj02	South	MSLP	January	-24	17	-40	-26
oaj03	South	600V	January	2	16	8	18
oaj04	South	200U	January	11	40	12	21
oaf01	South	SST	February	-60	-35	5	17
oaf02	South	SST	February	-20	8	-20	-8
oam01	South	SST	March	-24	12	-24	-10
oam02	South	MSLP	March	-28	-3	-38	-14
oaa01	South	SST	April	-35	10	-22	-4
oaa02	South	MSLP	April	-20	5	-23	-2
oaa03	South	200V	April	-8	-2	-15	6
obj01	Middle	Surf. Temp.	January	-16	6	14	25
obj02	Middle	MSLP	January	-20	20	-40	-26
obj03	Middle	925V	January	-11	-1	8	30
obj04	Middle	600V	January	4	16	7	20
obj05	Middle	600V	January	-20	-4	18	28

obj06	Middle	200V	January	10	22	20	30
obj07	Middle	200U	January	16	41	11	18
obf01	Middle	SST	February	-35	10	-20	-10
obm01	Middle	SST	March	-40	10	-22	-10
obm02	Middle	MSLP	March	-31	-2	-33	-15
oba01	Middle	MSLP	April	-22	3	-20	-5
oba02	Middle	MSLP	April	-12	8	4	10
ocj01	North	Surf. Temp.	January	-16	10	13	26
ocj02	North	MSLP	January	-48	-4	16	32
ocj03	North	MSLP	January	-20	16	-40	-30
ocj04	North	925V	January	-11	-1	8	30
ocj05	North	600V	January	6	16	8	18
ocj06	North	200V	January	13	25	20	30
ocj07	North	925U	January	-18	-10	10	27
ocj08	North	600U	January	-20	-4	22	27
ocf01	North	600V	February	-14	-2	1	9
ocm01	North	SST	March	-40	-10	-25	-10
oca01	North	SST	April	-30	-10	-18	-7
oca02	North	MSLP	April	-13	10	4	11
oca03	North	MSLP	April	-22	8	-23	-13

Table 2.2: Retreat Period model predictors

Predictor	Cluster	Parameter	Time Period	X1 (º)	X2 (º)	Y1 (º)	Y2 (º)
ral01	South	Surf. Temp.	July	16	24	-2	6
ral02	South	SST	July	-137	-113	-19	-9
ral03	South	SST	July	-40	-18	-31	-20
ran01	South	SST	June	-126	-138	-16	-7
ran02	South	600V	June	-4	4	7	15
ran03	South	200V	June	-9	-2	5	11
ran04	South	200V	June	-19	-9	16	28
ram01	South	MSLP	May	-80	-48	-15	-10
ram02	South	925V	May	-9	-1	17	28
ram03	South	925V	May	-30	-13	-1	10
ram04	South	200V	May	-19	-8	10	30
ram05	South	925U	May	-12	0	9	13
ram06	South	925U	May	-16	-2	16	20

raa01	South	MSLP	August	-42	-11	21	35
raa02	South	200V	August	16	24	7	20
rbm01	Middle	925V	May	-12	0	16	24
rbm02	Middle	200V	May	-22	-13	18	28
rbm03	Middle	925U	May	-16	-2	16	20
rbm04	Middle	600U	May	2	14	19	24
rbn01	Middle	200U	June	-25	-10	-20	-5
rbl01	South	MSLP	July	-40	-24	-28	-18
rbl02	Middle	200U	July	-20	3	13	20
rba01	Middle	200V	August	10	25	19	29
rba02	Middle	600U	August	11	28	15	21
rcm01	North	925V	May	-12	0	15	24
rcm02	North	600U	May	-16	-2	14	19
rcn01	North	600V	June	-4	4	6	15
rcn02	North	200U	June	-20	10	-17	-3
rcl01	North	MSLP	July	-45	-15	-30	-13
rcl02	North	200U	July	-22	-4	11	21
rca01	North	Surf. Temp.	August	-14	2	12	19
rca02	North	Surf. Temp.	August	12	23	6	15
rca03	North	Surf. Temp.	August	-39	-20	24	38
rca04	North	600U	August	16	28	16	21

A ‘best’ linear model was fitted for each lead time and for each period of interest. A generalized linear modeling (GLM) approach was selected, as it is flexible and general. In GLM (McCullagh and Nelder 1989), the response or the dependent variable *Y*, can be assumed to be a realization from any distribution in the exponential family with a set of parameter**s**. A smooth and invertible link function transforms the conditional expectation of *Y* to the set of predictors.

$$G(\mathrm{E}(Y)) = \eta = f(\boldsymbol{X}) + \varepsilon = \boldsymbol{X}\boldsymbol{\beta}^{\boldsymbol{T}} + \varepsilon \qquad (1)$$

G(·) is the link function, $\boldsymbol{X}$ is the set of predictors or independent variables, E(Y) is the expected value of the response variable and ε is the error. In a linear model the function G(·)is identity. Depending on the assumed distribution of Y there exist appropriate link functions (see McCullagh and Nelder 1989). The model parameters, $\boldsymbol{\beta}$, are estimated using an iterated weighted least squares method that maximizes the likelihood function as opposed to an ordinary least squares method in linear modeling. Here we fit a linear regression model – i.e., normality of variable Y and identity link function.

Models were fitted with different combination of predictors and for each the AIC was calculated. The best model was selected as the one that minimizes the Akaike Information Criteria (AIC). The AIC is calculated as follows:

$$AIC = 2k - 2L \tag{2}$$

where L is the logarithm of the likelihood function of the model with the predictor subset under consideration and k, is the number of parameters to be estimated in this model and it serves as a penalty. The AIC penalizes models with more number of predictors thus favoring parsimony. For the selected best model two performance metrics were computed – fitting R^2 which explains the variance captured by the model and cross validated R^2 in this, an observation is dropped, the model fitted using the rest of the observations and the dropped pointed is predicted. This indicates the variance explained by the model in a 'predictive' mode. To further assess the predictive capability of the models we performed leave 10% out cross-validation – in this 10% of observations are dropped at random and they are predicted using model fitted on the rest of the data. A final measure of model fit, root mean squared error (RMSE) is computed using the same drop 10% method as above. This is repeated 1,000 times and the median RMSE is selected, providing a robust assessment of the predictive skill.

The best model (or set of best predictors) based on AIC selects 2-3 predictors for almost all the lead times except for a few cases during withdrawal where it selects 4 predictors. The predictor sets and model skill scores can be found in Tables 2.3 (onset period) and 2.4 (retreat period).

Table 2.3: Onset Period GLM model statistics and predictor sets. Predictors from Table 2.1 above.

Onset South Cluster							
Lead Time	Predict Date	Model Fit R^2	CV Model Fit R^2	Median RMSE	Predictor 1	Predictor 2	Predictor 3
75 Days	1-Mar	0.442	0.352	2.279	oaj01	oaj02	n/a
45 Days	1-Apr	0.472	0.378	2.07	oaf01	oaf02	oam02
15 Days	1-May	0.471	0.365	1.987	oaa02	oaa03	oam02
Onset Middle Cluster							
Lead Time	Predict Date	Model Fit R^2	CV Model Fit R^2	Median RMSE	Predictor 1	Predictor 2	Predictor 3
75 Days	1-Mar	0.523	0.45	2.639	obj01	objo2	n/a
45 Days	1-Apr	0.32	0.238	2.681	obf01	obm02	n/a
15 Days	1-May	0.367	0.276	2.601	oba02	obm02	n/a
Onset North Cluster							
Lead Time	Predict Date	Model Fit R^2	CV Model Fit R^2	Median RMSE	Predictor 1	Predictor 2	Predictor 3
75 Days	1-Mar	0.582	0.491	2.101	ocf01	ocj01	ocj03
45 Days	1-Apr	0.301	0.186	2.693	ocf01	ocm01	n/a
15 Days	1-May	0.345	0.229	2.571	oca03	ocm01	n/a

Table 2.4: Retreat Period GLM model statistics and predictor sets. Predictors from Table 2.2 above.

Retreat South Cluster								
Lead Time	Predict Date	Model Fit R^2	CV Model Fit R^2	Median RMSE	Predictor 1	Predictor 2	Predictor 3	Predictor 4
75 Days	1-Jul	0.596	0.468	1.729	ram02	ram03	ran02	n/a
45 Days	1-Aug	0.521	0.36	1.84	ran03	ran04	ral01	ral02
15 Days	1-Sep	0.488	0.358	1.732	ral03	raa01	raa02	n/a
Retreat Middle Cluster								
Lead Time	Predict Date	Model Fit R^2	CV Model Fit R^2	Median RMSE	Predictor 1	Predictor 2	Predictor 3	Predictor 4
75 Days	1-Jul	0.74	0.631	3.181	rbm01	rbm03	rbm04	rbn01
45 Days	1-Aug	0.359	0.24	4.881	rbn01	rbl01	n/a	n/a
15 Days	1-Sep	0.534	0.302	4.719	rbl01	rba01	rba02	n/a
Retreat North Cluster								
Lead Time	Predict Date	Model Fit R^2	CV Model Fit R^2	Median RMSE	Predictor 1	Predictor 2	Predictor 3	Predictor 4
75 Days	1-Jul	0.7	0.573	2.709	rcm01	rcm02	rcn01	rcn02
45 Days	1-Aug	0.534	0.415	3.305	rcn01	rcn02	rcl01	n/a
15 Days	1-Sep	0.511	0.401	3.392	rcl01	rca03	rca04	n/a

Furthermore, predictor sets were remarkably consistent between the south and middle clusters, notable exceptions being the 1 April south cluster model containing February North Atlantic SST, and the 1 May south cluster model containing April Guinea Coast 200mb meridional winds. Guinea Coast 600mb meridional winds were found in the north cluster replacing South Atlantic MSLP in the 1 March and 1 April models. Plots of observed, estimated and cross-validated estimates of south onset cluster relative humidity are shown in Figure 2.15.

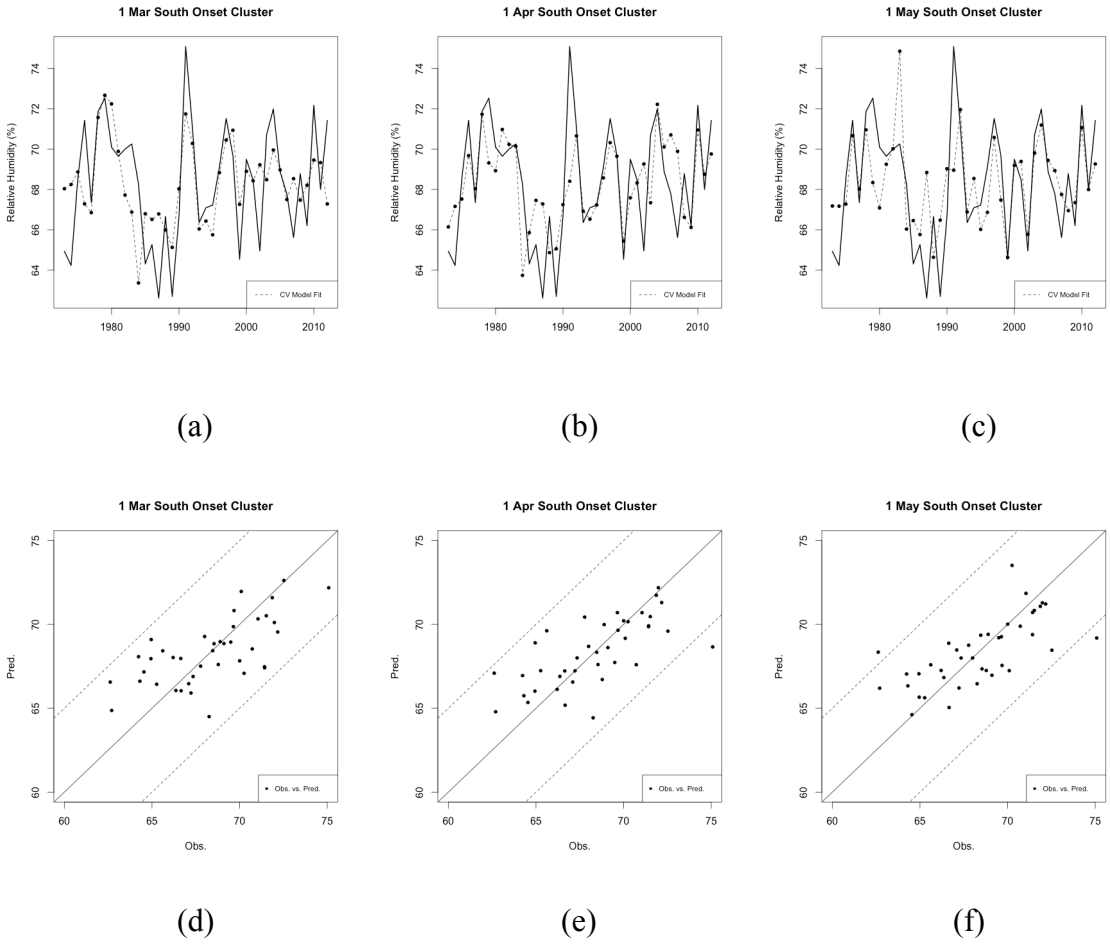

Figure 2.15: Onset South Cluster GLM models showing direct fit values and cross-validated values. (a), (b), and (c) show the cross-validated model fits for 1 March, 1 April, and 1 May. (d), (e), and (f) show the predicted vs. observed direct fit values for the 1 March, 1 April, and 1 May models (solid line indicates 1:1, dashed lines show ±5%)

It can be seen that the model estimates and predicts the values very well at all the lead times. The corresponding scatter plots of the observations and estimates (Figure 2.15 d-f) shows that almost all of the predictions fall within the 5% of the observed values (dotted lines indicate ±5% lines). It is interesting to note that the models exhibit good skill at all lead times, especially at 74-day lead time – as can be seen by the R^2 cross validated R^2 in Tables 2.3 and 2.4.

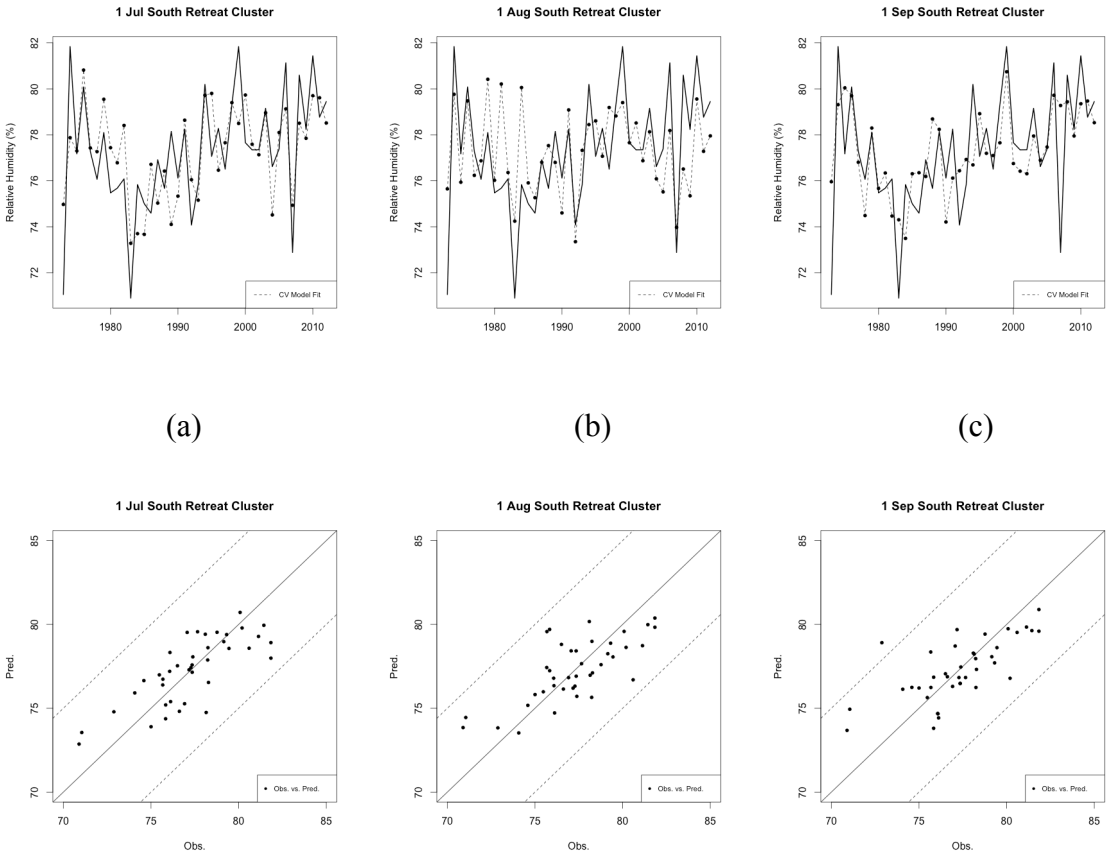

Figure 2.16: Retreat South Cluster GLM models showing direct fit values and cross-validated values. (a), (b), and (c) show the cross-validated model fits for 1 March, 1 April, and 1 May. (d), (e), and (f) show the predicted vs. observed direct fit values for the 1 March, 1 April, and 1 May models (solid line indicates 1:1, dashed lines show ±5%)

Forecasts of retreat period relative humidity also show good skill at all lead times including long lead. The retreat period model predictor sets are more varied; South Atlantic MSLP is a predictor for the middle and north clusters, but is not seen in the south cluster (Table 2.4). Both the south and north models contain predictors from the North Atlantic, MSLP, and SST respectively. Land surface-atmosphere interactions are responsible for the majority of the predictors, with Guinea Coast 925mb meridional winds, central Africa 600mb and 200mb winds, and central Africa surface temperature

showing up in the predictor sets. There are no other common predictors found between the models. Model and cross-validated estimates capture the observed variability very well and but one estimate fall within 5% of the observed values (Figure 2.16).

2.6 SUMMARY

The model results indicate skill in predicting relative humidity from climate variables. The predictions provide the mean relative humidity for the period of interest, which can inform an earlier or later end (or start) to the meningitis season. The best parameter sets for the models indicate that the strengths of the WAHL and South Atlantic anticyclone are the largest controls on relative humidity during monsoon onset. Secondary controls include the Gulf of Guinea SSTs, which influence the local MSLP and winds, and modify the cross-equator pressure gradient responsible for monsoon flow. Another secondary influence is the strength of the North Atlantic anticyclone, which along with the WAHL direct the strength of the hot, dry Harmattan winds from the northeast. These secondary influences appear to be responsible for much of the intercluster variability. Combined they have a large influence on the location of the Intertropical Front (ITF), the boundary between monsoon and Harmattan flows. During monsoon retreat, the strength of the South Atlantic anticyclone remains important, but surface – atmospheric interactions become the secondary controls. There is a lot of variability surrounding the predictors identified for each model; given the complexity of these interactions, become more difficult. This knowledge offers the *International Coordinating Group* a better understanding of the start and end of the meningitis season

which can provide a more informed decision making process while allocating vaccine in the region.

3 MENINGOCOCCAL MENINGITIS INCIDENCE FORECASTING

3.1 ABSTRACT

Meningococcal meningitis is endemic to Sub-Saharan West Africa and the region often sees widespread epidemics during the dry season. Incidence has been linked to environmental factors including relative humidity and this study attempts to use these links to forecast meningitis incidence in Nigeria, Chad, Benin, and Togo. Here we employed Poisson regression within a Generalized Linear Modeling framework to forecast incidences in the region using relative humidity and climate variables as predictors. We obtained very good skills at forecasting weekly meningitis incidence at lead times of 4, 8, and 12 weeks in the above four countries. Skillful forecasting of incidence could provide the international community managing meningitis outbreaks with additional decision-making tools allowing for better allocation of resources, better response times, and ultimately better disease prevention.

3.2 BACKGROUND AND MOTIVATION

Inland West Africa lies within the African 'meningitis belt' as defined by Lapeyssonnie (1963), a region where meningococcal meningitis (referred to hereafter as meningitis) is endemic. The belt experiences frequent epidemics, occurring every 7-14 years. *Neisseria meningitidis*, a bacterium, is the primary cause of meningitis, and is found in several serogroups. The 'A' serogroup (Nm A) is responsible for 80 – 85% of the cases in sub-Saharan Africa (WHO Fact Sheet Nº141), with the 'W135' serogroup (Nm W135) responsible for a majority of the remainder. The *International Coordinating Group for Vaccine Provision* (ICG) manages current disease mitigation efforts. As its name suggests, the ICG is primarily responsible for appropriating and distributing vaccine to the region. The ICG was established in 1997 following major meningitis outbreaks in 1995 and 1996 and is a partnership between the World Health Organization (WHO), Médecins Sans Frontières (MSF) and the International Federation of the Red

Cross and Red Crescent Societies. The ICG collaborates with technical partners including the U.S. Centers for Disease Control and Prevention. The decision-making structure of the ICG for mitigation efforts is outlined on the 22 September 2000 issue of *Weekly epidemiological record*, published by WHO (see Table 3.1).

Table 3.1: ICG meningitis monitoring and treatment strategy (from *Weekly epidemiological record,* 22 September, 2000, WHO)

	Population	
Intervention	> 30 000	< 30 000
Alert threshold / Seuil d'alerte ● Inform authorities / Informer les autorités ● Investigate / Enquêter ● Confirm / Confirmer ● Treat cases / Traiter les cas ● Strengthen surveillance / Renforcer la surveillance ● Prepare / Préparer	● 5 cases per 100 000 inhabitants per week / 5 cas pour 100 000 habitants par semaine	● 2 cases in 1 week / 2 cas en 1 semaine *Or / Ou* ● An increase in the number of cases compared to previous non-epidemic years / Une augmentation du nombre de cas par rapport aux années non épidémiques précédentes
Epidemic threshold / Seuil épidémique ● Mass vaccination / Vaccination de masse ● Distribute treatment to health centres / Distribuer traitements aux centres de santé ● Treat according to epidemic protocol / Prise en charge selon le protocole épidémique ● Inform the public / Informer la population	*If (1) no epidemic for 3 years and vaccination coverage <80% or (2) alert threshold crossed early in the dry season*[b] */* *Si 1) pas d'épidémie depuis 3 ans et couverture vaccinale <80% ou 2) seuil d'alerte franchi tôt dans la saison sèche*[b] ● 10 cases per 100 000 inhabitants per week / 10 cas pour 100 000 habitants par semaine *Other situations / Autres situations* ● 15 cases per 100 000 inhabitants per week / 15 cas pour 100 000 habitants par semaine	● 5 cases in 1 week */* 5 cas en 1 semaine *Or / Ou* ● Doubling of the number of cases in a 3-week period[c] / Doublement des cas sur une période de 3 semaines[c] *Or / Ou* ● Other situations should be studied on a case-by-case basis[b, d] Les autres situations doivent être étudiées au cas par cas[b, d]
	If there is an epidemic in a neighbouring area / En cas d'épidémie dans une zone proche ● the alert threshold becomes the epidemic threshold / Le seuil d'alerte devient le seuil épidémique	

[a] Recommendation of the Consensus meeting on detection of meningitis epidemics in Africa, Paris, 20 June 2000. – Recommandation de la Réunion de consensus sur la détection des épidémies de méningite en Afrique, Paris, le 20 juin 2000.
[b] Early in the dry season: before March. Other epidemic risk factor that may be considered: high population density. – Tôt dans la saison sèche: avant mars. Autre facteur de risque épidémique qui peut être pris en considération: forte densité de population.
[c] For example: *week 1*: 1 case; *week 2*: 2 cases; *week 3*: 4 cases. – Par exemple, *semaine 1* : 1 cas; *semaine 2*: 2 cas; *semaine 3*: 4 cas.
[d] For mass gatherings, refugees and displaced persons, 2 confirmed cases in 1 week are enough to vaccinate the population. – Pour les regroupements de populations, réfugiés et personnes déplacées, 2 cas confirmés en 1 semaine suffisent pour vacciner la population.

Incidence rate thresholds trigger reactive vaccination using a bivalent Nm A/C polysaccharide vaccine or a trivalent Nm A/C/W135 polysaccharide vaccine. A minimum of one week is needed to deploy resources to the district. Full immunological response takes roughly a week following the 1-2 weeks required for vaccination itself. For reactive campaigns to have an effect, vaccination needs to begin before peak incidence occurs. Lewis et. al. (2001) found the sensitivity and specificity of different thresholds using a

sub-district case data for Mali. The change in epidemic threshold from 15 to 10 cases per 100,000 provided roughly an additional week for vaccination. Forecasts of meningitis cases at longer lead times could provide the ICG with even greater additional time to respond to epidemics. For each week delay in vaccination, there is a 3-8% drop in the number of cases prevented (Lewis et. al. 2001).

Environmental factors have long been thought to influence meningitis incidence. Molesworth et al. (2003) compared historical cases of meningitis by district to a classification of environmental factors based on their seasonal cycle. Absolute humidity along with landcover provided the most robust prediction meningitis cases. Thomas et. al. (2006) used environmental factors to predict the annual incidence anomaly of meningitis by district in a study region including parts of Burkina Faso, Niger, Mali, and Togo. The best predictors of the incidence anomaly, found from annual cases between September and August, were August and January rainfall anomalies, and October and April dust anomalies. The strongest relationship when classified by landcover existed in savannah regions, with a linear R^2 value of 0.433. For all landcover types the R^2 value was 0.38. This model did not account for the effect of vaccination, underreporting of cases, and relied on satellite derived climate data, but still provided robust prediction of meningitis case anomalies. Perhaps the strongest demonstrated link between meningitis and environmental factors has been in identifying the start and end of the meningitis season. Sultan et. al (2005) investigated the start of the meningitis season, comparing it to the strength of the Harmattan winds. The seasonal start of season was strongly related to the week with highest wind speed at 1000mb ($R^2 = 0.85$) based on 9 years of data. Similar finding have been demonstrated by researchers focusing in smaller regions, including Besancenot et al. (1997) in Benin, Yaka et al. (2008) in Niger and Burkina Faso.

A conceptual model of meningitis epidemic occurrence was presented by Muller et. al. (2010) and is shown in Figure 3.1.

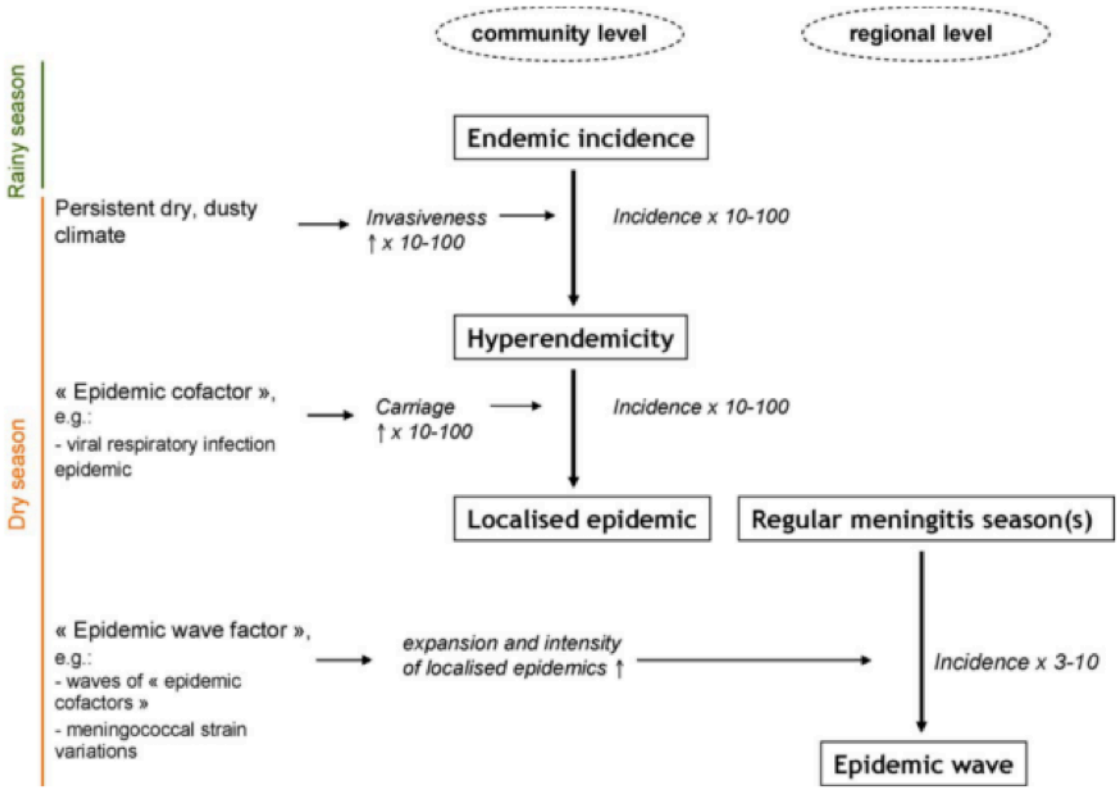

Figure 3.1: Conceptual meningitis model from Mueller et. al. (2010)

The model attempts to explain the large seasonal variation in meningitis incidence at the community and regional levels. In this model, environmental factors are responsible for a 10-100-fold increase in incidence, from an endemic to a hyperendemic state, brought about by a change to a dry dusty climate. Co-factors like upper respiratory infection, which reduces a body's mucosal defenses in the nose and throat provide conditions that encourage epidemics, with incidence increasing again 10-100-fold above the hyperendemic level. Large-scale prevalence of these cofactors and / or variation in meningitis strains produce regional epidemics: those that have historically occurred every 7 – 14 years in the 'Meningitis Belt'.

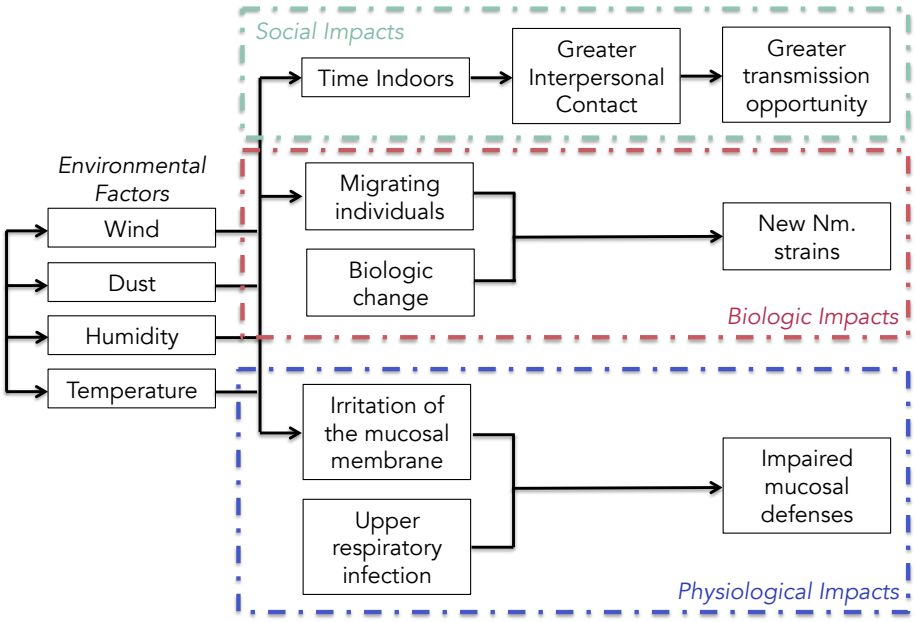

Figure 3.2: New Conceptual model of meningitis incidence

Figure 3.2 shows our conceptual model of meningitis incidence, identifying three classes of impacts: social, biologic, and physiological. We have made no attempt to quantify the relative impacts of each of the drivers, only to indicate their existence.

Environmental factors, wind, dust, humidity, and temperature, influence meningitis incidence in a number of ways. Socially, conditions during the dry season encourage individuals to spend more time indoors. As meningitis is transmitted person to person, this greater interpersonal contact offers more opportunity for disease transmission. Carriage rates of the same serogroup were higher for immediate family than for contacts outside the home suggesting that this increased opportunity does in fact result in higher transmission (Greenwood et. al. 1978; Hassan-King et. al. 1988; Gugnani et. al. 1989; Cheesbrough et. al. 1995; Boisier and Djibo 2006; Trotter and Greenwood 2007).

Direct physiological effects of low humidity, high temperature, and dust can irritate the mucosal membrane. This irritation, or upper respiratory infection can lead to impaired mucosal defenses, providing increased pathways into the body for meningitis. Asymptomatic carriage of meningitis is common and this pharyngeal carriage can induce natural immunity (Trotter and Greenwood, 2007). Kremastinov et. al. (1999) suggest this immunity can be caused by carriage of unencapsulated Nm (non-groupable - NG). Mueller et. al. (2008) examined the carriage of Nm NG and found it increases with humidity, from a rate of 1.6% in February to a rate of 8.6% in May / June. Carriage of virulent (encapsulated) meningitis remained constant at a rate of ~ 1.5%. The variation of Nm NG with humidity and the non-variation of virulent meningitis suggest that the ratio of the two could influence meningitis incidence.

Figure 3.2 above suggests that environmental factors, both direct and indirect, have a large influence on meningitis incidence. In Broman et. al. 2013 we investigated the interseasonal variability of one of these environmental factors, relative humidity, during monsoon onset and monsoon retreat. We showed skill in predicting this variability from climate variables and in this paper use both relative humidity and these climate variables to predict meningitis incidence.

Given our success in predicting relative humidity at long lead times, we looked to extend this prediction to meningitis incidence. Relative humidity, the identified climate predictors of relative humidity from Broman et. al. (2013), and prior meningitis incidence are used to predict weekly incidence of meningitis at lead times of 4, 8, and 12 weeks, useful for planning mitigation strategies. The data and basic diagnostics are first presented followed by the prediction method and validation. Results from application to incidence data from the four countries and discussion conclude the paper.

3.3 DATA AND DIAGNOSTICS

Three data sets are used - meningitis incidence; relative humidity from meteorological stations and large-scale climate data. The meningitis case data for a 5-7 year period spanning 2005 – 2012, were provided by the World Health Organization These data contains weekly case counts for four countries, Togo, Benin, Nigeria, and Chad which

are collected from sub-national districts and aggregated each week. The data is sparse in time as can be seen in Figure 3.3 that shows the percentage of districts reporting meningitis cases each week. Only weeks with at least 50% reporting were used in this analysis.

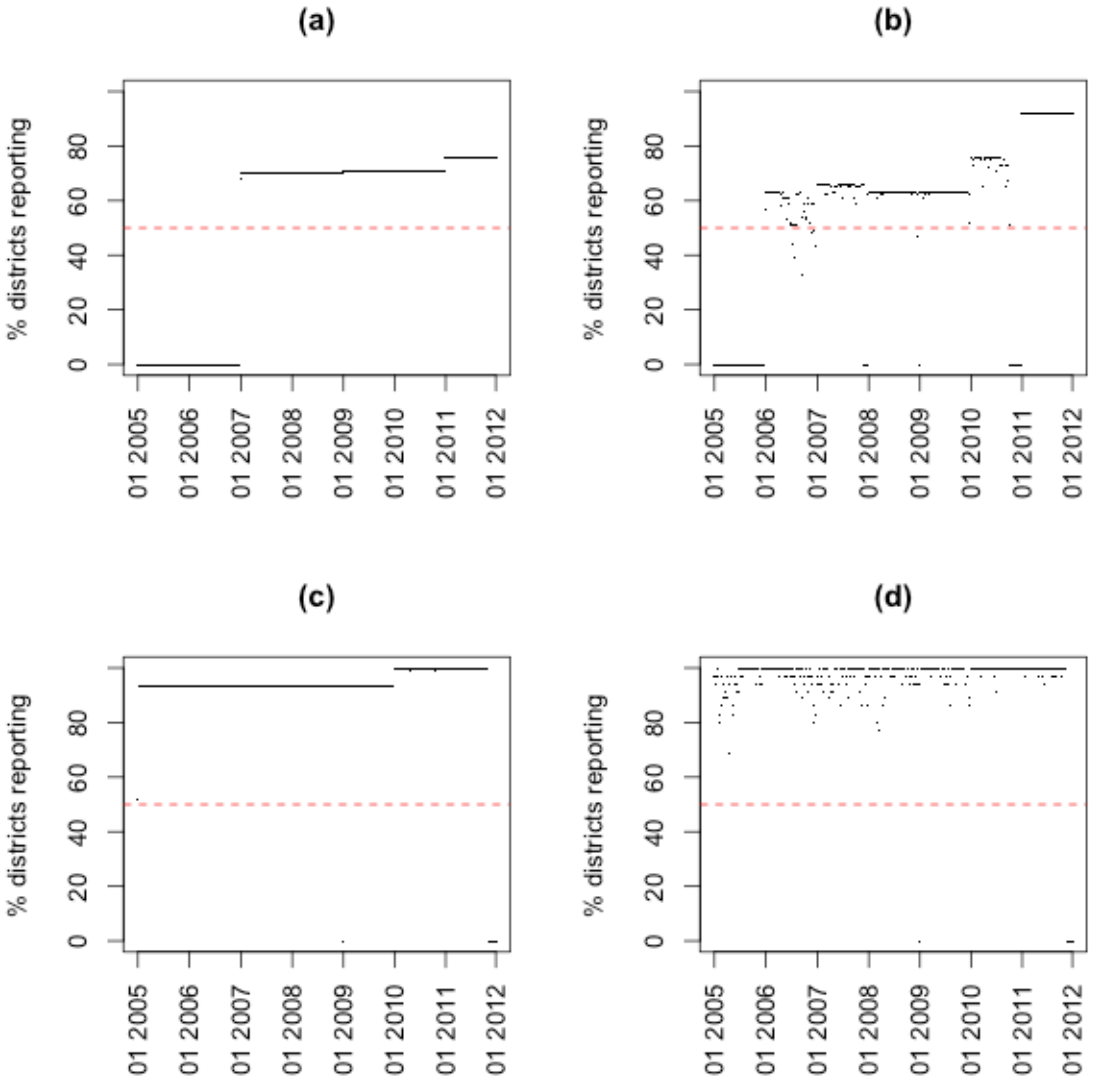

Figure 3.3: Meningitis case reports by week showing the percentage of districts within a country reporting for Nigeria (a), Chad (b), Benin (c), and Togo (d). The horizontal red line indicates 50%.

In order to identify the seasonal variability of meningitis incidences and to focus our analysis on the periods of importance, weekly average meningitis incidences (i.e., weekly climatology) were computed and shown in Figure 3.4 for Nigeria, Chad, and Togo + Benin combined. Two periods of interest are apparent: peak meningitis case season from weeks 1 to 13, and shoulder meningitis case season from weeks 14 to 20 (roughly 1 January to 31 March and 1 April to 20 May), indicated by the dashed boxes – these periods are defined as P1 and P2, respectively. The peak season follows the withdrawal period (Sep 15 – Oct 15) of the West African Monsoon and the shoulder season precedes the monsoon onset period (May 15 – Jun 30). Weekly data from these two periods were used in forecasting, described later. Nigeria and Chad have higher meningitis cases due to their bigger population. Benin and Togo have similar meningitis case climatologies and they are small countries that are neighbors. Therefore we decided to combine these two together for the forecasting analysis described later.

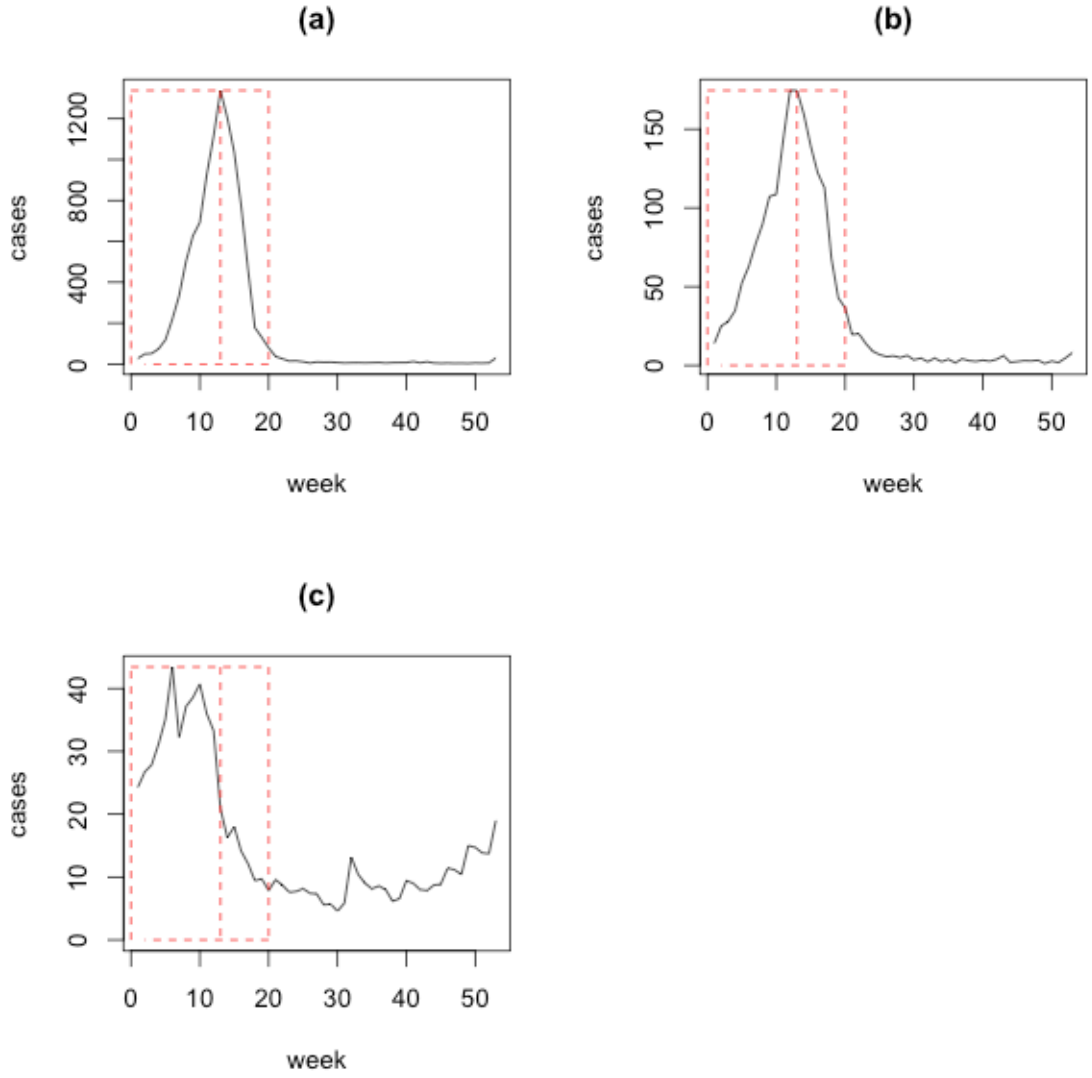

Figure 3.4: Mean weekly meningitis cases for Nigeria (a), Chad (b), Benin (c), and Togo (d). Dashed boxes indicate the peak meningitis period (left) and the shoulder meningitis period (right).

The World Meteorological Organization's Global Historical Climatology Network (GHCN) provided daily calculated relative humidity data. This network is a compilation of data from national meteorological services. In Chapter 2 we identified homogeneous clusters of stations from this network by their relative humidity during the monsoon onset and retreat periods using K-means clustering technique shown in Figure

3.5. Relative humidity was averaged across the stations in each cluster to develop 'cluster index' representative of each cluster.

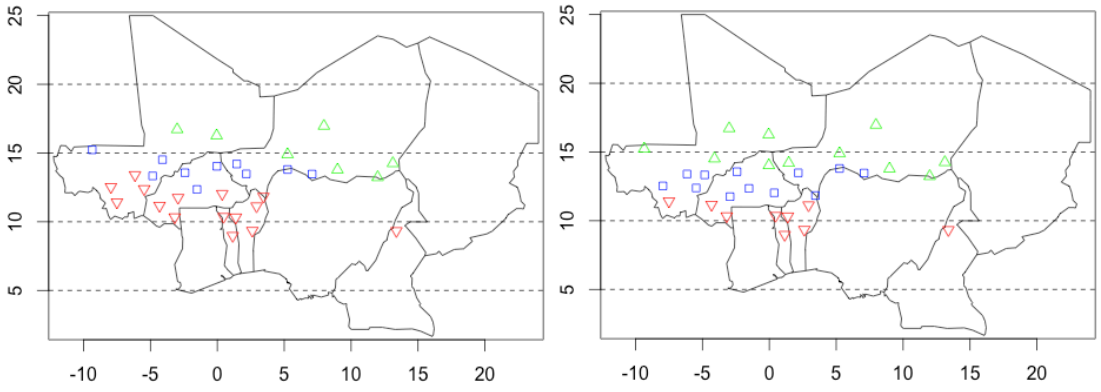

Figure 3.5: K-means identified station clusters for 15 May – 30 June relative humidity (a) and 15 September – 15 October relative humidity

The monsoon retreat period relative humidity is an indicator of residual moisture that will be present during period P1, while the onset season relative humidity impacts the timing and number of meningitis cases. Figure 3.6 shows the weekly time series of the cluster relative humidity indices during periods P1 and P2.

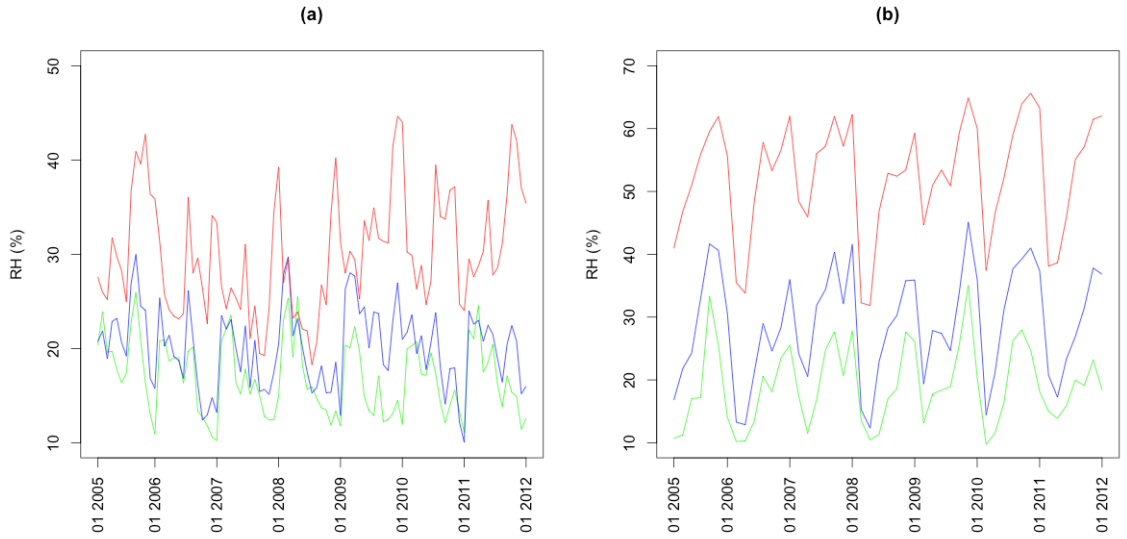

Figure 3.6: Cluster Index relative humidity time series showing north (green), middle (blue), and red (south) for weeks in peak meningitis (P1) period (a) and shoulder meningitis (P2) period (b)

The weekly cluster index relative humidity time series were correlated with weekly meningitis case counts at several lags for each country and are shown in Figure 3.7. It can be seen that there is a strong negative correlation between relative humidity and meningitis case counts, as is widely understood. As shown in our conceptual model, lower relative humidity leads to increased incidence in a number of ways, and this figure illustrates this relationship. Furthermore, the correlation is highest during 0-4 week lags.

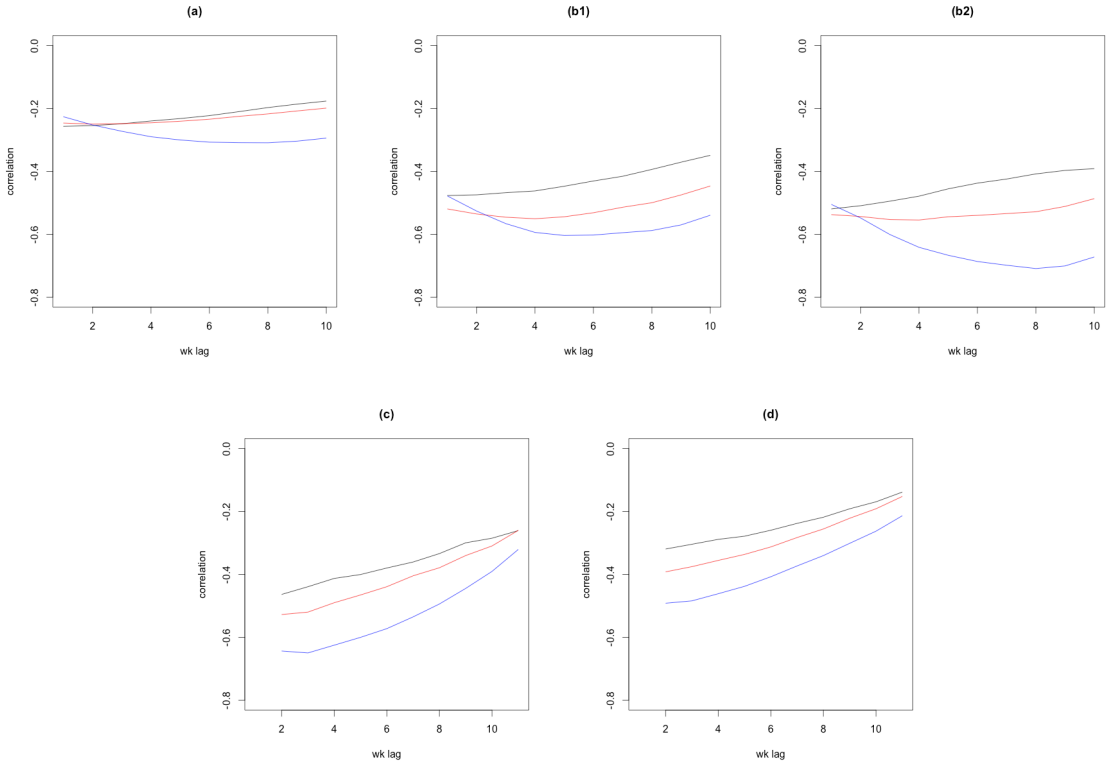

Figure 3.7: Correlation between peak period meningitis case counts and weekly lagged relative humidity for Nigeria (a), Chad (b1 – b2), Benin (c), and Togo (d). Black is north cluster RH, red is middle cluster RH, and blue is south cluster RH.

3.4 FORECAST METHODOLOGY

The Generalized Linear Modeling (GLM) framework (McCullagh and Nelder, 1989) is applied in this study for modeling and forecasting meningiris cases. The

implementation was done within R (2.15.2)[4]. Below we provide a brief description of the model and refer the readers to this and other references.

3.4.1 Model

GLM provides a statistical framework for modeling variables of different types (continuous, discrete, categorical, etc.). The assumption in GLM is that the response variable Y is realized from a distribution in the exponential family which is flexible to model a range of discrete and continuous distributions. A specified link function relates the expected value of Y to a set of predictors (McCullagh and Nelder, 1989).

$$G(E(_{ii})) = X_i\beta^T + e_i \quad \text{for i = 1, 2, …, N} \tag{1}$$

$G(\cdot)$ is the link function, X_i is the set of predictors or independent variables, $E(Y)$ is the expected value of the response variable, β^T is the transposed vector of fitted model parameters, and e_i is the error. Depending on data type, the appropriate link function is selected. Poisson distribution using the log link function was selected to model meningitis incidence as they are discrete data – this is also known as 'Poisson Regression'

$$Log(\lambda_i) = X_i\beta^T + e \quad \text{for i = 1, 2, …, N} \tag{2}$$

where λ_i is the parameter of the Poisson distribution for observation 'i'. An iterative least-squares method provides estimates of the model parameters, β, maximizing the likelihood function. Akaike Information Criteria (AIC, Akaike, 1974) is used to identify the best model predictor set. AIC is calculating using:

$$AIC = 2k - 2L \tag{3}$$

[4] R Core Team (2012). R: A language and environment for statistical computing. R Foundation for Statistical Computing,Vienna, Austria. ISBN 3-900051-07-0, URL http://www.R-project.org/

k indicates the number of predictors and L is the logarithm of the likelihood function of the model. Parsimony is encouraged by penalizing for additional predictors. The model is applied to meningitis incidences in periods P1 and P2 for each region to obtain the best set of predictors.

3.4.2 Validation

The fitted and estimated values are plotted and their R2 computed to indicate the strength of the relationship (0 being no relationship to 1 being a perfect relationship). Then we perform a drop-1 cross-validation in which at each observation point is dropped and the model is fitted on the remaining observations and, the dropped point is then predicted using the fitted model. This provides the model's ability in estimating in a predictive mode. The cross-validated model fits are measured using the adjusted root mean squared error (ARMSE), which is the ratio of RMSE and the standard deviation. Lower values (values closer to 0) are highly skillful.

$$ARMSE = \frac{\sqrt{\overline{(Y_{pred}-Y)^2}}}{\sqrt{\sum(Y_i-\bar{Y})^2}} \quad (4)$$

To stress the models further, drop 10% cross-validation is performed where 10% of the points are randomly dropped and the model is fit on the remaining observations. The dropped points are then predicted using the fitted model. This cross-validation is repeated for 1000 iterations to produce a distribution of RMSE values from which the median value is used to calculate the ARMSE.

3.5 RESULTS

Poisson regression models were fitted separately for the MM incidences in periods P1 and P2 at different lead times – 4, 8 and 12 weeks for P1, and 4 and 8 weeks

for P2. Forecasts were made on a weekly basis in the two periods at these lead times and skill scores computed for the lead times. The suite of predictors, shown in Table 3.2 include – lead time weekly relative humidity (4, 8 and 12 weeks) of the cluster index, relative humidity retreat period cluster index, two highly correlated climate predictors of monsoon onset season relative humidity identified in Broman et al., (2013) for forecasts in P2 period and cumulative meningitis case counts at the lead time (4, 8, and 12 weeks).

Table 3.2: Model predictors for P1 and P2

P1	P2
Week 1 – Week 13	*Week 14 – Week 20*
Retreat Period Relative Humidity Index	Onset Period Climate Predictors of Relative Humidity
Weekly Lagged Relative Humidity (at 4, 8, and 12 weeks)	Weekly Lagged Relative Humidity (at 4 and 8 weeks)
Weekly Lagged Cumulative Meningitis Incidence (at 4, 8, and 12 weeks)	Weekly Lagged Cumulative Meningitis Incidence (at 4 and 8 weeks)

For each region, Nigeria, Chad, or Benin + Togo, correlation between meningitis incidence and relative humidity from each of the clusters identified the appropriate cluster (not shown). For Nigeria, the middle cluster relative humidity was selected, the north cluster for Chad, and the south cluster for Benin + Togo. Retreat period cluster indices were included as predictors in P1 models only as a surrogate for soil moisture. Climate predictors were included as predictors for the P2 models only as they coincide with the P1 period (Jan – Mar). These climate predictors were restricted to the top two best-correlated climate predictors to encourage parsimony. These models were developed for Nigeria, Chad, and Benin + Togo lumped.

In total, fifteen models were produced, nine for the peak meningitis season (3 meningitis case time series and 3 lead times) and six for the shoulder meningitis season (3 meningitis case time series and 2 lead times). As mentioned above forecast were made for 4, 8 and 12 week lead times for the three meningitis case time series. Figures 8 - 10 show the results of peak meningitis season (P1 period) forecasts for Nigeria, Chad and Benin + Togo. Table 3.3 shows the suite of predictors selected in the best model via AIC,

which shows that the best model selects 2-4 predictors. Lagged relative humidity and lagged cumulative case counts (i.e., values at the lead time) were significant predictors for all models. The retreat relative humidity index was not used as a predictor for Nigeria, but is selected in all three of the Chad models and two of the Benin + Togo models Drop-1 cross validated estimates and the observed meningitis cases match very well for Nigeria (Figure 3.8 a-c) at 4-week and 8-week lead time and not that good for 12-week. The skills at 4 and 8 weeks especially, in cross-validated forecasting the high cases during 2008 is remarkable. The fitting skills (Figure 3.8 d-e), R2 and ARMSE are also quite good (Table 3.3). For Chad the performance is very good at all lead times (Figure 3.9 a-c) and this is indicated in the fitting skills (Table 3.3). Benin + Togo exhibit similar performance (Figure 3.10).

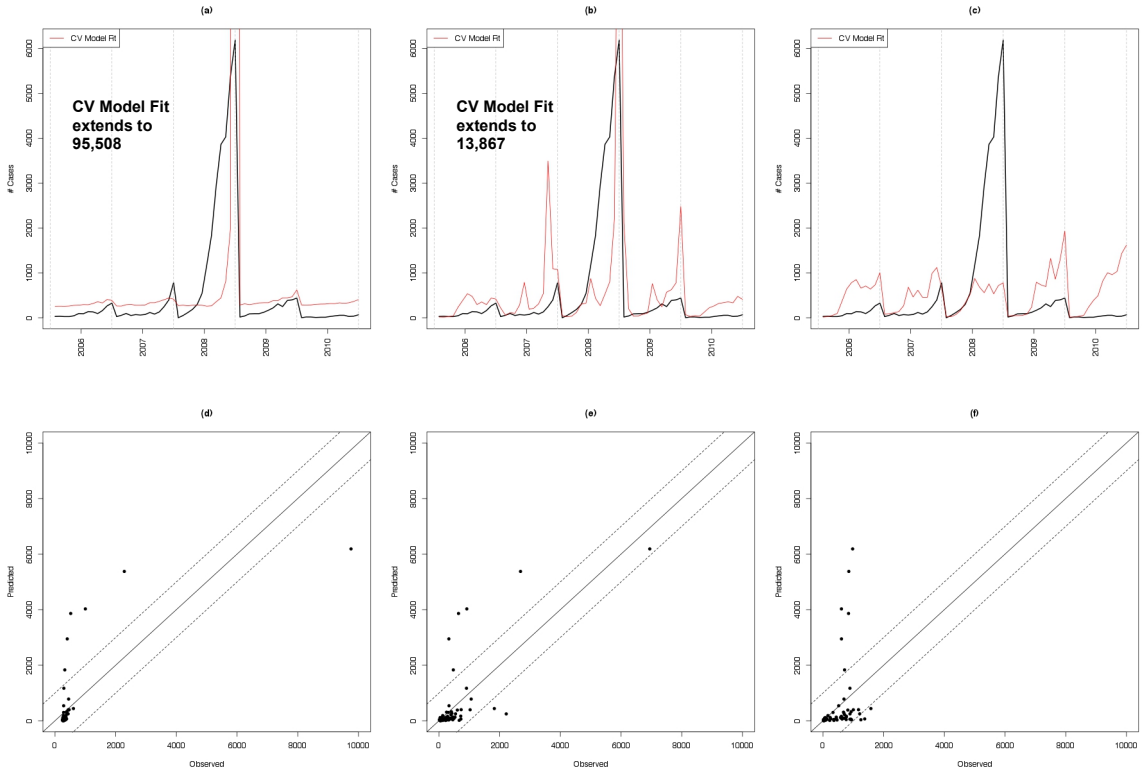

Figure 3.8: Nigeria 2007 – 2011 meningitis cases model results showing the cross-validated model fit at lead times of 4 weeks (a), 8 weeks (b), and 12 weeks (c), and the predicted versus observed at lead times of 4 weeks (d), 8 weeks (e), and 12 weeks (f). Dashed lines in (d-f) indicate +/- 1000 cases.

Country /Region	Period	Lead Time	Predictor 1	Predictor 2	Predictor 3	Predictor 4	RMSE	Model Fit R^2	CV Model Fit R^2
Nigeria	p1	4 Weeks	4wk Lagged Mid. Cluster RH	4wk Lagged Cumulative Case Counts	n/a	n/a	0.3262	0.5041	0.3481
Nigeria	p1	8 Weeks	8wk Lagged Mid. Cluster RH	8wk Lagged Cumulative Case Counts	12wk Lagged Mid. Cluster RH	12wk Lagged Cumulative Case Counts	0.3972	0.5329	0.3969
Nigeria	p1	12 Weeks	Mid. Cluster Retreat RH Index	12wk Lagged Cumulative Case Counts	12wk Lagged Mid. Cluster RH	n/a	0.411	0.0784	0.0256
Chad	p1	4 Weeks	4wk Lagged Cumulative Case Counts	4wk Lagged North Cluster RH	North Cluster Retreat RH Index	n/a	0.5218	0.7744	0.7225
Chad	p1	8 Weeks	8wk Lagged Cumulative Case Counts	8wk Lagged North Cluster RH	North Cluster Retreat RH Index	n/a	0.6788	0.7569	0.6889
Chad	p1	12 Weeks	12wk Lagged Cumulative Case Counts	12wk Lagged North Cluster RH	North Cluster Retreat RH Index	n/a	0.6248	0.6241	0.5184
Benin + Togo	p1	4 Weeks	4wk Lagged South Cluster RH	8wk Lagged South Cluster RH	8wk Lagged Cumulative Case Counts	12wk Lagged Cumulative Case Counts	0.6164	0.7569	0.7225
Benin + Togo	p1	8 Weeks	8wk Lagged South Cluster RH	8wk Lagged Cumulative Case Counts	12wk Lagged Cumulative Case Counts	South Cluster Retreat RH Index	0.6184	0.7569	0.7225
Benin + Togo	p1	12 Weeks	12wk Lagged South Cluster RH	12wk Lagged Cumulative Case Counts	South Cluster Retreat RH Index	n/a	0.6901	0.6241	0.5625

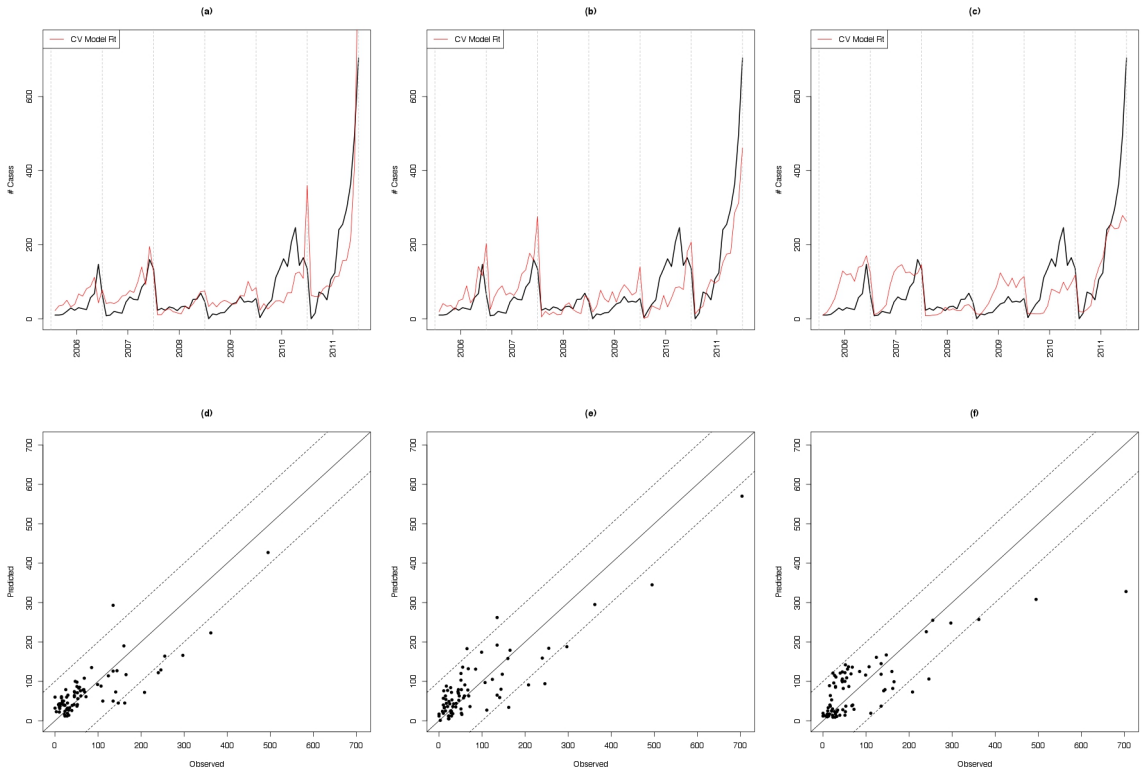

Figure 3.9: Chad 2006 – 2011 meningitis cases model results showing the cross-validated model fit at lead times of 4 weeks (a), 8 weeks (b), and 12 weeks (c), and the predicted versus observed at lead times of 4 weeks (d), 8 weeks (e), and 12 weeks (f). Dashed lines in (d-f) indicate +/- 100 cases.

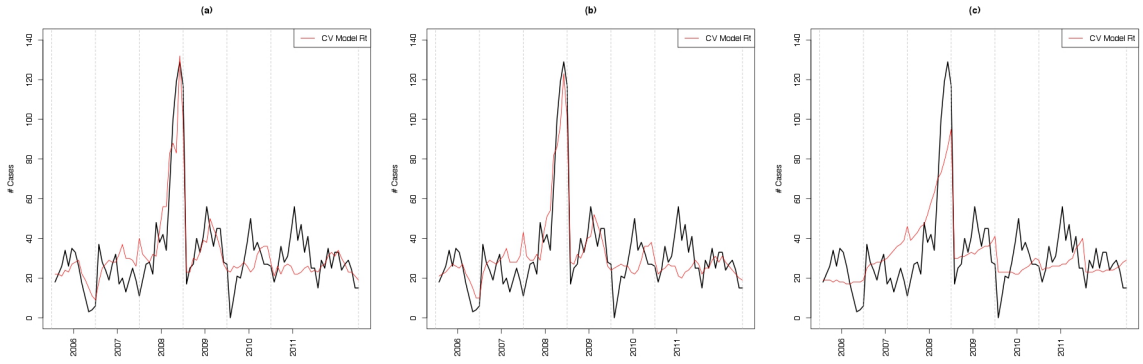

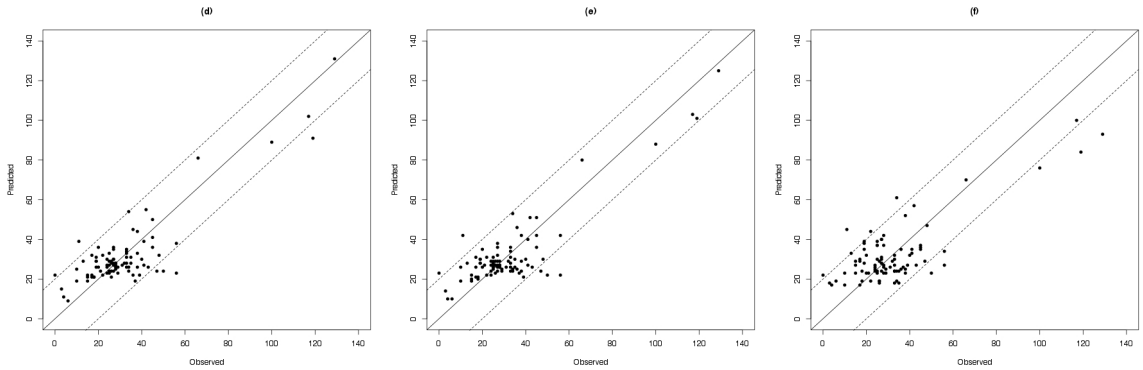

Figure 3.10: Benin and Togo 2005 – 2011 meningitis cases model results showing the cross-validated model fit at lead times of 4 weeks (a), 8 weeks (b), and 12 weeks (c), and the predicted versus observed at lead times of 4 weeks (d), 8 weeks (e), and 12 weeks (f). Dashed lines in (d-f) indicate +/- 20 cases.

Table 3.3: Peak meningitis period model predictors and RMSE.

Country /Region	Period	Lead Time	Predictor 1	Predictor 2	Predictor 3	Predictor 4	RMSE	Model Fit R^2	CV Model Fit R^2
Nigeria	p1	4 Weeks	4wk Lagged Mid. Cluster RH	4wk Lagged Cumulative Case Counts	n/a	n/a	0.3262	0.5041	0.3481
Nigeria	p1	8 Weeks	8wk Lagged Mid. Cluster RH	8wk Lagged Cumulative Case Counts	12wk Lagged Mid. Cluster RH	12wk Lagged Cumulative Case Counts	0.3972	0.5329	0.3969
Nigeria	p1	12 Weeks	Mid. Cluster Retreat RH Index	12wk Lagged Cumulative Case Counts	12wk Lagged Mid. Cluster RH	n/a	0.411	0.0784	0.0256
Chad	p1	4 Weeks	4wk Lagged Cumulative Case Counts	4wk Lagged North Cluster RH	North Cluster Retreat RH Index	n/a	0.5218	0.7744	0.7225
Chad	p1	8 Weeks	8wk Lagged Cumulative Case Counts	8wk Lagged North Cluster RH	North Cluster Retreat RH Index	n/a	0.6788	0.7569	0.6889
Chad	p1	12 Weeks	12wk Lagged Cumulative Case Counts	12wk Lagged North Cluster RH	North Cluster Retreat RH Index	n/a	0.6248	0.6241	0.5184
Benin +	p1	4 Weeks	4wk Lagged	8wk Lagged	8wk Lagged	12wk Lagged	0.6164	0.7569	0.7225

Togo			South Cluster RH 8wk Lagged South Cluster RH 12wk Lagged South Cluster RH	South Cluster RH 8wk Lagged Cumulative Case Counts 12wk Lagged Cumulative Case Counts	Cumulative Case Counts 12wk Lagged Cumulative Case Counts South Cluster Retreat RH Index	Cumulative Case Counts South Cluster Retreat RH Index			
Benin + Togo	p1	8 Weeks					0.6184	0.7569	0.7225
Benin + Togo	p1	12 Weeks				n/a	0.6901	0.6241	0.5625

For the shoulder season (P2 period), we issue forecasts at two lead times 4 and 8 weeks as no climate variables exist at 12 weeks to use as predictors (Figures 3.11 – 3.13).

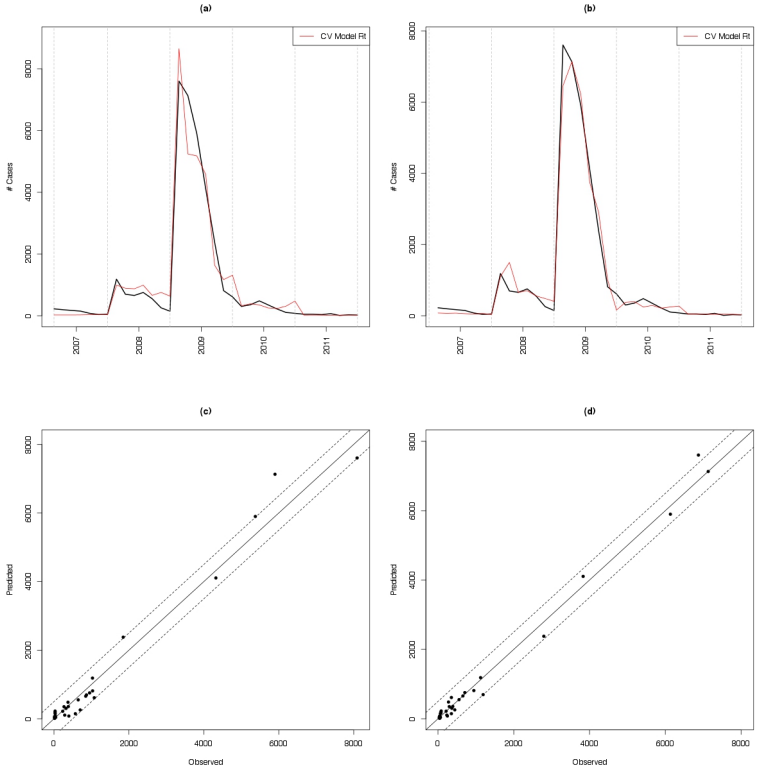

Figure 3.11: Nigeria 2007 – 2011 meningitis cases model results showing the cross-validated model fit at lead times of 4 weeks (a), and 8 weeks (b), and the predicted versus observed at lead times of 4 weeks (c), and 8 weeks (d). Dashed lines in (c-d) indicate +/- 500 cases.

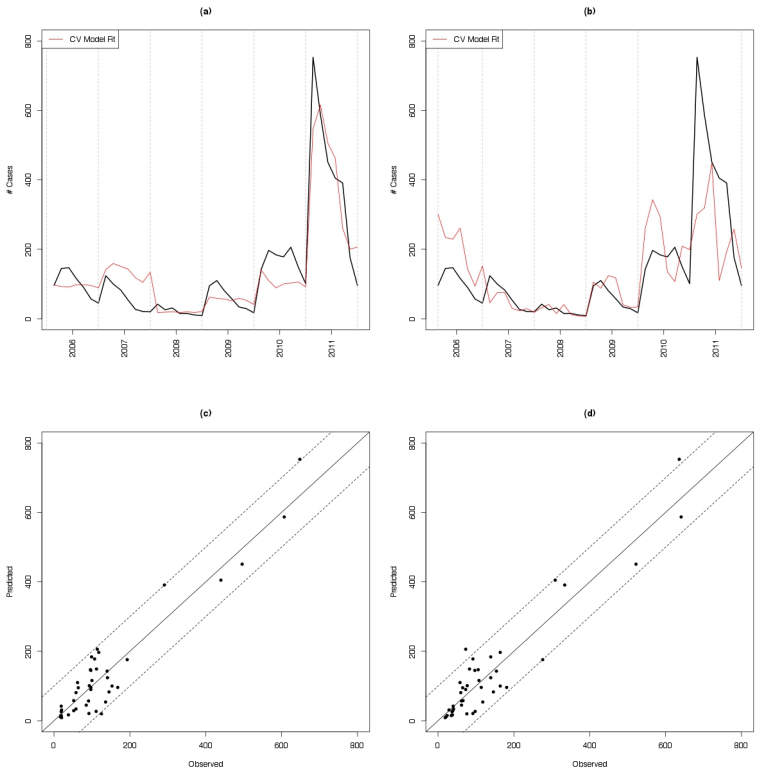

Figure 3.12: Chad 2006 – 2011 meningitis cases model results showing the cross-validated model fit at lead times of 4 weeks (a), and 8 weeks (b), and the predicted versus observed at lead times of 4 weeks (c), and 8 weeks (d). Dashed lines in (c-d) indicate +/- 100 cases.

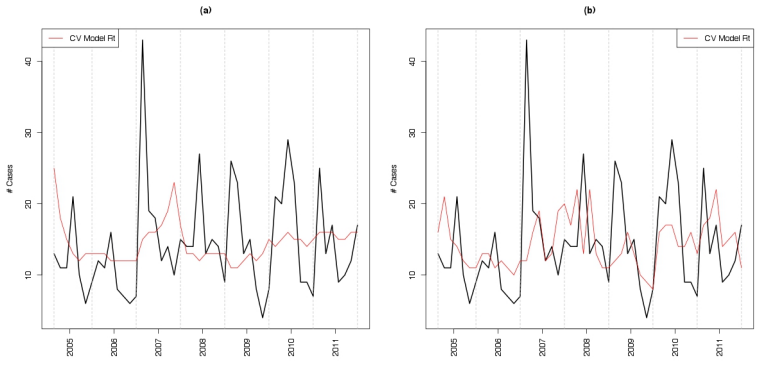

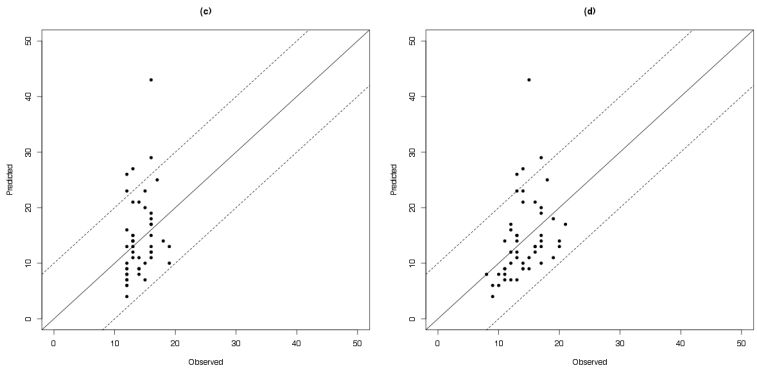

Figure 3.13: Benin and Togo 2005 – 2011 meningitis cases model results showing the cross-validated model fit at lead times of 4 weeks (a), and 8 weeks (b), and the predicted versus observed at lead times of 4 weeks (c), and 8 weeks (d). Dashed lines in (c-d) indicate +/- 10 cases.

The predictors used in the best model for each country and lead time are listed in Table 3.4. Also shown are cross-validated ARMSE and R2 values for each model.

Table 3.4: Shoulder Peak period model predictors and RMSE. * Climate predictors from Broman et. al. 2013.

Country /Region	Period	Lead Time	Predictor 1	Predictor 2	Predictor 3	Predictor 4	RMSE	Model Fit R^2	CV Model Fit R^2
Nigeria	p2	4 Weeks	4wk Lagged Mid. Cluster RH	4wk Lagged Cumulative Case Counts	Jan 925mb Zonal Winds (obj03)*	Jan 600mb Zonal Winds (obj05)*	0.662	0.9801	0.9409
Nigeria	p2	8 Weeks	12wk Lagged Mid. Cluster RH	12wk Lagged Cumulative Case Counts	Jan 925mb Zonal Winds (obj03)*	Jan 600mb Zonal Winds (obj05)*	0.5959	1	0.9801
Chad	p2	4 Weeks	4wk Lagged North Cluster RH	4wk Lagged Cumulative Case Counts	Jan 600mb Zonal Winds (ocj05)*	Jan 200mb Zonal Winds (ocj06)*	0.5967	0.9025	0.8281
Chad	p2	8 Weeks	8wk Lagged North Cluster RH	12wk Lagged North Cluster RH	8wk Lagged Cumulative Case Counts	Jan 200mb Zonal Winds (ocj06)*	0.6466	0.8836	0.4356
Benin +	p2	4 Weeks	4wk	4wk Lagged	Jan 600mb	n/a	0.8864	0.0729	0.0009

Togo			Lagged South Cluster RH	Cumulative Case Counts	Zonal Winds (oaj03)*				
Benin + Togo	p2	8 Weeks	12wk Lagged South Cluster RH	8wk Lagged Cumulative Case Counts	12wk Lagged Cumulative Case Counts	Jan 600mb Zonal Winds (oaj03)*	0.7872	0.1444	0.0361

All shoulder season models contain lagged relative humidity as a predictor at least one climate variable and lagged cumulative case counts. All the climate variables selected are from January, meridional winds at 925, 600, or 200mb. Figure 3.12 a-b shows the cross-validated estimates of MM cases in P2 period for Chad and Figure 3.12 c-d the scatterplot of fitted estimates. The model performs very well at both the lead times and in a cross-validated and fitting mode – also corroborated by lower ARMSE and higher R2.

3.6 SUMMARY AND CONCLUSION

We developed and validated Poisson regression models to predict weekly MM cases for countries in West Africa for the peak and shoulder periods of meningitis occurrence. Models were developed for Chad, Nigeria and Benin and Togo combined. The meningitis season is out of phase with the monsoon season – in that the start of the monsoon season (P2 period) coincides with the ending of the meningitis season and the monsoon retreat period marks the start of the meningitis season. The availability or lack thereof of moisture is key ingredient in the meningitis occurrence. Forecasts were made at 4, 8 and 12 week lead time and the predictors in the regression models involved relative humidity and meningitis cases at these lead times and large scale climate predictors for the P2 period. The models show very good skills – both fitting and cross validation at these lead times – especially for Chad and Nigeria which has the highest number of MM cases the models perform particularly well. This suggests that climate and meteorological features can help forecast MM cases skillfully, which will be of immense use in planning mitigation strategies by local agencies and WMO.

There are attributes that can be incorporated to the modeling approach to further improve the skills. Including dust and temperature as potential predictors could provide a measure of the influence of different environmental factors. Adjusting case counts to account for a potential depression in districts following a reactive vaccination campaign could provide a better measure of the true influence of environmental factors as compared to transport dynamics or variation in strains in outbreaks of meningitis. This modeling approach provided predictions of meningitis cases at weekly intervals, but over large geographic regions. Improved monitoring, including geo-locating cases, could allow this prediction to be made at the district or finer geographic location, and perhaps provide additional insight into the mechanisms that link environmental factors and meningitis outbreaks.

4 CONCULSION AND FUTURE WORK

4.1 CONCLUSION

Climate and health are inexorably linked as climate can influence health in numerous ways. The overarching goal of this forecasting is to provide additional inputs into the decision-making process used by the International Coordinating Group (ICG) for Vaccine Provision in managing meningitis outbreaks. It is hoped that these additional inputs could provide the ICG a way to more efficiently stage resources and improve response times.

The two linked studies described in Chapters 2 and 3 have shown success in modeling and forecasting regional climate (i.e., relative humidity) and meningitis incidences in the West African region, at long lead times.

The climate diagnostics and modeling studies performed in Chapters 2 provided an understanding of the seasonal variation of relative humidity within the West African Monsoon region. Prior investigation of climate in this region has focused on precipitation, winds, or dust. Large-scale ocean-atmospheric drivers of relative humidity were identified and it was shown that these drivers could be used to accurately predict relative humidity at long lead times. During the onset period, South Atlantic MSLP, Gulf of Guinea SST, and Sahara surface temperature were the three key drivers of variability of relative humidity. All influenced the cross-equator pressure gradient responsible for the monsoon winds that advect moisture inland. The picture was less clear during monsoon retreat except to say that land-atmosphere interactions were more important. Drivers included low, mid, and high-level winds, and surface temperature, all over the continent. The predictability of relative humidity indicates that these climate drivers have persistence, which imparts long lead skill in forecasting relative humidity.

In Chapter 3 we developed a Poisson regression model to forecast Meningitis incidences in Chad, Nigeria and Benin and Togo combined. The regression used relative humidity, climate variables and lagged incidences identified in Chapter 2. Meningitis forecasts had skill at all lead times, 4, 8, and 12 weeks. Predictions accurately identified the large spikes in incidence found in Nigeria in 2009 and in Chad in 2011. This indicates

that the models were able to identify those years where epidemics occurred, as well as identify the week of peak incidence. This is useful as it provides the location and timing of epidemics, even if total incidence predicted varies from actual incidence. The models also had few cases of over-prediction, indicating high incidence when none occurred, the exception to this being the 8-week P1 model for Nigeria during 2007. The lack of suitable meningitis case data led to forecasts at large spatial regions; it was hoped to be able to provide forecasts at the district level. The country-total forecasts presented here are still useful in suggesting where resources be staged, but is not able to indicate the center of incidence to inform which districts might be at risk for an epidemic. Additionally, fitting of the models relied on 5 – 7 years of case data; the demonstrated model skill was very good, but additional case data could improve forecasts or provide forecasts at longer lead times.

These studies have shown that investigation into the link between infectious disease and climate can provide useful information in disease management and mitigation. It is hoped that the results presented will be able to directly influence the decision process in managing meningitis outbreaks as well as inform future work into meningitis links to climate specifically and health and climate generally.

4.2 FUTURE WORK

The modeling framework developed for forecasting both relative humidity and meningitis incidences can be further extended. With relative humidity, the modeling should be extended to the dry season to identify climate links and provide climate variables to include in the peak meningitis season models. No climate variables were included in the dry season, P1 (Jan – Mar) meningitis models because no climate drivers of relative humidity during Oct – Dec were identified. The above extension of analysis of dry season climate will improve the meningitis incidence forecasts for the peak season.

Meningitis incidence forecasting models were found to be skillful at long lead times, and were able to identify spikes in incidence. A threshold exceedance score, examining the skill of the model in predicting incidence exceedance over the alert (5 cases / 100,000) and epidemic (10 cases / 100,000) levels currently used by the ICG

would provide an additional metric indicating the usefulness of the models. Furthermore, the threshold exceedances could be modeled directly using extreme value theory (e.g., Coles, 2001; Katz et al., 2002).

The inclusion of additional environmental factors such as temperature and dust, which are known to influence meningitis occurrence could further improve the forecasting skills. Incidence data used in forecasting were not adjusted for vaccination, which provides roughly three years of immunity with decreasing efficacy. Adjusting data for the depression of cases produced by vaccination would provide a less potentially biased dataset from which to model.

The explicit inclusion of social or physiological factors would require a better understanding of meningitis carriage, disease emergence, and social behavior. Given the wide variety of locations covered by this study area: rural and urban, plains and forest; along with different local cultures, any application of the theoretical model would have to be tailored to a local region.

BIBLIOGRAPHY

Besancenot, J. P., M. Boko, and P. C. Oke, 1997: Weather conditions and cerebrospinal meningitis in Benin (Gulf of Guinea, West Africa). *European Journal of Epidemiology*, **13**, 807–815.

Bracken, C., B. Rajagopalan, and J. Prairie, 2010: A multisite seasonal ensemble streamflow forecasting technique. *Water Resources Research*, **46**, W03532.

Caniaux, G., H. Giordani, J.-L. Redelsperger, F. Guichard, E. Key, and M. Wade, 2011: Coupling between the Atlantic cold tongue and the West African monsoon in boreal spring and summer. *J. Geophy. Res.*, **116**, C04003.

Cheesbrough, J. S., A. P. Morse, and S. D. Green, 1995: Meningococcal meningitis and carriage in western Zaire: a hypoendemic zone related to climate? *Epidemiology and Infection*, **114**, 75–92.

Coles S. An Introduction to Statistical Modeling of Extreme Values. London: Springer; 2001.

Colombini, A. and Coauthors, 2009: Costs for households and community perception of meningitis epidemics in burkina faso. *Clinical infectious diseases : an official publication of the Infectious Diseases Society of America*, **49**, 1520–1525.

Cook, K., and E. Vizy, 2006: Coupled model simulations of the West African monsoon system: Twentieth-and twenty-first-century simulations. *J. Climate*, **19**, 3681–3703.

Djibo S, Nicolas P, Campagne G, Chippaux JP. Pharyngeal carriage of Neisseria meningitidis in a school of Niamey, Niger. Med Trop (Mars) 2004; 64: 363–66.

Drobinski, P., B. Sultan, and S. Janicot, 2005: Role of the Hoggar massif in the West African monsoon onset. *Geophysical Research Letters*, **32**, 481–484.

Eltahir, E., and C. Gong, 1996: Dynamics of wet and dry years in West Africa. *J. Climate*, **9**, 1030-1042.

Fontaine, B., and S. Louvet, 2006: Sudan-Sahel rainfall onset: Definition of an objective index, types of years, and experimental hindcasts. *Journal of Geophysical Research*,

111, D20103.

Grantz, K., B. Rajagopalan, M. Clark, and E. Zagona, 2005: A technique for incorporating large-scale climate information in basin-scale ensemble streamflow forecasts. *Water Resources Research*, **41**, W10410.

Greenwood, B., 1999: Manson Lecture. Meningococcal meningitis in Africa. *Transactions of the Royal Society of Tropical Medicine and Hygiene*, **93**, 341–353.

Gugnani, H. C., and J. A. Uganabo, 1989: Nasopharyngeal, vaginal and anal carriage of Neisseria meningitidis in Nigeria. *The Journal of communicable diseases*, **21**, 41–45.

Haarsma, R. J., 2005: Sahel rainfall variability and response to greenhouse warming. *Geophysical Research Letters*, **32**, L17702.

Hagos, S. M., and K. H. Cook, 2008: Ocean Warming and Late-Twentieth-Century Sahel Drought and Recovery. *J. Climate*, **21**, 3797–3814.

Hassan-King, M. K., R. A. Wall, and B. M. Greenwood, 1988: Meningococcal carriage, meningococcal disease and vaccination. *J Infect*, **16**, 55–59.

Jackson, B., S. E. Nicholson, and D. Klotter, 2009: Mesoscale Convective Systems over Western Equatorial Africa and Their Relationship to Large-Scale Circulation. *Monthly Weather Review*, **137**, 1272–1294.

Janowiak, J., 1988: An Investigation of the Interannual Rainfall Variability in Africa. *J. Climate*, **1**, 240–255.

Kalnay, E. and Coauthors, 1996: The NCEP/NCAR 40-year reanalysis project. *Bulletin of the American Meteorological Society*, **77**, 437–471.

Kaplan, A., M. A. Cane, A. C. Clement, M. B. Blumenthal, B. Rajagopalan, and C. Bottoraley, 1998: Analyses of global sea surface temperature 1856-1991. *Journal of Geophysical Research: Oceans*, **103**, 18,567–18,589.

Katz, R.W., M.B. Parlange, and P. Naveau, 2002: "Statistics of extremes in hydrology."

Advances in Water Resources, **25**, 1287-1304.

Koster, R. D. and Coauthors, 2004: Regions of strong coupling between soil moisture and precipitation. *Science (New York, N.Y.)*, **305**, 1138–1140.

Kristiansen, P. a and Coauthors, 2011: Baseline meningococcal carriage in Burkina Faso before the introduction of a meningococcal serogroup A conjugate vaccine. *Clinical and vaccine immunology : CVI*, **18**, 435–443.

Kristiansen, P. a and Coauthors, 2013: Impact of the serogroup A meningococcal conjugate vaccine, MenAfriVac, on carriage and herd immunity. *Clinical infectious diseases : an official publication of the Infectious Diseases Society of America*, **56**, 354–363.

Lapeyssonnie, L., 1963: La méningite cérébrospinale en Afrique. *Bulletin of the World Health Organization*, **28**.

Lavaysse, C., C. Flamant, S. Janicot, D. J. Parker, J.-P. Lafore, B. Sultan, and J. Pelon, 2009: Seasonal evolution of the West African heat low: a climatological perspective. *Climate Dynamics*, **33**, 313–330.

Lewis, R., N. Nathan, L. Diarra, F. Belanger, and C. Paquet, 2001: Timely detection of meningococcal meningitis epidemics in Africa. *Lancet*, **358**, 287–293.

Lough, J. M., 1986: Tropical Atlantic sea surface temperatures and rainfall variations in subsaharan Africa. *Monthly weather review*, **114**, 561–570.

McCullagh, P., and J. A. Nelder, 1989: *Generalized Linear Models, Second Edition*. Chapman & Hall/CRC, 511pp.

Mohr, K. I., and C. D. Thorncroft, 2006: Intense convective systems in West Africa and their relationship to the African easterly jet. *Quarterly Journal of the Royal Meteorological Society*, **132**, 163–176.

Molesworth, A. M., M. C. Thomson, S. J. Connor, M. P. Cresswell, A. P. Morse, P. Shears, C. A. Hart, and L. E. Cuevas, 2002: Where is the meningitis belt? Defining

an area at risk of epidemic meningitis in Africa. *Transactions of the Royal Society of Tropical Medicine and Hygiene*, **96**, 242–249.

Molesworth, A. M., L. E. Cuevas, S. J. Connor, A. P. Morse, and M. C. Thomson, 2003: Environmental risk and meningitis epidemics in Africa. *Emerging Infectious Diseases*, **9**, 10, 1287–93.

Mueller, J. E., and B. D. Gessner, 2010: A hypothetical explanatory model for meningococcal meningitis in the African meningitis belt. *International journal of infectious diseases : IJID : official publication of the International Society for Infectious Diseases*, **14**, e553–9.

Nicholson, S. E., 2009: A revised picture of the structure of the "monsoon" and land ITCZ over West Africa. *Climate Dynamics*, **32**, 1155–1171.

Nieto, R., L. Gimeno, and R. M. Trigo, 2006: A Lagrangian identification of major sources of Sahel moisture. *Geophysical Research Letters*, **33**, L18707.

Nobre, Paulo, J. Srukla, 1996: Variations of Sea Surface Temperature, Wind Stress, and Rainfall over the Tropical Atlantic and South America. *J. Climate*, **9**, 2464–2479.

Ramel, R., H. Gallée, and C. Messager, 2006: On the northward shift of the West African monsoon. *Climate Dynamics*, **26**, 429–440.

Redelsperger, J.-L., C. D. Thorncroft, A. Diedhiou, T. Lebel, D. J. Parker, and J. Polcher, 2006: African Monsoon Multidisciplinary Analysis: An International Research Project and Field Campaign. *Bulletin of the American Meteorological Society*, **87**, 1739–1746.

Regonda, S. K., B. Rajagopalan, M. Clark, and E. Zagona, 2006: A multimodel ensemble forecast framework: Application to spring seasonal flows in the Gunnison River Basin. *Water Resources Research*, **42**, W09404.

Scott, A. A. J., and M. Knott, 1974: A Cluster Analysis Method for Grouping Means in the Analysis of Variance. *Biometrics*, **30**, 507–512.

Sultan, B., and S. Janicot, 2003: The West African monsoon dynamics. Part II: The

"preonset" and "onset" of the summer monsoon. *J. Climate*, **16**, 3407–3427.

Thomson, M. C., F. J. Doblas-Reyes, S. J. Mason, R. Hagedorn, S. J. Connor, T. Phindela, a P. Morse, and T. N. Palmer, 2006: Malaria early warnings based on seasonal climate forecasts from multi-model ensembles. *Nature*, **439**, 576–579.

Thorncroft, C. D., and M. Blackburn, 1999: Maintenance of the African easterly jet. *Quarterly Journal of the Royal Meteorological Society*, **125**, 763–786.

Trotter, C. L., and B. M. Greenwood, 2007: Meningococcal carriage in the African meningitis belt. *The Lancet infectious diseases*, **7**, 797–803.

Varaine, F. and Coauthors, 1997: Meningitis outbreaks and vaccination strategy. *Transactions of the Royal Society of Tropical Medicine and Hygiene*, **91**, 3–7.

Vizy, E. K., and K. H. Cook, 2002: Development and application of a mesoscale climate model for the tropics : Influence of sea surface temperature anomalies on the West African monsoon. *Journal of Geophysical Research: Atmospheres (1984–2012)*, **107**, D3, ACL-2.

Yaka, P., B. Sultan, H. Broutin, S. Janicot, S. Philippon, and N. Fourquet, 2008: Relationships between climate and year-to-year variability in meningitis outbreaks: a case study in Burkina Faso and Niger. *International Journal of Health Geographics*, **7**, 34

A. APPENDIX: ADDITIONAL FIGURES

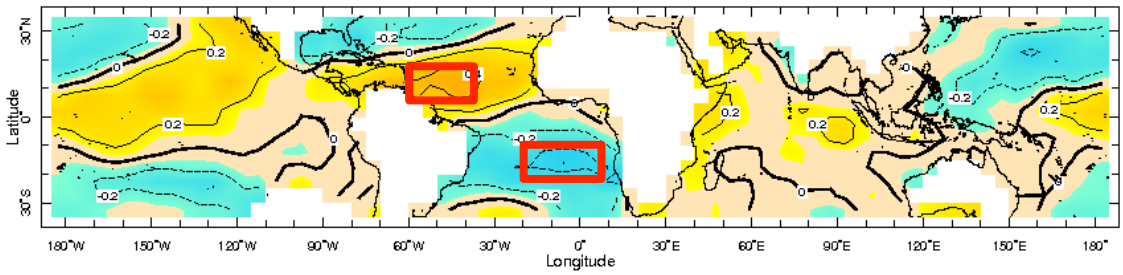

Figure A.1: Onset South Cluster correlation plot with February sea-surface temperature. Red boxes indicate regions used to produce predictors.

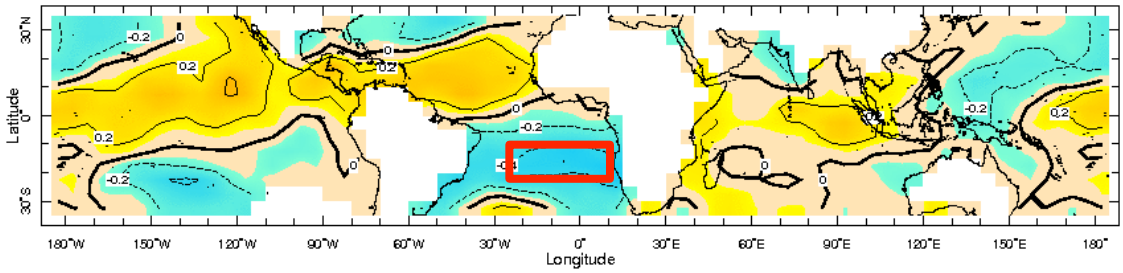

(a)

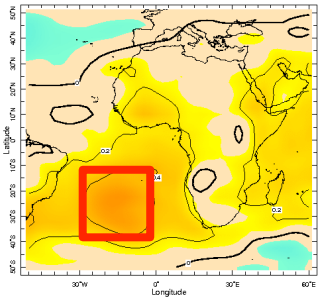

(b)

Figure A.2: Onset South Cluster correlation plots with March (a) sea-surface temperature and (b) mean sea-level pressure. Red boxes indicate regions used to produce predictors.

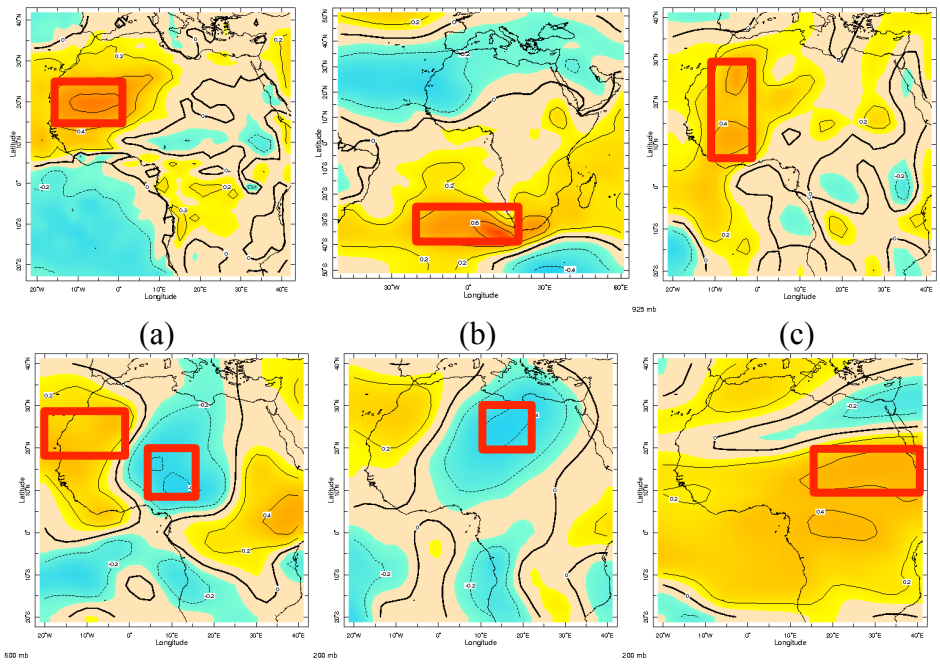

Figure A.3: Onset Middle Cluster correlation plots with January (a) surface temperature and (b) mean sea-level pressure, (c) 925mb zonal winds, (d) 600mb zonal winds, (e) 200mb zonal winds, and (f) 200mb meridional winds. Red boxes indicate regions used to produce predictors.

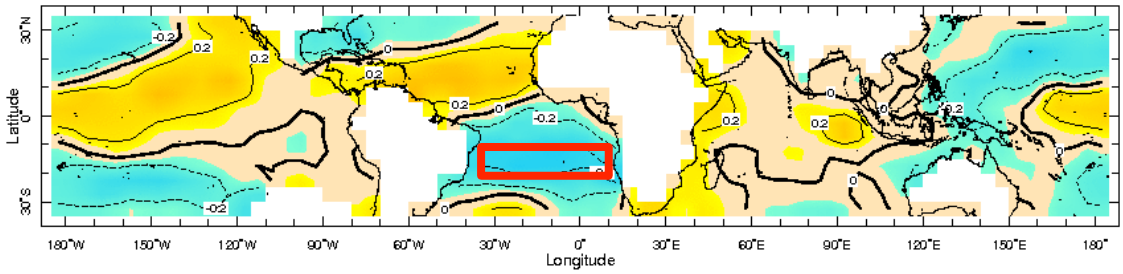

Figure A.4: Onset Middle Cluster correlation plot with February sea-surface temperature. Red boxes indicate regions used to produce predictors.

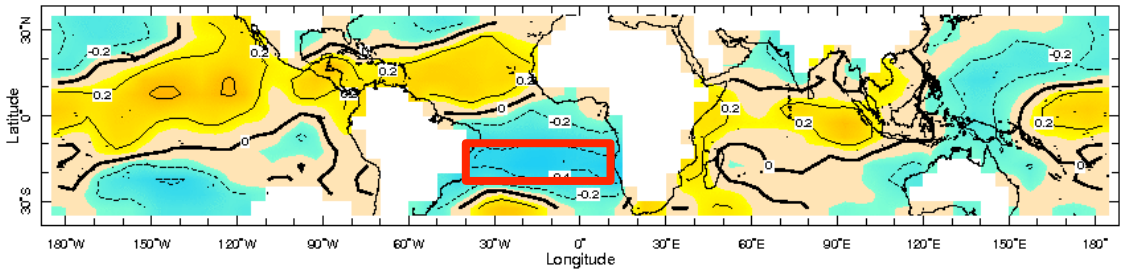

(a)

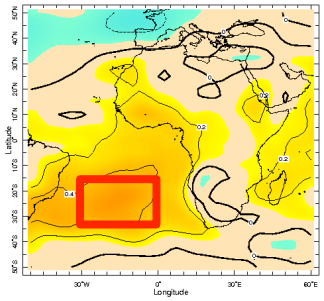

(b)

Figure A.5: Onset Middle Cluster correlation plots with March (a) sea-surface temperature and (b) mean sea-level pressure. Red boxes indicate regions used to produce predictors.

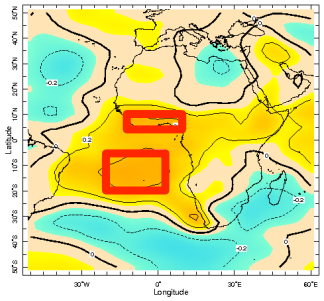

Figure A.6: Onset Middle Cluster correlation plot with April mean sea-level pressure. Red boxes indicate regions used to produce predictors

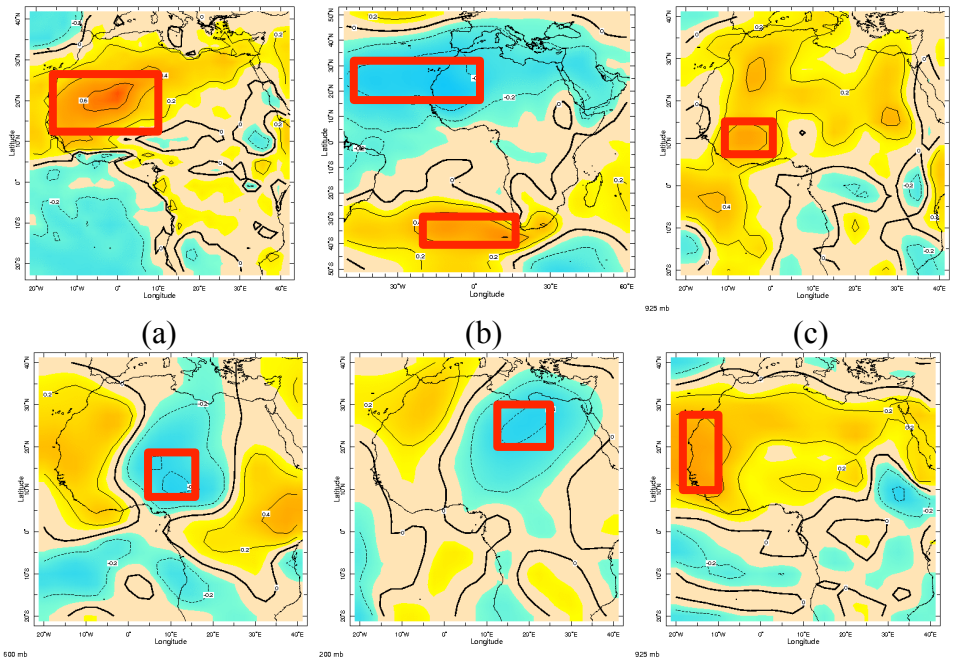

(a) (b) (c)

(d) (e) (f)

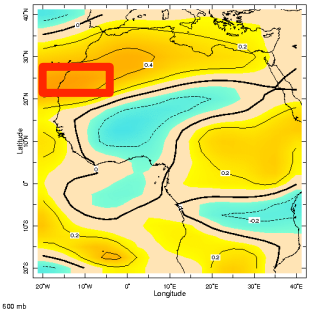

(g)

Figure A.7: Onset North Cluster correlation plot with (a) surface temperature, (b) mean sea-level pressure, (c) 925mb zonal winds, (d) 600mb zonal winds, (e) 200mb zonal winds, (f) 925mb meridional winds, and (g) 600mb meridional winds. Red boxes indicate regions used to produce predictors.

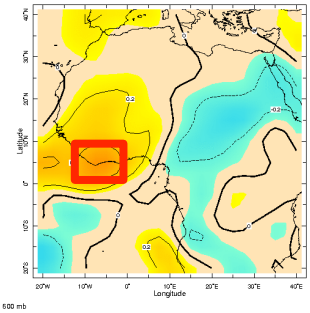

Figure A.8: Onset North Cluster correlation plot with February 600mb zonal winds. Red boxes indicate regions used to produce predictors.

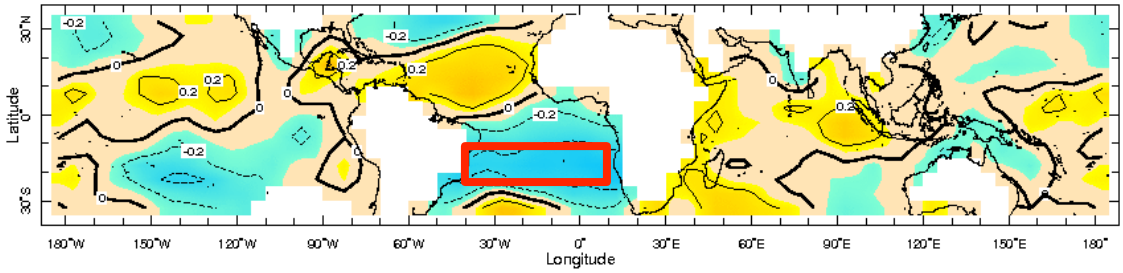

Figure A.9: Onset North Cluster correlation plot with March sea-surface temperature. Red boxes indicate regions used to produce predictors.

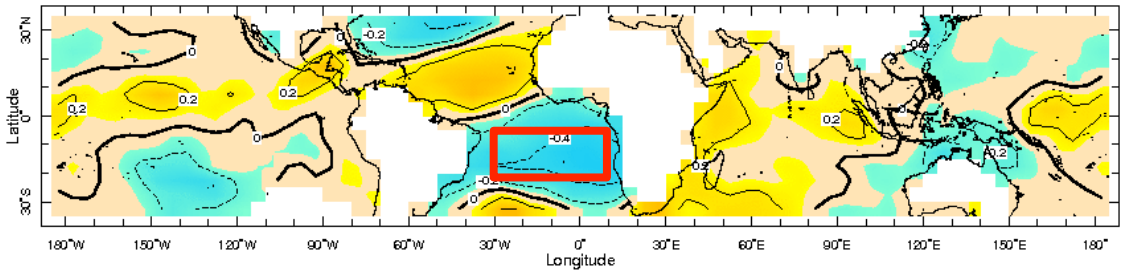

(a)

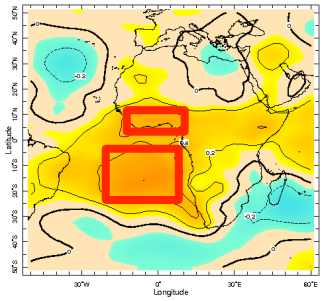

(b)

Figure A.10: Onset North Cluster correlation plots with April (a) sea-surface temperature, and (b) mean sea-level pressure. Red boxes indicate regions used to produce predictors.

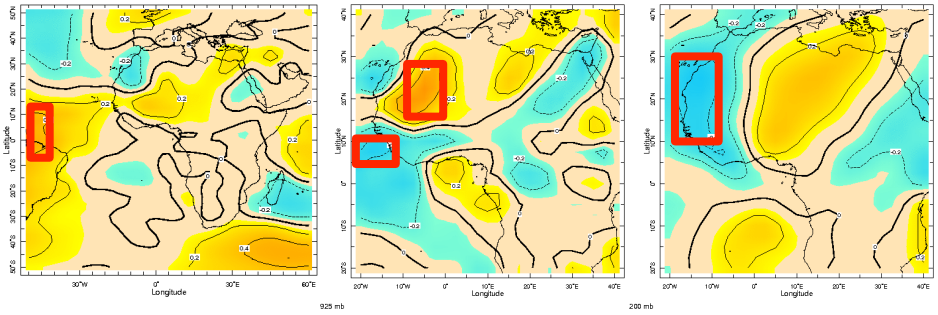

(a) (b) (c)

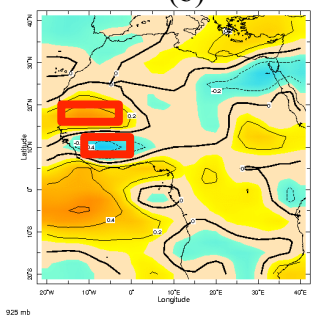

(d)

Figure A.11: Retreat South Cluster correlation plots with May (a) mean sea-level pressure, (b) 925mb zonal winds, (c) 200mb zonal winds, and (d) 200mb meridional winds. Red boxes indicate regions used to produce predictors.

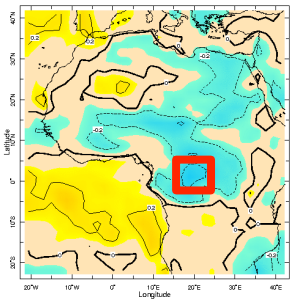

(a)

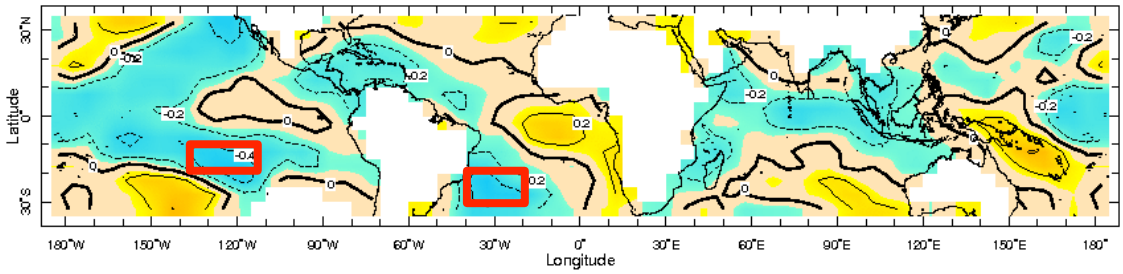

(b)

Figure A.12: Retreat South Cluster correlation plots with July (a) surface temperature, and (b) sea-surface temperature. Red boxes indicate regions used to produce predictors.

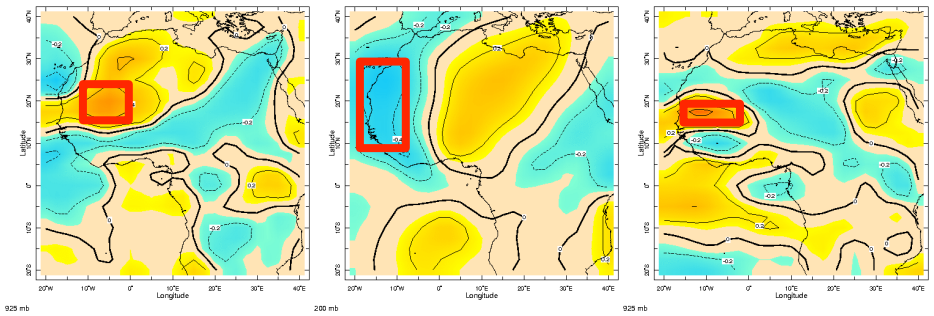

(a) (b) (c)

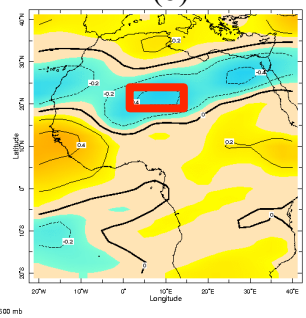

(d)

Figure A.13: Retreat Middle Cluster correlation plots with May (a) 925mb zonal winds, (b) 200mb zonal winds, (c) 925mb meridional winds, and (d) 600mb meridional winds. Red boxes indicate regions used to produce predictors.

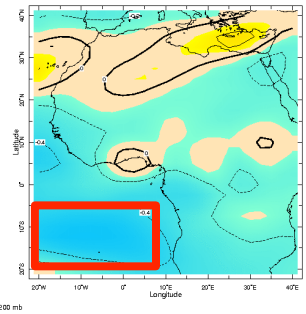

Figure A.14: Retreat Middle Cluster correlation plot with June 200mb meridional winds. Red boxes indicate regions used to produce predictors.

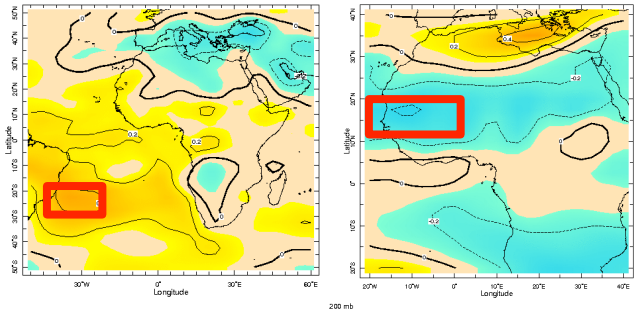

(a) (b)

Figure A.15: Retreat Middle Cluster correlation plot with July (a) mean sea-level pressure, and (b) 200mb zonal winds. Red boxes indicate regions used to produce predictors.

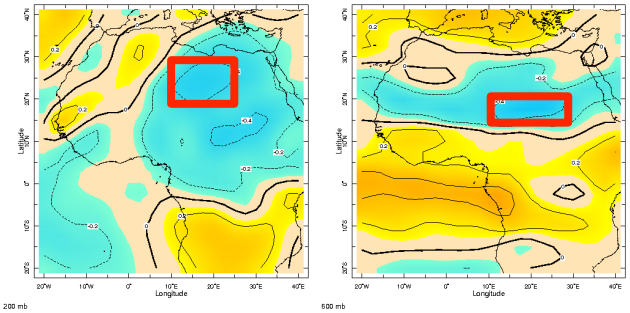

(a) (b)

Figure A.16: Retreat Middle Cluster correlation plots with August (a) 200mb zonal winds, and (b) 600mb meridional winds. Red boxes indicate regions used to produce predictors.

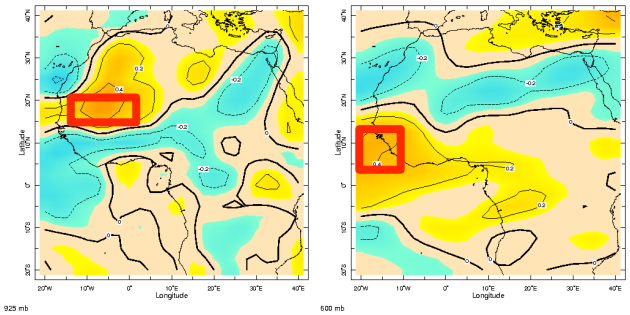

(a) (b)

Figure A.17: Retreat North Cluster correlation plots with May (a) 925mb zonal winds, and (b) 200mb meridional winds. Red boxes indicate regions used to produce predictors.

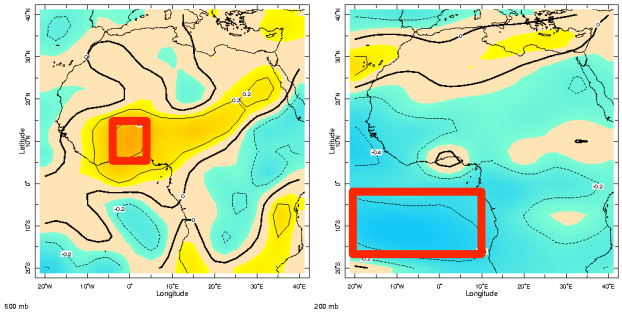

(a) (b)

Figure A.18: Retreat North Cluster correlation plots with June (a) 600mb zonal winds, and (b) 200mb meridional winds. Red boxes indicate regions used to produce predictors.

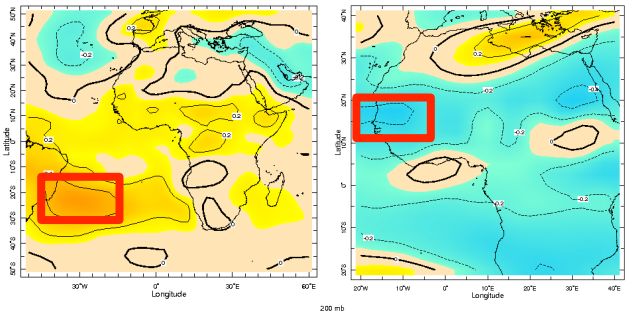

(a) (b)

Figure A.19: Retreat North Cluster correlation plots with July (a) mean sea-level pressure, and (b) 200mb meridional winds. Red boxes indicate regions used to produce predictors.

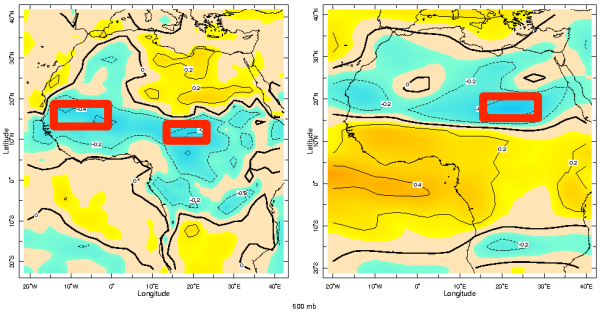

(a) (b)

Figure A.20: Retreat North Cluster correlation plots with August (a) surface temperature, and (b) 600mb meridional winds. Red boxes indicate regions used to produce predictors.

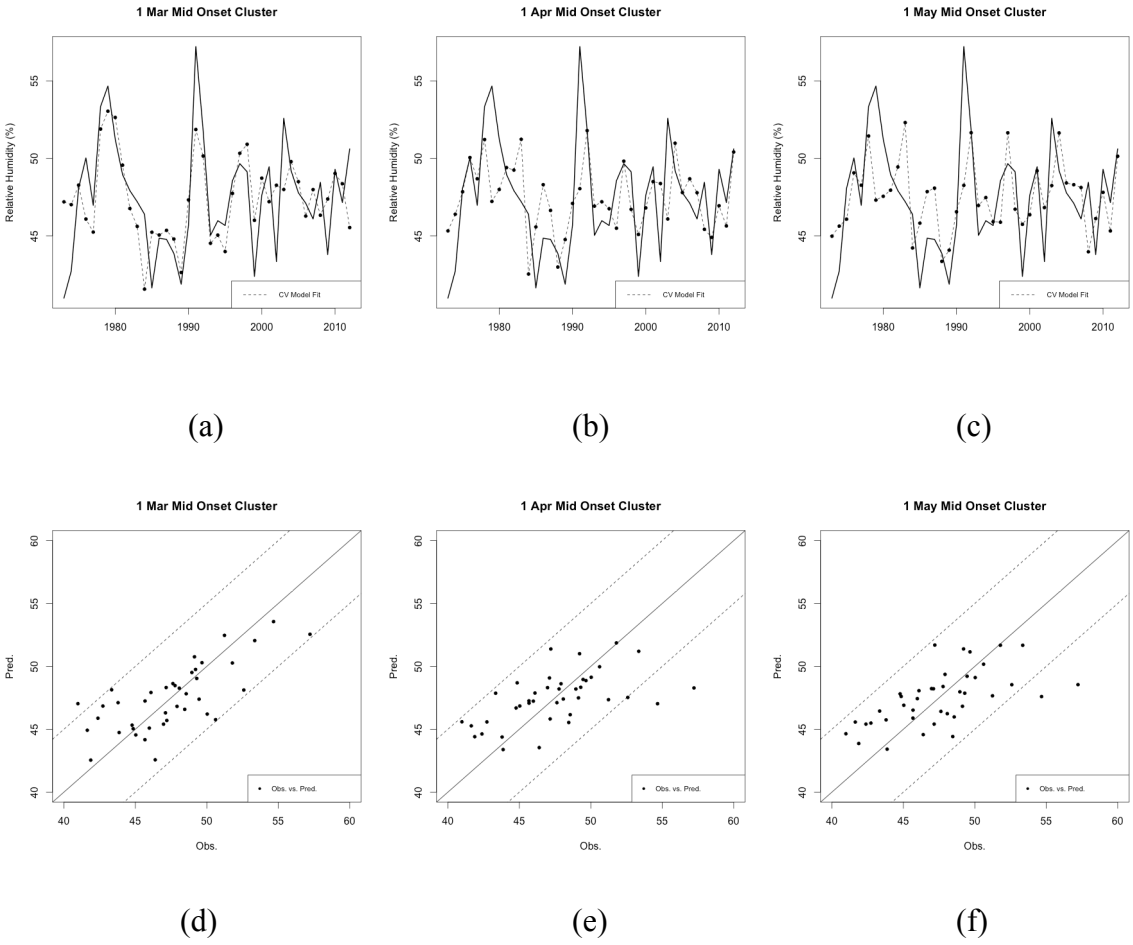

Figure A.21: Onset Middle Cluster GLM models showing direct fit values and cross-validated values. (a), (b), and (c) show the cross-validated model fits for 1 March, 1 April, and 1 May. (d), (e), and (f) show the predicted vs. observed direct fit values for the 1 March, 1 April, and 1 May models (solid line indicates 1:1, dashed lines show ±5%)

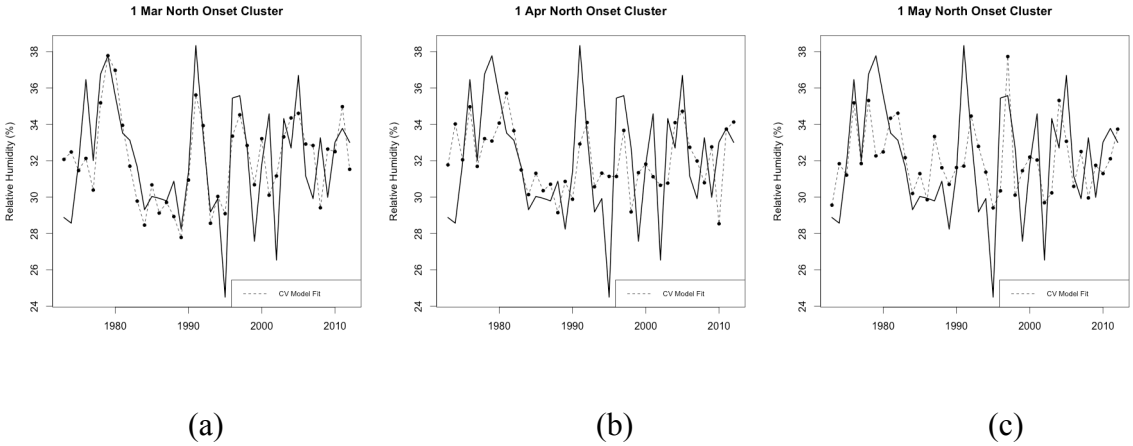

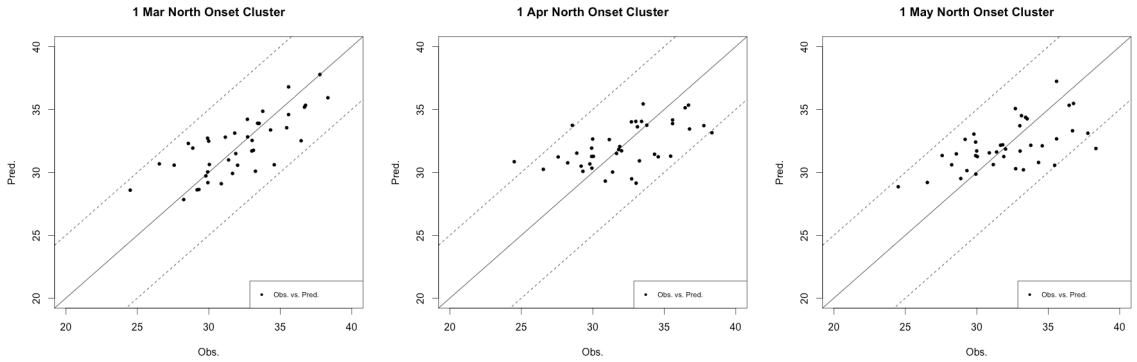

(d) (e) (f)

Figure A.22: Onset North Cluster GLM models showing direct fit values and cross-validated values. (a), (b), and (c) show the cross-validated model fits for 1 March, 1 April, and 1 May. (d), (e), and (f) show the predicted vs. observed direct fit values for the 1 March, 1 April, and 1 May models (solid line indicates 1:1, dashed lines show ±5%)

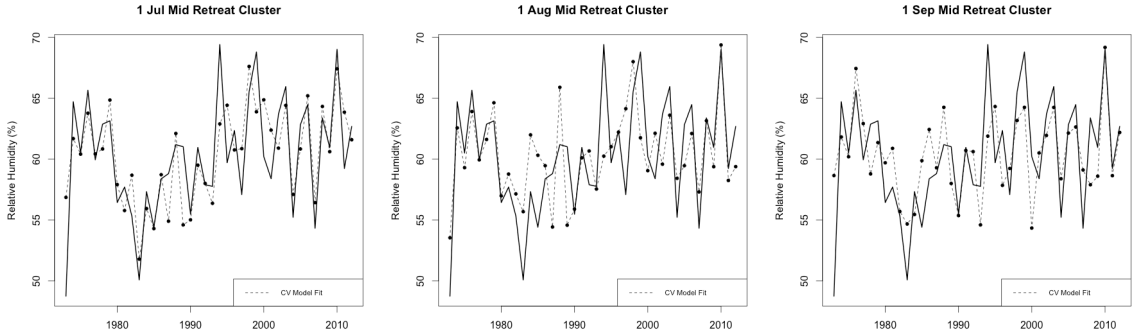

(a) (b) (c)

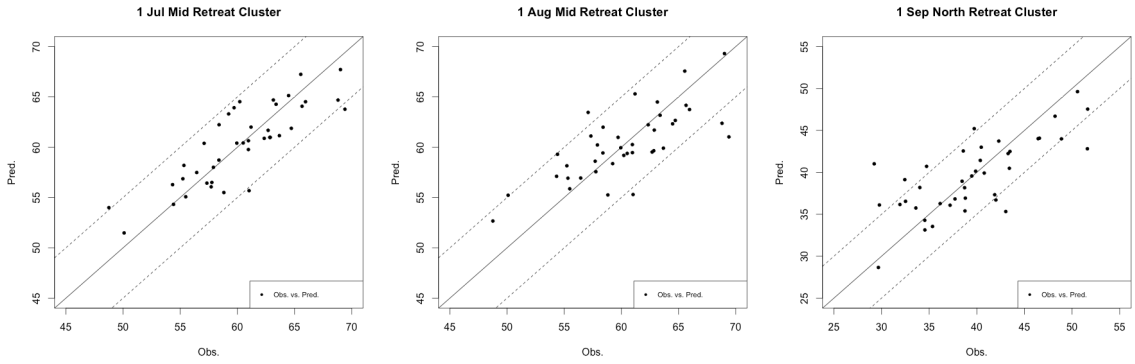

(d) (e) (f)

Figure A.23: Retreat Middle Cluster GLM models showing direct fit values and cross-validated values. (a), (b), and (c) show the cross-validated model fits for 1 July, 1 August, and 1 September. (d), (e), and (f) show the predicted vs. observed direct fit values for the 1 July, 1 August, and 1 September models (solid line indicates 1:1, dashed lines show ±5%)

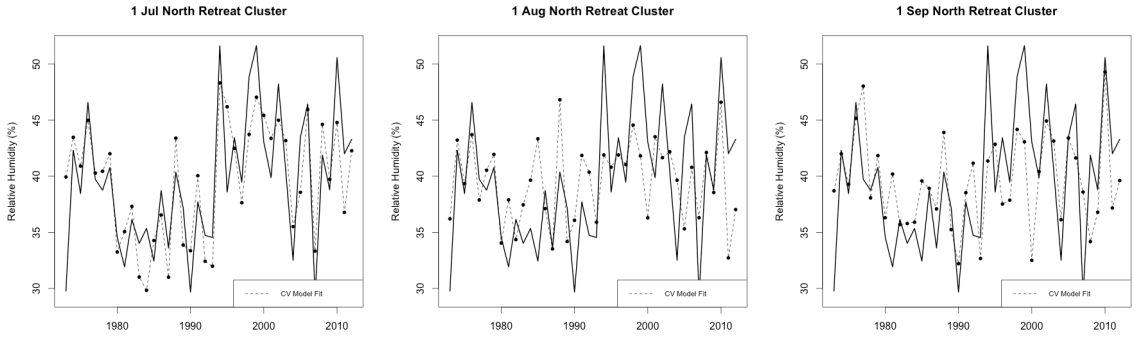

(a) (b) (c)

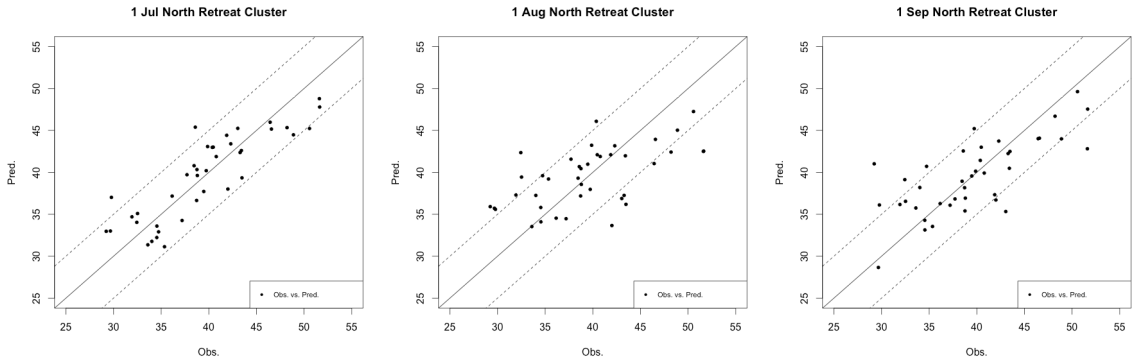

(d) (e) (f)

Figure A.24: Retreat North Cluster GLM models showing direct fit values and cross-validated values. (a), (b), and (c) show the cross-validated model fits for 1 July, 1 August, and 1 September. (d), (e), and (f) show the predicted vs. observed direct fit values for the 1 July, 1 August, and 1 September models (solid line indicates 1:1, dashed lines show ±5%)